Republic of Iraq
Ministry of Higher Education
and Scientific Research
University of Babylon / College of Sciences
Chemistry Department

Removal of Some Dyes Using Nanocomposites Derived From Polyaniline and Chitosan with Some Metal Oxides as a new Adsorbents.

A thesis

Submitted to the Council of the College

of Science, University of Babylon in a

Partial Fulfillment of theRequirements

for the Degree of Doctorate of

Philosophy in Chemistry

By

Karrar Majeed Obaid Mohammed

B.Sc. College of Sciences - University of Babylon 2016

M.Sc. College of Sciences - University of Babylon 2018

Supervised By

Asst. Prof. Dr.: Ahmed Saadoon Abbas

Asst. Prof. Dr.: Yahya Fahim Obeed

2023 A.D **1445 A.H**

يَرْفَعِ اللَّهُ الَّذِينَ آمَنُوا مِنكُمْ وَالَّذِينَ

أُوتُوا الْعِلْمَ دَرَجَاتٍ وَاللَّهُ بِمَا تَعْمَلُونَ

خَبِيرٌ

صدق الله العظيم

سورة المجادلة: الآية 11

Supervisor Certification

We certify that this thesis entitled, **"*Removal of Some Dyes Using Nanocomposites Derived From Polyaniline and Chitosan with Some Metal Oxides as a new Adsorbents.*"** Is prepared under our supervisions, by **"*Karrar Majeed Obaid Mohammed*"**. It is done at the Department of Chemistry, College of Science at the University of Babylon in partial fulfillment of the requirement for the degree of **Doctorate** of Philosophy in chemistry at the University of Babylon and this work has never been published anywhere else.

Signature:

Name: **Asst. Prof.Dr.**
Ahmed Saadoon Abbas
Title: Assaint Professor
Address: Babylon University
College of Science, Chemistry
Date: / / 2023

Signature:

Name**: Asst. Prof.Dr.**
Yahya Fahim Obeed
Title: Assaint Professor
Address: Babylon University
College of Science, Chemistry
Date: / / 2023

In view of the available recommendation, I forward this thesis for debate by the examining committee.

Signature:

Name: Prof.Dr.
Abbas Jasim Atiyah
Title: Professor
Address: Head of Department
Date: / / 2023

Committee Certification

We, the examiner committee, certify that we have read the thesis entitled"**Removal of Some Dyes Using Nanocomposites Derived From Polyaniline and Chitosan with Some Metal Oxides as a new Adsorbents**" and examined the student (***Karrar Majeed Obaid Mohammed***) in its contents at 13 / 7 / 2022, and that in our opinion it is accepted as a thesis for the degree of **Doctorate** of Philosophy in chemistry with **(Excellent)** estimation.

Signature:

Name: **Dr. Ahmed Ali Abdulsahib**
Title: Professor
Address: Babylon University
College of Sciences, Chemistry
Date: / / 2023
(Chairman)

Signature:
Name: **Dr. Ibtihal Kadim Kareem**
Title: Professor
Address: Kufa University
Faculty of Education for Girls
Date: / / 2023
(Member)

Signature:
Name: **Dr. Angham G. Hadi**
Title: Assistant Professor
Address: Babylon University
College of Sciences, Chemistry
Date: / / 2023
(Member

Signature: Ahmed s.
Name: **Dr. Ahmed Saadoon Abbas**
Title: Assistant Professor
Address: Babylon University
College of Sciences, Chemistry
Date: / / 2023
(Member and Supervisor)

Signature:
Name: **Dr. Aseel Mushtaq Kadim**
Title: Assistant Professor
Address: Babylon University
College of Scinece for Girls
Date: / / 2023
(Member)

Signature:
Name: **Dr.Zahraa Hashim Athab**
Title: Assistant Professor
Address: Babylon University
Environmental Research and Studies Center
Date: / / 2023
(Member)

Signature:
Name: **Dr. Yahya Fahim Obeed**
Title: Assistant Professor
Address: Babylon University
College of Sciences, Chemistry
Date: / / 2023
(Member and Supervisor)

Approved by the College Committee on Graduate Studies

Signature:
Name: **Prof.Dr. Mohammed Hadi Shinen Alshammari**
Title: Professor
Address: Dean of College of Science – University of Babylon.
Date: / / 2023

Declaration

I, ***Karrar Majeed Obaid Mohammed***, the researcher, who conducted this study entitled **"*Removal of Some Dyes Using Nanocomposites Derived From Polyaniline and Chitosan with Some Metal Oxides as a new Adsorbents*"** is submitted in a partial fulfillment of the requirements of a ***Ph.D.*** in Chemistry. The research is carried out during the period **1-2-2022 to 17-7-2023** at the Department of Chemistry, College of Science, University of Babylon**.**

The study is carried out under the supervisions of ***Asst.Prof.Dr: Ahmed Saadoon Abbas*** and ***Asst.Prof.Dr: Yahya Fahim Obeed*** at the Department of Chemistry, College of Science, University of Babylon.

I confirm that the work presented in this thesis has not been previously submitted for a degree Ph.D. at any higher educational institute. In addition, I declare that all the information in this document has been obtained and presented in accordance with academic rules and ethical conduct, I have fully cited and referenced all material and results that are original to this work or where information has been derived from other sources, I confirm that this has been indicated in this thesis.

Karrar Majeed Obaid

Dedications

To the Imam Mahdi (calf God reappearance)

To the supporter of my life, my father

To my great mother, for her support, assistance, and kindness, all thanks and appreciation to you.

To my Brothers and sisters … who supported me all Time.

To my friends … who supported me all time

To my master's supervisor, Dr. Kasim Hassan Kadim, who passed away due to the Corona virus

Karrar Majeed Obaid

Acknowledgements

In The Name of Allah Most Gracious, Most Merciful

In the beginning, I would like to express my great appreciation to the Almighty, Allah for His support in enabling me to complete this dissertation.

Special thanks go to my supervisors ***Assist.Prof.Dr: Ahmed Saadoon Abbas*** *and* ***Assist.Prof.Dr: Yahya Fahim Obeed,*** *greatly for enriching my knowledge.*

I would like to express my deep and special thanks to my family.

I wish to thank Babylon University, the Collage of Science, and the Department of Chemistry for offering me the scholarship and facilitating.

In addition, I would like to thank all Chemistry staff members, the Department of Chemistry for their help and inspiration.

Also, I would like to express my deep and special gratitude to my best friends, who helped and encouraged me a lot during three years ago.

Karrar Majeed Obaid

Summary

The present study is divided in to two parts. **First part of thesis** deals with the synthesis of a new types of multifunctional material Polyaniline/Nb_2O_5/MnO_2 and Polyaniline/Nb_2O_5/Cr_2O_3 Nanocomposites were prepared by chemical Polymerization from aniline monomer in the presence of metal oxides (Nb_2O_5,Cr_2O_3 and MnO_2) and an oxidant (ammonium persulfate) in acidic aqueous solution for removal dye from water. Herein, the Nanocomposites was found to be a favorable adsorbents for wastewater treatment due to their high adsorption and efficiency, self-regeneration, low cost and easy synthesis. These Nanocomposites were characterized by different techniques such as Fourier Transform Infrared Spectroscopy (FTIR), X-ray diffraction (XRD), UV/Visible, Thermo gravmetric analysis (TGA), Zeta potential analysis(ZPA) and scanning electron microscopy (SEM). While surface morphology was examined by SEM examination, XRD analysis validated the structure of Polyaniline/nanomatrial composites. In Polyaniline /NPs composites, their functional groups were identified by using FTIR spectroscopy, and the shifting of the peaks towards the higher wave number side has been discovered to demonstrate the interaction between the polymer and the nanoparticles in produced Adsorption.

The Polyaniline/Nb_2O_5/MnO_2 and Polyaniline/Nb_2O_5/Cr_2O_3 Nanocomposites using to adsorb methyl orange dye (MO). The results showed that polyaniline Nanocomposites doped with Nb_2O_5 and MnO_2 nanoparticles had a higher adsorption efficiency (~ 97.75%) than that found in PANI with Cr_2O_3 and MnO_2 (~ 94.2%).).The maximal adsorption capabilities of the PANI/Nb_2O_5/Cr_2O_3 and PANI/Nb_2O_5/MnO_2. A similar amount of adsorbents 148 mg/g and 84 mg/g, respectively. The optimum conditions for the methyl orange reactions with Polyaniline/Nb_2O_5/MnO_2 where the dose was 100 mg, temperature 298 K, and pH

value is 7, while with Polyaniline /Nb_2O_5/Cr_2O_3 Nanocomposites the dose is 50 mg, temperature 298, and pH value was 9.

Second part of thesis study deals with the synthesis a new type of multifunctional material Chitosan/Nb_2O_5/MnO_2 and Chitosan/Nb_2O_5/Cr_2O_3 Nanocomposites were prepared by situ chemistry approach in the presence of metal oxides (Nb_2O_5,Cr_2O_3 and MnO_2) and in acidic aqueous solution. the Nanocomposites were found to be a favorable adsorbents for wastewater treatment due to its high adsorption and efficiency, self-regeneration, low cost and easy synthesis. These Nanocomposites were characterized by different techniques such as Fourier Transform Infrared Spectroscopy (FTIR), X-ray diffraction (XRD),UV/Visible, Thermo gravimetric
analysis (TGA), Zeta potential analysis(ZPA) and scanning electron microscopy (SEM). These synthesized Chitosan/Nb_2O_5/MnO_2 and Chitosan/Nb_2O_5/Cr_2O_3 were used as adsorption against toxic dyes such as bromocresol green (BCG) and direct yellow 50 (DY50). The higher adsorption efficiency of bromocresol green (BCG) by Chitosan/Nb_2O_5/ MnO_2 90.65% while Chitosan/Nb_2O_5/Cr_2O_3 88.5%. the maximum adsorption capacity was determined to be (93,43) mg/g. for Chitosan/Nb_2O_5/ MnO_2 & Chitosan/Nb_2O_5/Cr_2O_3 respectively. The optimum conditions for the bromocresol green reactions with Chitosan /Nb_2O_5/MnO_2 where the dose was 150 mg, temperature 298 K, and pH value is 7,while with Chitosan /Nb_2O_5/Cr_2O_3 Nanocomposites the dose is 550 mg, temperature 313, and pH value is 10.

The higher Removal dye of direct yellow (DY50) by Chitosan/Nb_2O_5/ MnO_2 and Chitosan/Nb_2O_5/Cr_2O_3 (98.1% and 95.41%)respectively. the maximum adsorption capacity is determined to be (200,351.5) mg/g .for Chitosan/Nb_2O_5/ MnO_2 & Chitosan/Nb_2O_5/Cr_2O_3 respectively. The optimum conditions for the

direct yellow 50 reactions with Chitosan /Nb_2O_5/MnO_2 where the dose is 50 mg, temperature 298 K, and pH value was 3,while with Chitosan /Nb_2O_5/Cr_2O_3 nanocomposites the dose is 25 mg, temperature298, and pH value was 4.

.

Table of Contents

List of Tables

Table of Figures

Table of Abbreviations and Symbols

Abbreviations and Symbols	*The Meaning*
Abs	Absorbance
APS	Ammonium persulfate
Bg	band gap
C	Concentration
C_o	Initial Concentration
C_e	Equilibrium Concentration
CD	Circular Dichroism
CS	Chitosan
CB	conductivity band
CH	Chitin
^0C	Centigrade
D	Crystallite Size
1D	One Dimensional
DI	Deionized Water
Eg	Energy Gap
FTIR	Fourier Transform Infrared Spectroscopy
FE-SEM	Field Emission Scanning Electron Microscopes
GO	Graphene Oxide
HOMO	Highest Occupied Molecular Orbital
K	The Scherrer Constant
k	Empirical Constants for Adsorbent
Kf	Freundlich Constants
LUMO	Lowest Occupied Molecular Orbital
m	Mass of Adsorbent
NPs	Nanoparticles

NMs	Nanomaterial
NSs	Nanostructure semiconductor
PANI	Polyaniline
UV-Vis	Ultra Violet light in the range from 315 to 380 nm
QDs	quantum dots semiconductor
qe	Adsorption capacity
SEM	Scanning Electron Microscopy
TGA	Thermogravmetric analysis
T	Temperature
XRD	X-rays Diffraction
ZPA	Zeta Potential Analysis
Θ	Diffraction angle (Bragg's angle)
λ	Wavelength of X-rays reaction

Chapter 1

Introduction & Literature Survey

I. Introduction

Nanoparticles and its structures have drawn the attention of materials developers due to their unique properties. In the past ten years, there has been a lot of interest in Nanomaterial's, which are materials with structural features [such as grain or particle size] of at least one dimension in the range of 1-100 nm. Materials such as composites, metals, ceramics and polymers can all be employed as nanostructures[1].

Nanomaterials are in the middle of the process of downsizing, between the atomic and quantum scales and the bulk scale. They are not an additional stage in the process. Atomic physics principles do have an effect on some material properties at the nanoscale, however, this effect is in direct contrast to the bulk properties. Nanotechnology and its utilization in the modern era were anticipated and received the most significant attention as a distinct field of study because of their unique physical and chemical properties as well as their biological uses[2].This technique is mostly used for the creation, modification, the development of their properties while taking into consideration their potential, the use of promising materials, and size, dimensions, shape, and morphology of magnetic and crystal structures. Intriguing nanoscale physics, chemistry, and biomedical studies are all included in the field of nanoscience. compounds that are both inorganic and organic, with cutting-edge technological advancements and difficulties[3, 4].

1.1 Nanotechnology and nanomaterials

Environmental safety is one of the many scientific and technical areas that nanotechnology affects. Water and wastewater treatment are examples of environmental uses of nanotechnology where various nanomaterials use adsorption and separation processes, as well as a number of other techniques[5], to remove contaminants, germs, and other dangerous substances. a wide range of composites, different shapes, and active components.

Many methods exist to create nanomaterials, the most common is to add functions to them. Nanostructures have facilitated a practical solution that provides abundant water. Because of the small surface area of its microfacets, the interface is extremely specialized.[6] Due to their properties and potential for environmental remediation, nanomaterials have emerged as a significant topic in environmental research. Nearly all of the nanoparticles discussed here are nanoparticles. In the upcoming years, the use of nanoparticles in wastewater treatment is projected to provide many significant hurdles, including the possibility for aggregate build-up, issues with insoluble separation, toxicity to both human and environmental health properties, and remediation potential[7].

Nanomaterials have also become a hot topic in environmental research because of their potential for use in remediation[8].

1.1.1Classification of Nanomaterials

Nanomaterials can be made as a film, rod, or dot and can vary in size along simply one, two, or all three dimensions. There are various nomenclatures used to describe the dimensions of nanomaterials, and this causes confusion because some refer to the confinement dimensions (or nanoscale size), which are distinct from the bulk-like dimensions that a nanomaterial appears to possess[9] . The definition of nanomaterials includes 0D, 1D, 2D, and 3D nanostructures[10]. Clusters and

spheres are examples of 0D nanomaterials; wires, nanofibers, and rods are examples of 1D nanomaterials; plates, films, and networks are examples of 2D nanomaterials; and liposomes are examples of 3D structures. The characterisation of these nanostructures requires the use of sophisticated techniques like spectroscopy and microscopy[11].

1.1.2 Properties of nanomaterials

Particles' physicochemical qualities change significantly as they grow from micrometer to nanoscale size. Nanomaterials display radically different features from normal materials due to their small size. dimensions of materials with similar constituents. In essence, there are two factors that make nanomaterials' properties significantly differ from one another materials[12, 13].

1.1.2.1 Surface Effects

More atoms are found on the particle's surface than inside its internal core when particle size decreases. For instance, particles of a diameter of 30 nm contain 5% surface atoms, those of 10 nm have 20%, and those of 3 nm have 50%. [14].

The surface area to volume ratio is extremely large in nanomaterials that have a large percentage of surface atoms. Surface properties and characteristics have the greatest influence on the majority of physical and chemical interactions between materials. As a result, compared to materials that are micrometer-sized but have the same composition, nanomaterials will have greater surface-dependent material properties. The characteristics of the interface and the behavior of the particles are affected by the properties of the nanoparticle's surface [15]. Figure (1.1) illustrates the effect of decreasing particle size on the percentage of surface area that is proportional to particle size.

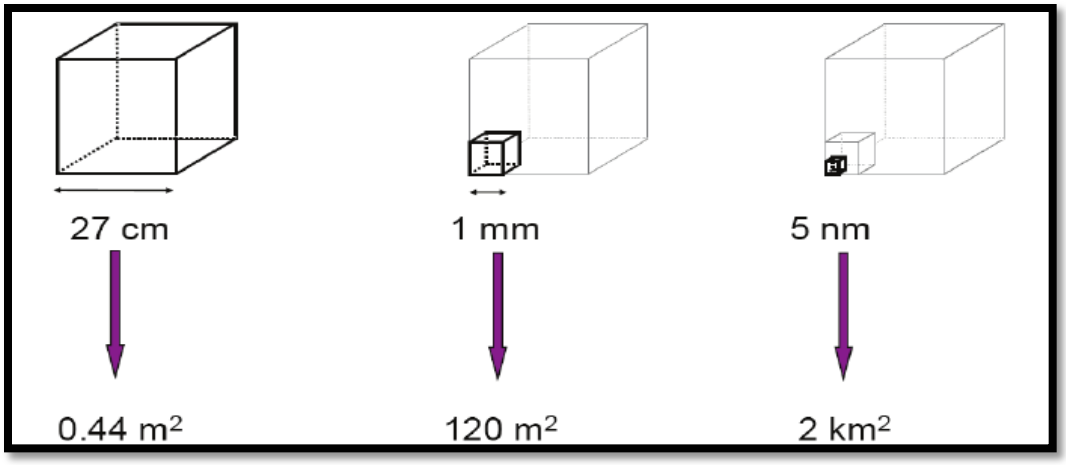

Figure 1.1. A schematic showing how a cube's surface area increases as particle size decreases **[16]**

1.1.2.2 Quantum confinement Effects

The quantum confinement phenomena in low-dimensional semiconductor systems was initially described about 25 years ago. The overall crystalline structure in an is maintained at the nanoscale. However, due to quantum confinement, nanocrystals have features similar to molecules. distinct electrical states that clearly exhibit size dependence. Extensive research has been conducted to look into size dependent qualities over the last ten years. of semiconductors with an emphasis on their optical properties, such as their luminescence and absorption [17].

Excitons in quantum dots (QDs), a semiconductor, are constrained in all three spatial dimensions. They consequently possess characteristics halfway between those of discrete molecules and those of bulk semiconductors. Quantum size effects are typically found in nanocrystallites less than 10 nm, whereas size effects are seen in semiconductor crystals measuring 10-100 nm. There are two main differences between the physicochemical characteristics of nanocrystalline particles and those of bulk materials[18].

Due to the high surface to volume ratio in the crystalline lattice, there are a lot of atoms there. Second, the charge carriers are enclosed in three dimensions as a result of the electronic bands splitting into various energy levels. This causes the bandgap to widen with smaller particles, leading to quantum confinement of charge[19].

1.2 Conducting polymers

Because they combine the chemical applications, electrochemical characteristics, and mechanical qualities of polymers with the electrical properties of semiconductors and metals, conductive polymers are a particular family of materials that can be referred to as synthetic metals[20]. These organic materials are semiconductors or true metallic electrical conductors. Their main strength is how easily they can be processed. The mechanical properties of plastics, such as elasticity, malleability, flexibility, etc., are combined with high electrical conductivity in these synthetic plastics. They can also be improved by using the various organic synthesis processes[21].

Many methods are available, including chemical, electrochemical, laser, injection-based, and non-redox methods, all of which can be employed to modify conjugated polymers. The most common form of doping is oxidative doping, which removes electrons from the conjugated system via chemical or electrochemical means. With the assistance of nearby counter-ions, this procedure is called "p-doping," which creates a positively charged backbone that is sustained by Coulombic forces. By augmenting the n-doping system with electrons, which increases the number of n-electrons in the system, negatively charged polymers are created[22, 23]. This form of doping, however, results in a lightly doped polymer. Doped polymers are typically created from the monomer starting material in a

single phase because the oxidative doping process typically occurs simultaneously with polymerization.[24]. Chemical structures of typical conductive polymers are shown in Figure (1.2).

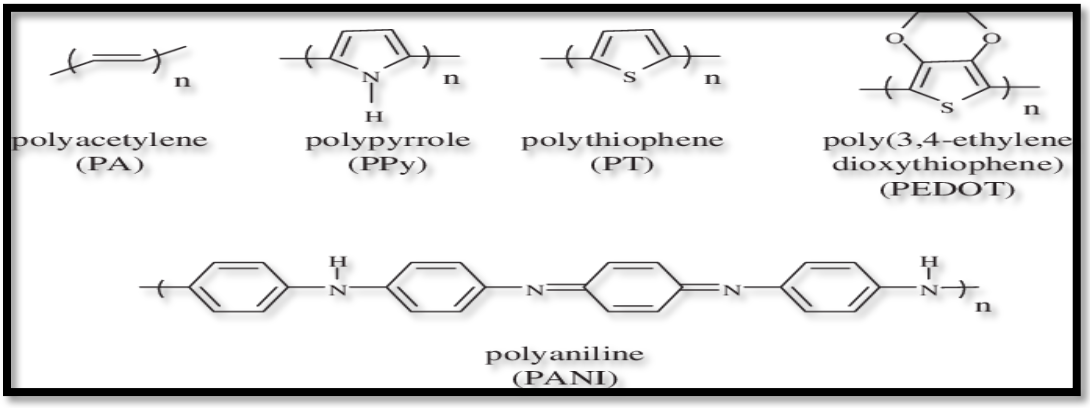

Figure 1.2 Typical conductive polymer chemical compositions [25]

1.3 Properties of polymer Nanocomposites

In addition to being influenced by the characteristics of each parent component, the unique features of Nanocomposites and the degree to which host matrix material's attributes are enhanced depend on[26] :

- The nature of the interface adhesion between the matrix.
- The percentage of inclusions that are filled with nanoparticles.
- The properties of nanoparticles.
- The volume of nanofillers.
- The appearance of the interphase as it developed at the interface with the matrix.
- The morphology of the system.

To augment or create new properties in Nanocomposites, the large surface area of the nanoparticles must be maintained; otherwise, they will tend to cluster or agglomerate. Because these larger aggregates would serve as flaws and limit the property's increase, nanoparticles should be consistently distributed throughout the matrix in order to achieve the greatest property increase[27]. Figure (1.3) illustrates type of dispersing nanoparticles in the host matrix material.

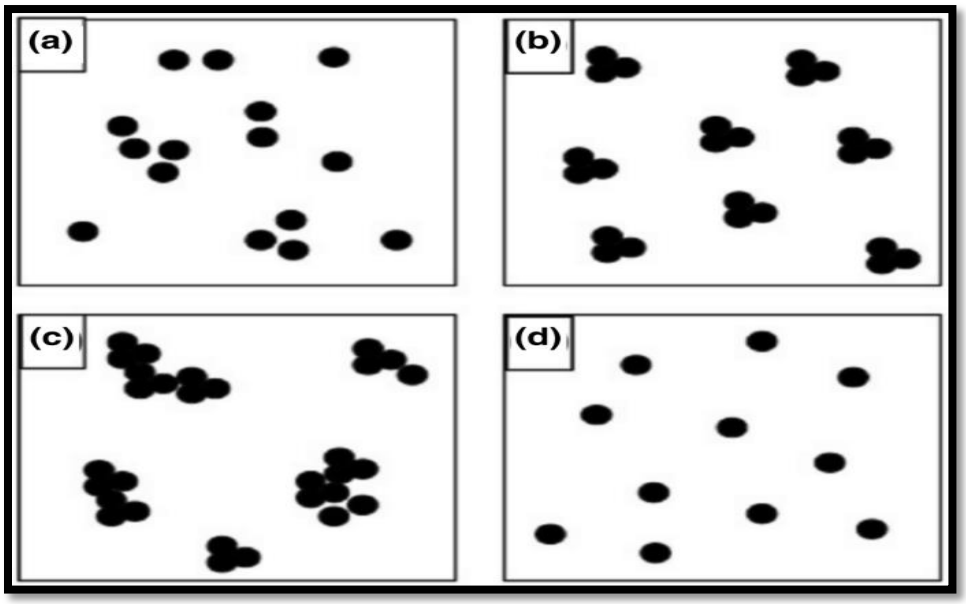

Figure 1.3. Nanoparticle dispersion and distribution inside the matrix**(a) "good distribution but poor dispersion, (b) poor distribution and poor dispersion, (c) poor distribution but good dispersion, (d) good distribution and good dispersion are examples of dispersion patterns"** [27].

1.4 Polyaniline (PANI)

Many applications have looked into the properties of Polyaniline (PANI), including its mechanical, electrical, optical, physical, thermal, chemical, and morphological characteristics. For adsorbents based on PANI, the most researched characteristics are hydrophobicity, surface charge, and both functional groups and

morphology. PANI is a very important class Among the family of conducting polymers, it stands out for its simplicity high environmental stability and synthetic materials[28].

The word "polyaniline" is originally created in 1862 to describe a family of polymers (also called "mers") that have as many as 1000 monomers in them. Even though the majority of the structural characterization of polyaniline has been accomplished in the past 20 years or so, this knowledge is fairly well understood, the large number of publications in the past five years suggests that polyaniline is still being studied extensively[29].

Potential applications for polyaniline include electrochromic devices, corrosion-resistant paint, and sensors[30]. Polyaniline is particularly advantageous and appealing for usage in electromagnetic shielding devices, solar cells, displays, light battery electrodes, and sensors due to these applications[31].

PANI exhibits semiconducting properties that are frequently observed in inorganic semiconductors due to their capacity to modify certain features, such as conductivity, density, color, and permeability to gases and liquids, in response to external forces[32, 33]. Reduced and oxidized states of polyaniline can cause color changes that can be utilized in sensors and electrochromic devices[34].

1.4.1 Structure and Morphology

Conducting polymers have -conjugation because of the polymer backbone, which is composed of carbon, hydrogen, and heteroatoms like nitrogen or sulphur. Polyaniline, a conventional phenylene base polymer, has a chemically flexible -NH-group that is edged on both sides by a phenylene ring. This -NH-group can be utilized to detect the properties of polyaniline, including protonation, de protonation, and many physicochemicals[35].

PANI exists in three different states: completely reduced (also known as leucoemerald base; LB), half-oxidized (also known as emerald base; EB), and fully

oxidized (also known as pernigraniline;). Additionally, it is said that emerald, in all three of its states, is PANI's most conductive form when it has undergone the doping procedure (emerald salt), as well as being the most stable.[36] In the fundamental structure of emeralds, the sizes of the amines (-NH-) and imines (=N-) are the same. However, neither the fully oxidized pernigraniline base nor the fully reduced leucoemeraldine base of PANI conduct electricity[37]. Except for polyacetylene, which has a doubly degenerate ground state, polyaniline only exists in the pernigraniline form[38].Figure (1.4) illustration chemical structure of polyaniline.

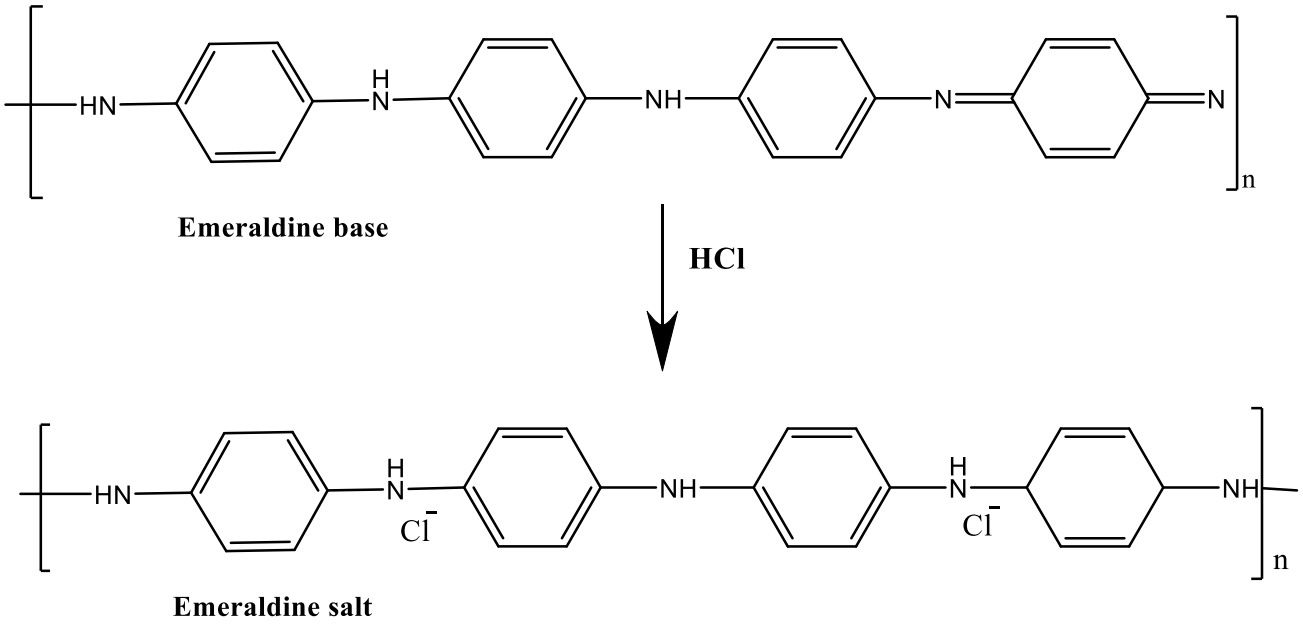

Figure1.4Chemical structure of polyaniline[39]

PANI can be found in both its reduced and oxidized states. The reduced units come equipped with two amine groups and two benzenoid rings[40]. On the other hand, the oxidized units exhibit one quinoid ring, one benzenoid ring, and two imine groups. As a result of variations in the proportion of oxidized to reduced units within the polymer, PANI is able to exist in several different oxidation states. A noteworthy example of a more reduced form is leucoemeraldine, which contains

only benzenoid rings, contrary to pernigraniline, the most oxidized form featuring two quinoid and two benzenoid structures. The emeraldine form of PANI boasts a superior level of conductivity in contrast to its other oxidation states, due to its optimal balance of reduced and oxidized units [41, 42].

Sharing replicated units are one quinoid ring that encircles imine (N=) groups and three benzene rings divided by amine (NH) groups. The polyaniline structure forms double bonds using four electrons, two pairs of carbon atoms in the ring, and a quinoid ring within the polymer chain's framework. PANI has multiple forms that can exist in a range of H+ salt forms, including their basic form. The conductive PANI structure, also known as the emeraldine salt (PANI-ES), exhibits advantageous transport properties[43].

The quantity of electrons or degree of oxidation, and quantity of protons or degree of protonation, have a direct impact on the polyamine's conductivity[44]. The ideal conductivity range for PANI is a controlled 10^{-10} to 10^{1} Scm^{-1}.

1.4.2. Applications of Polyaniline

For clinical diagnostics and environmental monitoring, many researchers have recently focused on the creation of printable electrochemical sensor systems that are least expensive. Consuming polyaniline's redox characteristics has required a lot of effort. Several organizations have investigated various mass-affordable manufacturing techniques to create suitable thin films of PANI in order to gain the greatest sensing applications. This observation revealed that, provided they are inkjet-printable, nano-dispersions have a lot of potential for sensing applications [45]. The two-dimensional pattern, thickness, and conductivity of the polyaniline inkjet-printed films can be precisely controlled, demonstrating the level of accuracy possible with inkjet printing[43]. Numerous other applications, including energy storage, displays, organic light-emitting diodes, etc., are also possible for polyaniline.

Polyaniline is used in many different businesses and aspects of daily life. They are only briefly discussed here[46].Figure (1.5) show the application of polyaniline

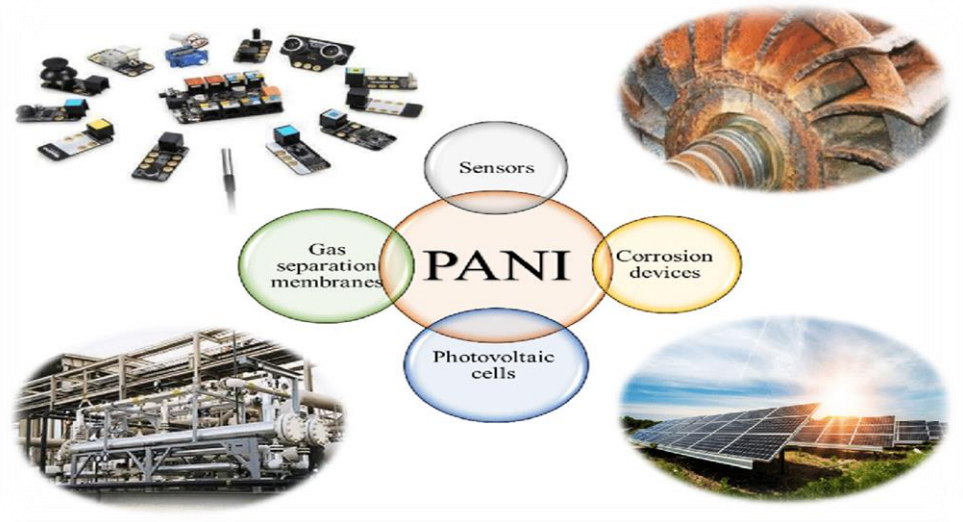

***Figure 1.5 Polyaniline in different applications*[43].**

1.5. Chitosan

Chitosan is a biopolymer containing a linear polysaccharide based on glucosamine units that can be made by deacetylating of chitin[47]. Chitosan is regarded as a versatile and a non-toxic raw material, both biodegradable and frequently used[48]. It has been utilized innumerous industries, such as food production, agriculture, and medical, textiles, wastewater treatment, etc. However, its more widespread application was somewhat constrained due to its acidic disintegration[49, 50].

Chitosan that has been cross-linked is insoluble in acid solution, which increases its stability. However, cross-linking frequently comes at the expense of the hydroxyl and amino groups in chitosan, resulting in a reduction in chitosan's capacity for adsorption[50]. Cross-linked chitosan would undergo further protonation for the improvement of the positively charged characteristic of

chitosan in order to increase its adsorption capacity. An increase in positively charged traits would make anion dye removal easier [51, 52]. Figure (1.6) show the structure of chitosan.

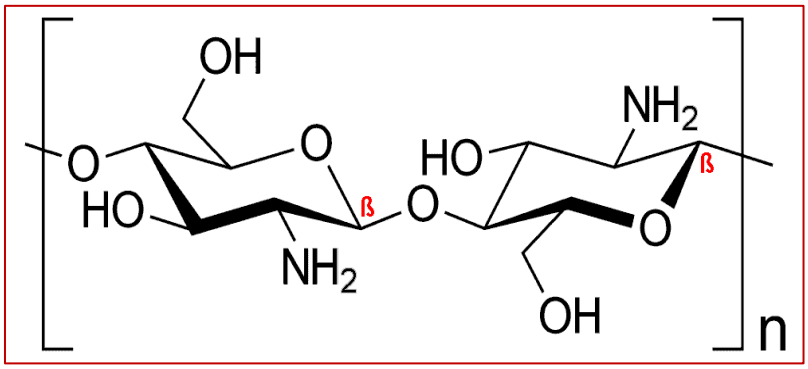

Figure 1.6 The chemical structure of chitosan

1.5.1. Chitosan crystallinity

Chitosan is believed to have a hierarchical structure that is composed of numerous crystalline domains that are linked by both intra-and intermolecular hydrogen bonds.[52] Also, the capacity of chitosan to bind substances is influenced by the degree of crystallinity because it restricts the substance from accessing internal or amino binding sites[53] . Measuring the hydrophility of the polymer samples is an indirect method for estimating crystallinity. Less water is absorbed because water sorption takes place in the hydrophilic polymers' non-crystalline (amorphous) domains. A sample that is more crystalline will absorb more moisture, and vice versa. Studies on the sorption of water vapor by chitosan samples revealed that the samples' ability to sorb increased with their deacetylation degree (DD) [54]. The effect of the samples' crystallinity on their capacity for sorption was used to explain this result.

1.5.2. Disadvantages of Chitosan as adsorbent

The attributes of an adsorption performance include a high affinity for the target contaminant species, a large capacity for adsorption, selectivity, the speed of adsorption, and the potential for the adsorbent to be regenerated. The interaction between the adsorbent and the adsorbate, for example, is one physical and chemical component that affects all of these properties[55]. The adsorbent's surface area, particle size, surface-accessible active sites, pH of the solution, temperature, and contact time are just a few examples of the physical and chemical parameters that affect all of these features. When employed in its natural state, chitosan still has significant drawbacks, such as a low specific surface area, non-selectivity, crystallinity, a low adsorption capacity, instability in acidic environments, and a lack of sites that are ideal for ionized organic dye adsorption. Chitosan is not widely utilized in adsorption-based applications due to the aforementioned disadvantages[56].

1.5.3. Modification of Chitosan for adsorption

Physical or chemical alterations are frequently required to increase the adsorption capacity of chitosan for different adsorbates. Adsorption mechanisms must be recognized, and appropriate modification techniques must be created, in order to modify and improve chitosan's adsorption ability[57, 58]. Crosslinking and graft co-polymerization, the creation of composites, and the inclusion of substituents are popular methods for chemically altering chitosan. a few others These techniques have been used to transform chitosan into other materials[59]. to enhance its functionality for different applications, depending on chitosan's porosity A chitosan-based substance is lyophilized to maintain and improve it, and then squeeze and then react with aqueous ammonia [60, 61].

1.5.3.1. Physical modification

Commercial chitosan is available in flake or powder form, however, due to its varying degree of deacetylation, limited specific surface area, weak mass transfer resistance, and narrow pore structure, it is not suitable for use in practical applications. The physical state of chitosan has a significant impact on the degree to which it absorbs substances and the speed of this absorption[62]. To increase access to interior adsorption sites and reduce crystallinity, chitosan is physically altered by being transformed from a powder into its smaller, more porous, and higher specific surface area forms [62, 63]. The quantity of -NH_2 groups per unit area increases as a result of Chitin deacetylation, because there are more functional groups available for interaction with the solvent or adsorbate. Consider the various chitosan adsorbents available, including fibers, sponges, gels, films, nanoparticles, beads, and microspheres, all of which have been demonstrated to have a lower degree of crystallinity[67]. These chitosan materials have a variety of different morphologies, instead of the usual powder-based systems, this has facilitated a broader range of uses.

1.5.3.2. Chemical modification

The chitosan molecule has been chemically modified by means of cross-linking [68, 70] and grafting[71]. The chitosan backbone holds several active chemical groups such as -OH and -NH_2, which make possible various chemical reactions, among them amide formation. Esterification, etherification[72], and Schiff base reactions [73] are among the transformations that result due to these chemical activities[74-75]. Chitosan enhancement can be achieved through its chemical modification, yielding a derivative with superior adsorption capacity and greater chemical stability. When cross-linked, chitosan becomes less soluble in acidic

settings. Glutaraldehyde and Epichlorohydrin are two frequently utilized cross-linking agents. Varying the composition of the cross-links changes the textural and surface properties of chitosan, hence adjusting its adsorptive characteristics. Creating a three-dimensional network, cross-linkers serve as molecular connectors between polymers and enhances the chemical stability of the system when exposed to acidic environments. By introducing additional functional groups, cross-linkers can alter the adsorbent structure, affecting its solubility and hydrophile-lipophile profile. Moreover, the extent of cross-linking can control the amount of water that the adsorbent can soak up. Chitosan adsorbent materials can be tailored with adjustable textural attributes and adsorption capabilities by selectively choosing the type and quantity of the cross-linker used [78, 79].

Grafting is distinct from cross-linking, which involves covalently bonding tiny molecules like monomers or pre-polymers to the polymer backbone. By attaching long, flexible polymers to the polymer backbone, some of the drawbacks of chitosan can be overcome, including low potential for hydrogen bond formation with an adsorbate because of strong competitive intermolecular interactions between CHI chains, limited electrostatic interactions, low hydrodynamic volume, and low adsorption capacity [80, 81]. The technique of graft copolymerization, which increases the number of surface functional groups on a polymer adsorbent, is a crucial step in this process. For this method, the monomers must have polymerization capabilities and contain reactive functional groups suitable for enhanced adsorption. Numerous monomers, including those with vinyl groups such as acrylamide[71], acrylic acid[82], and itaconic acid[83], have been used for grafting. Subsequently, these materials demonstrate better adsorption performance and properties than unmodified polymers.

1.6. Semiconductors

Semiconductors are solid materials that are either crystalline or amorphous, they are thought to have a property between a metal and an insulator.[84] The typical band gap (BG) values listed in table (1-1) can be used to categorize solid materials.[85-87]

Table 1.1. Classification of solid materials according to energy gap magnitudes at room temperature.

Type of solid	**Metal**	**Semimetal**	**Semiconductor**	**Insulator**
Eg values (eV)	**No Eg**	Eg ≈ 0	0 < Eg < 4 or 5	Eg ≥ 4 or 5

According to the band theory, the conductivity and valence bands of every solid are HOMO and LUMO, respectively, both of which have lower energies. For semiconductors and insulators, the energy gap between the valence band and conduction band can be between 0.7 and 6-7 eV, this varies depending on the type of solid, but it is the same in metals[87, 88].

When extra electronic levels (donor or acceptor) are introduced into the forbidden semiconductor gap as a result of specific impurities or defects in the crystal lattice, p- and n-type semiconductors are created, the resulting requirements are listed in tables (1-2)[89].

Table 1.2.The generated requirements of p-type and n-type of semiconductor.

p-type	*n-type*
An electronic hole, known as an electron-defect one, is left behind when the valence band electrons are extracted from the empty acceptor level, which is located close to the band.	The donor level, which is referred to as an electron-excess semiconductor one, is located near to the conductivity band.
P-type semiconductors can be created when Fermi level is close to VB.	When the Fermi level is close to CB, an n-type semiconductor is produced.
Such as Cr_2O_3.	Such as MnO_2,Nb_2O_5.

1.6.1. Metal oxide semiconductor nanostructures

The practical and theoretical significance of metal oxide semiconductor nanostructures in biological, environmental science, and analytical chemistry applications makes them appealing and significant for nanosensor research[90].

One dimension metal oxide NSs' semiconducting, piezoelectric, and pyroelectric characteristics are crucial optoelectronics is the most well-liked research field for these nanostructures, sensor and actuators [90]. High surface area to volume ratio, low toxicity, environmental friendliness, chemical stability, and biocompatibility are all characteristics of metal oxide NSs. Therefore, when utilized as a biomimetic membrane that can detect, for instance, proteins and maintain their activity, metal oxide NSs also exhibit the quick electron transfer capabilities needed to enhance nanomaterial performance.[91-93].

These metal oxides such us MnO_2,Nb_2O_5 and Cr_2O_3 can be used to create nanodevices for optoelectronic and sensing applications because they have unique

and appealing morphologies such as nanowires, nanorods (NRs), nanotubes, nanoleaves, and nanoflowers, among others.

Niobium, which is part of the group V metals, bonds with oxygen to form Nb_2O_5 when it's in the +5 oxidation state. Other oxides are compared to niobium pentoxide (Nb_2O_5), which is a semiconductor with a moderate bandgap of 3.4 eV. The Nb_2O_5 has been of interest to science because of its exceptional physical and chemical properties and isotropic structure. It's ideal for many different photoelectrodes, electrochromic displays, gas sensors, microelectronics, and displays for field emission[94-96].

Environmental remediation through photocatalysis with Nb_2O_5 nanoparticles has been previously investigated. Nb_2O_5 presents promising prospects in this field due to its surface acidity, stability in water, redox properties, and photocatalytic traits, all of which are intrinsically linked to its structure [97, 98]. With regards to Nb_2O_5, literature has explored several primary phases: pseudohexagonal TT-Nb_2O_5 at low temperatures, orthorhombic T-Nb_2O_5 when the amorphous oxide reaches temperatures of 600 and 800°C, and monoclinic H-Nb_2O_5 when heated to approximately 1100°C[99]. These phases' crystallization circumstances, however, are subject to a number of variables: starting materials, synthesis methods, and heat treatment conditions. Of note, the T-Nb_2O_5 structure consists of an octahedron constructed from NbO_6 with unique net parameters of a = 6.17, b = 29.32, and c = 3.94. At the corners, 4 linked blocks come together to form its crystalline structure[100].

manganese dioxide (MnO_2) can exist in a variety of structural forms, such as types, sizes, shapes, and so on, depending on how the basic structural unit (MnO_6) octahedron, is connected. In light of the numerous[101].

Three different types of MnO_2 structures have been identified: chains, layered or sheet structures, and three-dimensional structures. The Co-precipitation method is commonly employed due to its low cost and wealth of advantages. Nanostructure manganese dioxide has been recognized as the ideal electrode material for energy storage devices like super capacitors, also known as electrochemical capacitors[102, 103].

MnO_2 is recognized as one of the most significant catalysts due to its accessibility, low toxicity, and environmental friendly. One of the many different types of transition metal oxides is manganese oxide (MnO_2). Due to its unique characteristics, MnO_2 is one of the most attractive oxides. MnO_2 is a semiconductor with a low band gap and high optical constant that exhibits ferroelectric and catalytic properties[104, 105]. The type of MnO_2 nanoparticles produced by the hydrothermal method and the co-precipitation approach are not the same. By analyzing powder XRD and SEM techniques, it is possible to determine if a MnO_2 nanoparticle is actually MnO_2 or not.

Chromium trioxide Due to its wide band gap (3 eV), Cr_2O_3 is one of the successful semiconductors and much investigated compounds [106]. At lower temperatures, Cr_2O_3 has the characteristics of a p-type semiconductor .This class of p-type metal oxide semiconductors may make good candidates for a variety of uses in optical storage systems and gas sensors .[107]These Cr_2O_3 uses depend on their structure, phase, form, size, and synthesis methods in addition to the presence of suitable dopants, including zinc oxide . [108] For instance, the combination of nanomaterials with a high surface area to volume (smaller particle size) and strong chemical activity has been a significant topic of current research.

1.7. Adsorption

The process of ions, molecules or atoms from a gas or liquid phase interaction to a solid's surface is called adsorption. Adsorbent response is caused by the large surface area of semiconductor metal oxides. Adsorbate is the term for a substance that binds to a solid surface. Rapid responses and high sensitivity are achieved with nanostructured films that are thin[109]. Physisorption and chemisorption are the two subcategories of the adsorption process. Physisorption is brought on by weak Van der Waals forces between the adsorbent and adsorbate, which may be caused by London dispersion effects, persistent dipole moments in adsorbed molecules, or polarization in molecules[110].

The distinctive qualities of the interacting species are kept, and there are no chemical modifications during physisorption. The creation of chemical bonds or chemical interactions between the adsorbent surface and the adsorbate is what causes chemisorption[111]. The many adsorption mechanisms include electrostatic interactions, hydrogen bonds, hydrophobic interactions On adsorbents with polar functional groups, hydrogen bonding is one potential mechanism for the adsorption of polar organic molecules .The electrostatic interaction can be the main controlling mechanism for the adsorption of ionic or ionisable adsorbates on activated carbon.

Interactions between unbalanced charge distributions between the aromatic rings of carbon materials and electron-rich or electron-deficient systems can result in the adsorption of aromatic organic compounds.[112, 113] Aside from its physical properties (specific surface area and pore size distribution), activated carbon also has chemical properties, including the presence of inorganic elements and the characteristics of its surface, such as the quantity and type of oxygen-

containing functional groups, the acidity and basicity of the surface, the surface groups, and the eight surface charges of the carbon material. expressiveness in Figure (1.7) Adsorption terminology basics.

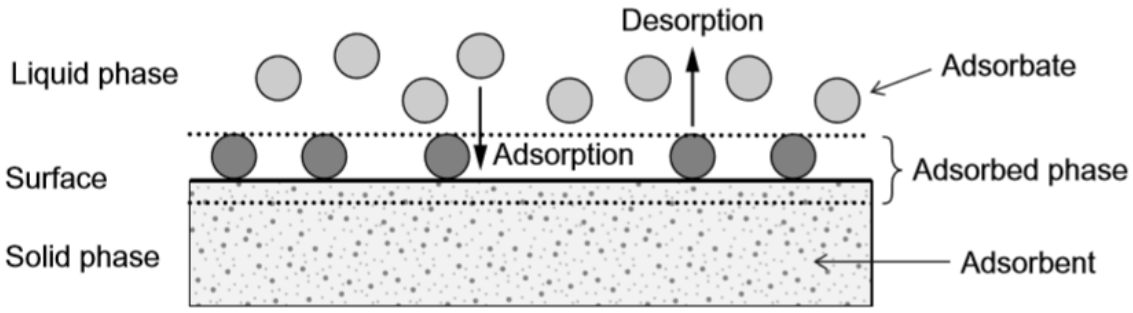

***Figure 1.7. Fundamental terms of adsorption process*[114]**

1.7.1. Adsorption from Solution

The adsorption process between the adsorbent and the solution is of great importance, but its understanding is still limited. Despite the availability of many research papers published on it, most of the studies that dealt with this topic are interested in The surface of non-polar carbon, which has been studied by many researchers Factors affecting physical adsorption[115]. In a solution, adsorption is different from Any change in the concentration of the solution has an impact on the process of adsorption because adsorption in solids occurs when the adsorbent material contains at least two substances, a solvent or a solute (these are competing for the location of effective adsorbent surfaces, which results in interference of the adsorbed type of adsorbent or adsorbent solvents). It is important to keep in mind that the phase before adsorption, known as desorption, involves removing the adsorbed particles from the adsorbent surfaces and then returning them. Adsorption often takes place at a temperature high enough to cause chemical reactions. The forces holding the adsorbent to the adsorbent surface together[116].

1.7.2 Factors Influencing the Adsorption Process

1.7.2.1 Effect of equilibrium time

It is the period of time when the adsorbent and adsorbent have reached equilibrium. To put it another way, the period of time, which could be for hours, days, or even weeks, during which there is no drop in the concentration of the solution.

1.7.2.2 Nature of adsorbate

The physical characteristics of the adsorbate material have an impact on the adsorption process since adsorption rises with mass. The chemical composition of the adsorbate material has an impact on the adsorption process as well because aggregates ,Effectiveness, polarity, and solubility in solvents of the adsorbent composition and absence thereof the capacity for adsorption increases with decreasing adsorbent solubility in the solution. All these elements it plays a significant part in figuring out how much the adsorbent's surface is interfered with and how well it adsorbs, and because of these differences in characteristics, one of the components will adsorb to the other rather than the other, which is known as selective adsorption, especially in multi-component systems[117].

1.7.2.3 Effect of pH

The activity of the hydrogen ion in the process of adsorption is mostly a result of the solution's acidity changing because the adsorbent, adsorbent surfactant, and solvent are all affected by the pH function. This result is brought about via competition. They consequently have a positive or negative impact on the (-OH) and (+H) ions' adsorbent, adsorbent surfactants, and solvent. Adsorbent surface changes from one substance to another depending on the solution isotherms of

adsorption, the amount or capacity of the adsorbent material, and other factors [118].

1.7.2.4 Effect of ionic strength

Ionic strength has an impact on the adsorption process. due to the addition of adsorbent particles making the electrolytes more soluble in the solvent, adsorption may either decrease or increase when the electrolyte's ionic strength rises. The amount of adsorption will rise as a result. Due to their competition with the adsorbent on the adsorbent surface, strong electrolytes may also have an impact on the adsorption process[119].

1.7.2.5 Types of Adsorption and the Influence of Temperature

Adsorption stubbornness results from temperature effects on the material and the adsorption rate as the rate of adsorption increases. Adsorption, despite being a process, grows with rising temperature and shrinks with decreasing temperature. Don't be afraid Adsorption will increase and decrease in an exothermic process at low temperatures[120].

1.7.2.6 Nature of adsorbent

Adsorption effectiveness is largely influenced by the chemical composition, among other physical and chemical factors. In regards to the amount of polar aggregates or non-polar aggregates present on the adsorbent surface, The polarity, the presence of basic or acidic groups, the distribution and size of the pores on the surface, together with surface area, are other elements that obviously influence the adsorption process. The decline is higher the more surface area there is. Due to the size of the adsorbent's particles, the more active sites there are on the surface, the higher the adsorption capacity[121].

1.7.2.7 Adsorbent surface area

The surface area of the adsorbent surface can be increased to boost adsorption, which increases the adsorption capacity because It is crucial to adsorption because it increases the amount of active sites on the adsorbent surface.

1.7.2.8 Concentration of Adsorbate

As the concentration increases, the amount of adsorbent also increases, and this causes the adsorption rate to rise, increasing the adsorption capacity. The rate of mass transfer and diffusion on the adsorbent surface.

1.8 Adsorption Isotherms

It is also known as The relationship between the amount of adsorbate material on a surface and the pressure in the case of a gas (and the concentration of the equilibrium in the case of a solution) for the adsorbent material at constant temperatures (the adsorption isotherm), and it describes an adsorption process in equilibrium between the solution and the solid phase of the adsorbent surface. Adsorption isotherms come in a variety of shapes and sizes. Their abundance is helpful in learning about the orientation of adsorbate molecules on the adsorbent surface, identifying the kind of adsorption, determining the thickness of the adsorption retention layer, and studying the thermodynamics of the adsorption process.

1.8.1 Isotherm Langmuir model

The Langmuir equation assumes that no adsorbate migrates to the surface of the adsorbent, that maximal adsorption corresponds to a monolayer of adsorbate molecules that is saturated, and that the adsorption energy is constant[122].The intermolecular interactions become weaker the more distant you are from the

adsorption surface because every adsorption site has an energy that is equivalent[123]. The following equation represents the Langmuir model(1.1):

$$\frac{\mathbf{Ce}}{\mathbf{qe}} = \frac{\mathbf{Ce}}{\mathbf{qm}} + \frac{\mathbf{t}}{\mathbf{qmKL}} \ldots\ldots\ldots\mathbf{(1.1)}$$

The variables qm and KL are derived from the slope of the line and its intersection with the abscissa Ce and ordinate Ce/qe, respectively.

1.8.2 Freundlich isothermal model

The Freundlich model takes into account both the complexity of the adsorbent's surface and the exponential distribution of the energy of the active sites. The Freundlich model is expressed in equation (1.2).:

$$\mathbf{log\ qe} = \mathbf{log\ KF} + \frac{\mathbf{1}}{\mathbf{n}}\ \mathbf{log}\ \boldsymbol{ce} \ \ldots\ldots\ldots\ldots(\mathbf{1.2})$$

KF denotes the Freundlich constant,qe adsorption capacity (mg/g), and heterogeneity factor (n), which denotes the number of layers, according to Eq. (1.2). The Freundlich linear equation was found by plotting log qe versus log Ce. Then, using the intercept and gradient, KF and n were mathematically determined[124].

1.8.3 Temkin isotherm model

The interactions that take place between the species and the adsorbate during adsorption are especially taken into account by a part of the Temkin isotherm model [125]. Equation (1.3) gives a description of the Temkin model:

$$\mathbf{qe} = \mathbf{A} + \mathbf{B\ log\ Ce} \ldots\ldots\ldots(\mathbf{1.3})$$

The letters A and B in this context represent the constant for the Temkin isotherm (L/g) and the heat of sorption constant (J/mol), respectively. Plots of qe against Ce were employed to derive the Temkin linear equation.

1.9.Adsorption of Dyes

Pollution caused by dyes has become a hazardous problem for both water environments and the well-being of people, due to its toxicity and possible to cause cancer [126]. While dyes are a essential in everyday living, particularly in the textile, cosmetics, printing, and pharmaceutical sectors, their close association with these industries has resulted in serious concerns regarding water pollution [127]. Therefore, a vast amount of funding has been invested specifically towards the effective removal of dye from water solutions. As compared to other methods, such as ion exchange and membrane filtration, adsorption has been recognized as a successful option for eliminating dye from water solutions, given it is a relatively straightforward, affordable, and impressive approach. The problem of post-adsorption adsorbent collection is a more recent issue of concern. The importance of having adsorbents that are cost-effective and efficient at removing dyes from wastewater and allowing for quick regeneration cannot be overstated. Various materials, including active carbon, alumina, zeolite, and polymer, have been identified as effective adsorbents to handle organic dye pollutants. Refer to Figure (1.8) for a description of the process of dye adsorption.

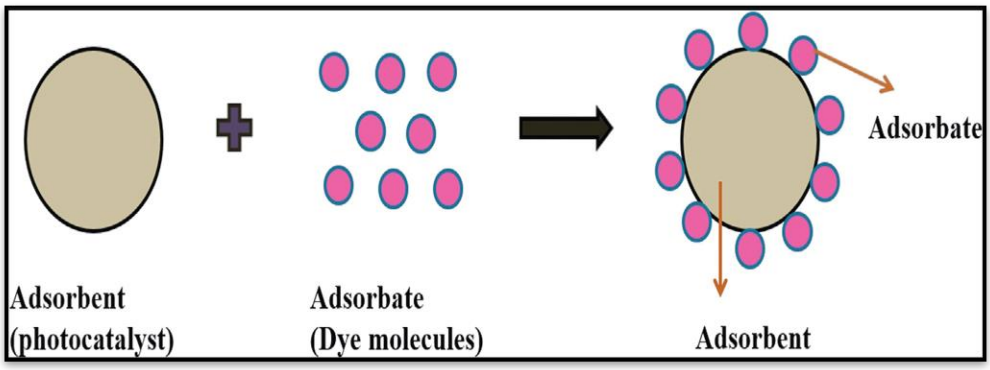

Figure 1.8.The dye adsorption process using adsorbent **[131]**

1.10. Dyes

Dyes are the most widely employed materials as color yields in industrial especially, they are applied in the textile, cosmetics and foodstuffs. Dyes are very important due to their applications in all aspects of human life. However, the production volume of dyes around the worldwide are increase. Over the last few decades, more attention about discharged of about (10–15%) of the dyes into the environment. So, there is a major environment problem came from colored wastewater and frequently cause eco-toxic hazardous . In addition, decrease of efficiency of water caused by dyes. Examples of such dyes are methyl orange (MO). With this in mind treatment of dyes or dyestuff before discharge to the environment catch more attentions.

Two types of treatment techniques could be used recently: chemical and physical treatment, examples of such techniques are liquid chromatography, precipitation, ion exchange and electrochemical [132]. but the problems with these techniques are expensive or some of them not effective, subsequently, researchers try to find other way not expensive, more active, easy to use and be able to recycle to use many time to remove dye from waste water. Among these way more focused

on the adsorption process, researcher have been investigated several selective adsorbent material in this area such as zeolites[133], chitosan[134] and clay.

The majority of dyes are organic chemicals, and they are divided into different classes based on the application technique and chemical character. Hence, it is discovered that there are more than 100,000 commercially available dyes. The colorful pigments could take the form of an insoluble fine powder. in thick liquids or water. The presence of active groups called chromophores, a radical structure made up of double conjugate bonds, is what gives pigments their color[135]. In addition to the division listed in Table (1.3), dyes can also be divided into groups based on how they are applied during the dyeing procedure. Originally used to color cellulose fibers, reactive dyes are a type of highly colored organic dye that is employed in the textile coloring business. It is still frequently used in the textile industry due to its remarkable coloring and stability capabilities.

Table 1.3. Classification of pigments.

Dye class	Description
Acid	Water-soluble anionic compound
Basic	Water-soluble, applied in weakly acidic dye baths; very bright dyes
Direct	Water-soluble, anionic compounds; can be applied directly tocellulosics without mordants (or metals like chromium and copper)
Dispers e	Not water-soluble
Sulfur	Organic compounds containing sulfur or sodium sulfide
Vat	Water-insoluble; oldest dyes; more chemically complex

1.10.1 Azo dyes

Many artificial azoic aromatic dyes (monoazoic, diazoic, triazoic, or polyazoic) have one, two, three, or more (N = N) groups attached to the benzene and naphthalene rings. Several functional groups, including methyl, nitro, triazine amine, chloro, hydroxyl, and sulphonate, typically replace these rings[136, 137]. Azo dyes are extensively employed in the cosmetics, pharmaceutical, paper printing, food, beverages, textiles, and clothing industries. Azo dyes are widespread in the textile industry due to their abundance (around 80%), excellent stability, low cost, and a variety of hues[138]. Methyl orange (MO), a mono-azo dye, is commonly employed as an indicator for titrating strong acids and bases as well as for assessing the alkalinity of water. The food, textile, printing, pharmaceutical, and other industries all make extensive use of it[139].

MO's ionic composition renders it nonvolatile and less disposed to aerobic biodegradation in soil and water. It could also stick to surfaces in water that are made of clay, minerals, and debris[140]. The two different tautomeric forms of acid-base indicators, benzenoid and quinonoid, have different structures and colors. The red quinonoid form of MO is more common at pH levels higher than 3.1. At pH levels higher than 4.4, the yellow benzenoid form becomes more abundant[141, 142]. The structure of MO in an acidic and basic medium is shown in Figures 1.9. When OH ions are introduced, a hydrogen ion will be lost from the N-N bond between the benzene rings.

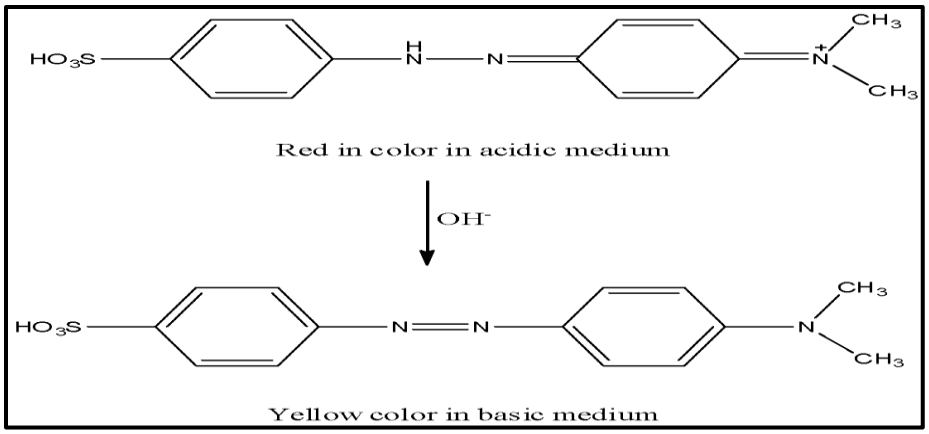

Figure 1.9. MO in acidic and base medium.

1.10.2.Sulfur Dyes

It is one of the smaller dye groups when compared to other dye groups. An alkaline reducing solution containing a reducing agent, specifically sodium sulfide, is used to apply these colours to cotton. These dyes are essential from an economic standpoint due to their excellent wash fastness properties and reasonable pricing. Bromocresol green (BCG) is a synthetic dye that belongs to the triphenylmethane family. It frequently escapes from factories as watery effluents, where it seriously harms the environment. It is widely used in many other applications, not just in the textile sector[143, 144]. The chemical compound 2,6-dibromo-4-[7-(3,5-dibromo-4-hydroxy-2-methyl-phenythiabicyclo[4.3.0]nonane) is known as bromocresol green (BCG). A triphenylmethane dye called -9,9-dioxo-8-oxa-9 -3-methyl-phenol) is employed in DNA gel electrophoresis as a tracking dye and a pH indicator. Because of its high salt concentration, the sodium salt of BCG is highly ionizable in water, which results in it having two different forms in aqueous solutions: lactoid and quinoid. This is dependent on the pH of the solution. The lactoid (neutral) form is more prevalent in acidic solutions, while the quinoid (anionic) form is more prevalent in alkaline conditions[145]. The Bromocresol Green (BCG) structure is shown in figure (1.10).

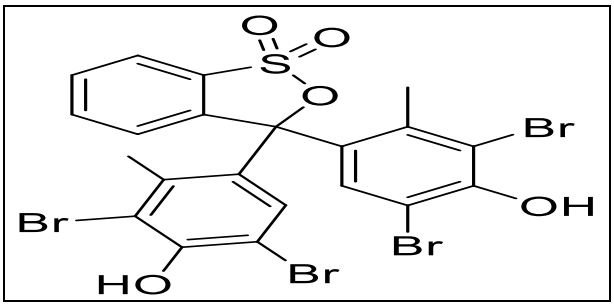

Figure 1.10. Structure of BCG dye.

1.10.3.Direct Dyes

Anionic dyes that are soluble in water and have a strong affinity for cellulosic fibers are called direct dyes. Aqueous solutions containing electrolytes are used to dye these functional dyes. Primary applications of direct dyes are for paper, cotton, and regenerated cellulose; nylon is a less common option. The treatment procedures of these dyes offer them the ability to acquire wash fastness features. As direct dyes have a natural affinity for cotton, the need for mordents during cotton dyeing has been replaced. It's important to note that Direct Yellow (DY50) is a specific type of direct dye. The solution appears yellow. Frequently utilized in the paper and leather industries, as well as for cotton coloring, DY50 is a diazo dye that shows resistance against both acidic and alkaline solutions. Its molecular structure is depicted in Figure 1.11, with a chemical formula of $C_{35}H_{24}N_6Na_4O_{13}S_4$. The dye's λmax measures at 403 nm[146]

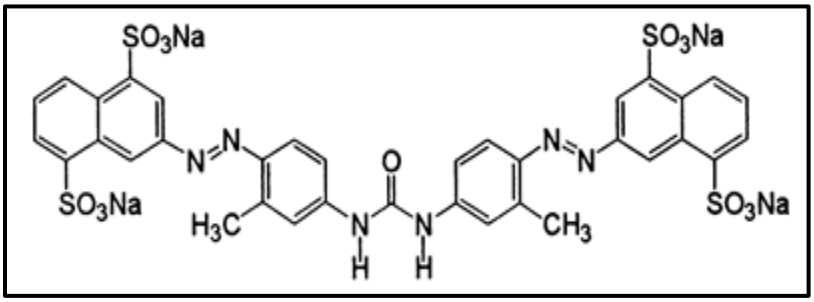

Figure 1.11. Structure of Direct yellow 50 dye.

1.11.Literature Review

In 2011, Reza Ansari and Zahra Mosayebzadeh used methyl orange (MO), a common azo dye, to examine from aqueous solutions using polyaniline that has been coated on wood sawdust (PANI/SD) [147].Investigations were also conducted on how certain significant factors, including pH, beginning concentration, sorbent dosage, and contact time, affected the uptake of MO solution. It was discovered that PANI/SD may be utilized to effectively remove azo dyes from aqueous solutions, including MO. The adsorption models of Langmuir and Freundlich were used to assess experimental results. The chosen adsorbents' kinetic characteristics for the adsorption of MO dyes are also presented. Chemical regeneration of the utilized adsorbents was also explored in order to examine the feasibility of desorption for frequent application. Desorption or dye recovery and it was discovered that regeneration of the adsorbent (PANI/SD) was quite doable and of good performance. The use of modified sawdust with polyaniline for the removal of azo dye in textile wastewater treatment is very promising.

In 2014, Vito Rizzi and co-workers [148].they conducted a study with a primary focus on the potential applications of Chitin films under various situations,

including lowering the intrinsic pH, enhancing hydrophobicity through ethanol treatment, and neutralizing CH films to increase their absorption capacity. 86 Direct Yellow Long-term dehydrated one and neutralized acid CH film end up being the best films for removing dye from water. Also, the decrease of the contact time improves the outcomes by reducing the acidity of the CH solution throughout the film formation. For each film under consideration, the effect of the initial dye concentration has been investigated, and the quantity of dye adsorption as a function of time t, qt (mg/cm^2), has been assessed.

In 2016, Jadhav Smita and co-workers[149]. Studied The chemical oxidative polymerization of aniline with doping of an organic acid (oxalic acid) is used to create a polyaniline nano-adsorbent, which is then used to adsorb methyl orange color from wastewater. Maximum decolorization occurred at pH 3 after 5 hours of contact time, according to the study's findings. With 0.03 g of the adsorbent, a clearance rate of almost 92% of methyl orange was accomplished at 50°C.

In 2017, Marjan Tanzif and co-workers created a polyaniline nano-adsorbent and used it to absorb the methyl orange dye from the aqueous solution[150]. The study's findings showed that as the initial dye concentration was raised, the nanoadsorbent's dye adsorption capacity increased from 3.34 to 32.04 mg/g and from 3.28 to 30.28 mg/g andthe maximum adsorption capacity was estimated to be 75.9 mg/g . At 65 °C and 25 °C, the concentrations range from 10 to 100 mg/L. Also, for the dye methyl orange, dye adsorption equilibrium was reached in 60 minutes.

In 2018, Pinki Chakraborty and co-workers used hydrogen peroxide (H_2O_2) as an oxidant, iron chloride ($FeCl_{22}H_2O$), and vanadyl sulphate ($VOSO_4H_2O$) as co-catalysts, respectively, polyaniline was produced by a chemical oxidative

polymerization process at room temperature [151]. The produced polymers were examined using high resolution powder X-ray diffraction, Fourier transform infrared spectroscopy, Raman, UV-Visible, photoluminescence spectroscopy, thermogravimetric analysis Field Emission Scanning Electron Microscopy (FE-SEM), and Transmission Electron Microscopy (TEM) techniques. Results of the study at room temperature, the ordered polyaniline absorbed about 93% of the Methyl Orange dye in under 30 minutes.

In 2018, Neha V. Nerkar and Subhash B. Kondawar In this study describe the chemical interaction of the dye molecule with the polyaniline/zinc oxide (PANI/ZnO) nanocomposite for the safe removal of methyl orange (MO) dye from aqueous solution[152]. In situ polymerization has been used to create the PANI/ZnO nanocomposite. Due to its higher porosity than pure PANI, PANI/ZnO nanocomposite was found to be the most promising choice for dye adsorption. PANI/ZnO nanocomposite was combined with a MO dye solution and employed for the adsorption process in the current experiment. UV-Vis spectroscopy was used to study color removal, and the spectra were recorded for a set amount of time in order to validate the kinetic model. More MO elimination is achieved by PANI-ZnO nanocomposite than by pure PANI and ZnO nanoparticles. A finding of dye removal of 87.5% was made.

In 2019, K. Haitham and co-workers examined the adsorption of methyl orange (MO) dye from aqueous solutions, immobilized polyaniline on glass plates (PANI/glass) and its powder form [153]. Extensive analysis had been done on the effects of operational variables such pH, sorbent dosage, beginning concentration, contact time, aeration rate, and the thermodynamics of MO uptake. PANI/glass and PANI powder had maximum adsorption capacities (qmax) of 93 and 147 mg/g, respectively. This study demonstrated that PANI that had been immobilized had

the special benefit of convenient usage and reuse over a long period of applications.

In 2019, J. Vidya and co-workers they in-situ oxidative polymerization of Polyaniline- $BiVO_4$ nanocomposites employing aniline monomer in the presence of hydrochloric acid and bismuth vanadate nanosheets[154]. By using field emission scanning electron microscopy, X-ray diffraction spectroscopy (XRD), and other techniques, the adsorbents' physiochemical characteristics were examined. By observing the adsorption of the methyl orange dye over a period of two hours, the adsorption behavior of PANI and PANI - $BiVO_4$ Nanocomposites was assessed. The adsorption effectiveness of the PANI - $BiVO_4$ Nanocomposites is 99%, which is higher than that of pure PANI (70%). The monolayer sorption of MO on PANi-$BiVO_4$ and the homogeneity of the adsorption sites are depicted by the Langmuir isotherm model. After five cycles, analysis of the nanocomposite's reusability revealed 78% of adsorption.

In 2019, Mohammadi, R and co-workers [155].This research involved the preparation and characterization of titanium dioxide (TiO_2), TiO_2/graphene (TiO_2/GO), and polyaniline-TiO_2/graphene (polyaniline-TiO_2/GO) catalysts using a variety of analysis techniques, including X-ray diffractometer, transmission electron microscope, scanning electron microscope, energy-dispersive X-ray spectroscopy, Brunauer-Emmett-Teller, and diffuse reflectance spec The elimination of methyl orange, an anionic dye, from aqueous solutions was used to test the produced materials' photocatalytic activity and adsorption potential. The polyaniline-TiO_2/GO Nanocomposites demonstrated high photocatalytic activity, which is partially attributable to polyaniline's sensitizing effects and the low recombination rate resulting from the electron-scavenging ability of graphene

oxide. The Polyaniline-TiO_2/GO Nanocomposites had a maximum adsorption capacity of around 69.23 mg g^{-1} for methyl orange.

In 2019, E Salmalian and co-workers [156].In this work, bromocresol green dye was removed using chitin nanofibers, a valuable natural resource. For color removal, the impacts of effective factors including pH (2–7), adsorbent dosage (0.25–2.5 gram), starting concentration (0.2-2 $mg.L^{-1}$), temperature (20–45 °C), and contact time (5–30 min) were examined. The outcomes demonstrated that pH affects color adsorption, and pH=6 was chosen as the ideal value. This concentration was chosen as the best example since it removed 92.75% of the color at a concentration of 0.4 $mg.L^{-1}$. The ideal dose of bromocresol green was determined to be 1.5 g while accounting for the absorbent's cost. The ideal contact period for these two was thought to be 10 minutes at 25°C. parameters, which shows how brief this treatment's duration was. The findings demonstrated that bromocresol green removal and reduction from aqueous solutions—and therefore wastewaters containing various colors—can be significantly influenced by chitin nanofibers. High pressures and temperatures are not necessary for this process to be repeated in the textile industry's diluted wastewater treatments.

In 2019, Dan Liu and co-workers were reported use chitosan poly(methacrylate) composites for the adsorption of bromocresol green from aqueous solutions [157].Scanning electron microscopy, Fourier transform infrared spectroscopy, and thermogravimetric analysis were used to characterize the produced composites. The impacts of experimental factors, such as sample pH and adsorption period, were also evaluated. The bromocresol green removal by the proposed adsorbent was also investigated. The Freundlich model adequately represented the adsorption isotherm, and 40 minutes of shaking at pH 2.0 resulted in a maximum adsorption capacity of 39.84 g mg^{-1}. Green bromocresol adsorption

After three repetitions of the recycling test, the bromocresol green with chitosan poly(methacrylate) composites' adsorption percentage maintained over 97%.

In 2020, Monika Duhan and Raminder KaurIn was studied the methyl orange (MO) was adsorbed out of its aqueous solution using nanofibers made of polyaniline (PANI) [158]. The traditional interfacial polymerization approach was used to create PANI nanofibers in an acidic solution with ammonium persulfate as the oxidant. PANI nanofibers are discovered to be ideal for the adsorption of anionic dyes like MO because of their positively charged backbone. The impact of key adsorption factors, including starting dye concentration, pH, and contact time, was also investigated. The equilibrium values of these factors were found to be 7 mg L^{-1}, pH 7, and 80 min, respectively. The pseudo-second order model was found to best fit the experimental data (R^2 = 0.99). An analysis of the Freundlich isotherm revealed.

In 2020, Cuijuan Xing and co-workers they used Ammonium persulfate was used as an oxidant in the effective synthesis of polyaniline (PANI) nanofibers[159]. Investigated was the methyl orange (MO) adsorption behavior on PANI at various parameters. the maximal adsorption capacity (Qe) at 313 K was determined using the Langmuir adsorption model. The MO adsorption on PANI followed the pseudo-second-order kinetic model, according to a kinetic analysis. PANI nanofibers may be used as inexpensive and effective adsorbent materials to remove organic contaminants from water, according to experimental data.

In 2020, Chao Lv and co-workers [160].they used an in-situ polymerization method in a hydrothermal reactor using Fe_3O_4 as an intercalant and GO (graphene oxide) as a template for PANI to create a lamellar PANI-GO-Fe_3O_4 hybrid nanosheet adsorbent. The PANI-GO-Fe_3O_4 hybrid adsorbent has a high adsorption

capacity of 181.0 mg/g for methyl orange (MO) dyes in addition to the benefits of simple magnetic separation ability. At 298 K, 313 K, and 333 K, the adsorption isotherms were well fitted by the Langmuir model. The removal rates of MO dyes by PANI-GO-Fe_3O_4 can still reach 76.3% even after 5 cycles of adsorption and desorption. This work offers a fresh approach to the promotion of separate high-performance adsorbents for the contamination of waste water with ionic dyes.

In 2020, Bharatraj Singh Rathore and co-workers Using the batch adsorption approach, chitosan-polyaniline-copper(II) oxide (CH-PANI-CuO) Nanocomposites has been created[161]. It was examined using UV-Vis, transmission electron microscopy (TEM), scanning electron microscopy (SEM), X-ray diffraction, and Fourier transform infrared (FTIR) (TEM). The nanocomposite's surface was rough and porous with pleats, as revealed by the SEM and TEM, which is likely to have improved dye adsorption. For methyl orange dye, the maximum percentage of dye degradation was reported to be 94.6%. The findings of the FTIR analysis and the desorption investigation verified the presence of the hydroxyl and amino functional groups. The outcomes unmistakably show that methyl orange may be removed from aqueous solution using the polymer matrix as an adsorbent.

In 2020, Eman Alabbad[146] According to the findings, the solution pH, sorbent dosage, initial DY50 concentration, contact time, and temperature all had an impact on the removal of DY50 by the modified chitosan. The Langmuir, Freundlich, and Temkin isotherms were fitted to the experimental data, and the Langmuir isotherm provided the best fit. By, the elimination percentage was 97.9%.0.05 g of sorbent dosage and 100 ppm of the Direct Yellow 50 dye starting concentration, and chemisorption components after three hours.

In 2021, Sudhindra Pete and co-workers Used a PANI-MWCNT composite was used to swiftly and efficiently remove methyl orange (MO), an azo dye that is carcinogenic and significantly pollutes water[162]. We examined the composite made by in-situ oxidative polymerization using FT-IR, XRD, and TEM techniques. At 30 °C, the MO adsorption process' pseudo-second-order kinetics (R^2 0.99), with a rate constant of 5.265 10^{-4} g mg^{-1} min^{-1}. The maximum adsorption capacity (qm) of the equilibrium data is found to be 149.25 mg/g, and the data's best fit to the Langmuir isotherm model is discovered. Because both the Freundlich constant (1/n) and the Langmuir constant (RL) were less than 1, the adsorption method is beneficial. Additionally, the used adsorbent demonstrated exceptional recyclability after being cleaned with 1 M HCl.

In 2021, L. I. Abd Ali and co-workers [163].In this study, a novel class of multifunctional material PANI/NiO/MnO_2 Nanocomposites was created for the first time by chemically polymerizing aniline monomer in an acidic aqueous solution with metal oxides (NiO and MnO_2), an oxidant (ammonium persulfate), and methyl orange (MO) dye. Due to its excellent adsorption, the PANI/NiO/MnO_2 Nanocomposites was discovered to be an advantageous adsorbent for wastewater treatment. The information showed that PANI Nanocomposites doped with MnO_2 and NiO nanoparticles had a greater adsorption efficiency (97%). We looked at the adsorption circumstances, including the medium's pH, the initial dye concentration, the dosage of the adsorbent, and the adsorption time. The PANI/NiO/MnO_2 nanocomposite's experimental adsorption capacity (248.4 mg/g). Up to four times may the PANI/NiO/MnO_2 adsorbent be recycled.

In 2021, Milad Abniki and Ali Moghimi were studied use of chitosan functionalized magnetic carbon nanotubes in aqueous samples for preconcentration, detection, and removal of trace levels of colored effluent is novel

and quick[164]. This process uses a two-phase system with functionalized magnetic carbon nanotubes and chitosan in the acceptor phase and an aqueous phase with bromocresol green in the donor phase. The experiment was conducted in two stages: first, bromocresol green was extracted from an aqueous solution, and then, using an ethanol solvent, for desorbed the dye from surface . UV-Vis spectrophotometer analysis was performed on the samples. The effect of organic solvent, the pH of the donor and acceptor phases, the extraction time, interfering species, and the volume of the elution solvent were some of the extraction parameters that were examined. The thorough description of the bromocresol green adsorption isotherm Langmuir model, and the greatest adsorption capacity was 28.49 mg g^{-1}. For bromocresol green, the preconcentration factor and limit of detection were 14.3 and 7.5 g L^{-1}, respectively. There is a linear range between 0.1 and 20 mg L^{-1}. The magnetic carbon nanotubes with chitosan functionalization (Fe_3O_4 /MWCNT-CN) also showed a great potential for eliminating bromocresol green from water samples.

In 2022, A. Bekhoukh and co-workers exmained the removal of methyl orange (MO) by utilizing a novel adsorbent made from activated carbon (AC) and polyaniline reinforced by a direct oxidation chemical process[165]. TGA, FTIR, XRD, and PANI/CA were used to characterize the produced materials. greatest values for total mesoporous volume (around 0.038 cm^3 g1) and specific surface area (near 332 m^2 g^{-1}). Demonstrated a significantly higher MO elimination capacity than PANI (46.82 mg g^{-1}), which was 192.52 mg g^{-1} at 298 K and pH 6.0. Also, the adsorption, kinetics, and isothermal analyses of the process were investigated utilizing a number of different factors, including pH, MO concentration, and contact time. The Freundlich model did not fit experimental

results as well as the Langmuir model did. After five cycles of regeneration experiments, findings that were suitable.

In 2022, Alabbad, E. A and co-workers, Direct yellow dye 50 (DY 50) was extracted and removed using a customized chitosan crosslinked isovanillin (CCIV) polymeric adsorbent made utilizing homogeneous catalysis[166]. This was accomplished through fast adsorption caused by an electrostatic attraction between the dye molecules and CCIV frameworks. To ascertain the impact of contact time, incubation temperature, solution pH, initial dye concentration, and adsorbent mass, the removal efficiency of DY 50 was methodically examined. In addition, the adsorbent appeared to have a novel tribocatalytic energy impact for dye decompositions. This is validated by comparing the removal from friction, which is supposed to encourage the production of reactive oxygen species, to the removal from agitation (friction). Up to 83.3% of the initial DY 50 load was eliminated within and practically immediately after the DY 50 adsorption began. In addition, the adsorbent appeared to have a novel tribocatalytic energy impact for dye decompositions. This is validated by comparing the removal from friction, which is supposed to encourage the production of reactive oxygen species, to the removal from agitation (friction). The DY 50 adsorption was nearly immediate, with up to 83.3% of the initial DY 50 load being removed in as little as 10 minutes, and then 90-97.9% of the DY 50 load being removed by physicochemical adsorption using 0.05 g of CCIV bio sorbents after 45-180 min at room temperature.

In 2023, Abdel-Basit Al-Odayni and co-workers employed, polyaniline (PANI) as a precursor to produce nitrogen-rich activated carbon (PANI/AC), which provides one potential technique of converting nitrogen-containing polymeric waste into a practical adsorbent [167]. PANI/AC is created and examined using FTIR, SEM, BET, TGA, and CHN elemental composition after being chemically

activated using a 4:1 mixture of KOH and a PAn precursor. Its structural characteristics support its potential as an adsorbent material. Methyl orange (MO) concentration (C_0 = 50, 100, and 200 ppm), contact duration (0–180 min), and adsorbent dosages (20, 40, and 80 mg per 250 mL batch) were employed to determine the adsorption performance. (405.6 mg/g) The adsorption capacity (qe) was perfect.

In 2023, Neza Rahayu Palapa and co-workers [168]The potential of $M^{2+/}$Al intercalated chitosan has been examined in this study, as well as its excellent capacity to decrease dyes in an aqueous solution. An anion exchange technique and coprecipitation in a nitrogen atmosphere were used to create $M^{2+/}$Al intercalated chitosan. The ability of $M^{2+/}$Al intercalated chitosan to preserve the particle size of direct dyes was examined using selectivity adsorption (direct green, direct red, and direct yellow). $M^{2+/}$Al intercalated chitosan was tested using kinetic, isothermal, and thermodynamic parameters to assess the adsorption process. When the Langmuir isotherm and pseudo-second order models were used to fit the kinetic data, the qmax values for Zn/Al-chitosan and Mg/Al-chitosan were 294.11 mg/g and 322.58 mg/g, respectively.

1.12. The aims of the Study

1-Preparation the tertiary Nanocomposites PANI/Nb_2O_5/ MnO_2 and PANI/Nb_2O_5/ Cr_2O_3 by using the oxidative polymerization .

2- Preparation the tertiary Nanocomposites CS/Nb_2O_5/MnO_2 and CS/Nb_2O_5/Cr_2O_3 by using the oxidative polymerization.

3- Characterized the prepared catalyst by different techniques such as Fourier Transform Infrared Spectroscopy (FTIR), X-ray diffraction (XRD), UV/Visible, Thermo gravmetric analysis (TGA), Zeta potential analysis(ZPA) and scanning electron microscopy (SEM).

4- Study adsorption of dyes (MO,BCG,DY50) and estimates optimum condition such as optimum dosage of the Nanocomposites, initial of concentration of dye, effect of temperature and effect of pH solution.

5- Study Adsorption isotherms:(Langmiur ,Friundlich and Temkin isotherm model)

Chapter 2
Materials and Methods

2.1 Materials and Methods:

2.1.1. Chemicals and Instruments:

As can be seen in tables (2-1), all of the chemicals employed in this study were used without being purified in any way.

Table 2 -1. Chemicals used in the study purity and compound supplied

No.	Chemicals	Chemical formula	Company Supplied	Purity %
1	Aniline monomer	$C_6H_5NH_2$	Sigma-Aldrich/ Germany	99.5%
2	Ammonium persulfate	$(NH_4)_2S_2O_8$	Sigma-Aldrich / United *States*	98%
3	Acetone	C_3H_6O	Monobind/ USA	99.99%
4	Acetic acid	CH_3COOH	Sigma-Aldrich / United *States*	99%
5	Bromocresol green	$C_{21}H_{14}Br_4O_5S$	Textile dyes	90%
6	Chitosan (CS)	$C_6H_{11}NO_4$	British Drug House/ British	98%
7	chromium(III) oxide	Cr_2O_3	Panreac	98%
8	Direct yellow 50	$C_{35}H_{24}N_6Na_4O_{13}S_4$	Textile dyes	88%
9	Ethanol	C_2H_5OH	British Drug House/ British	99.99%
10	Hydrochloric acid	HCl	British Drug House/British	37%
11	Manganese oxide	MnO_2	Panreac	98%
12	Methyl orange	$C_{14}H_{14}N_3NaO_3S$	Thomas Baker/India	90%
13	Niobium Oxide	Nb_2O_5	Fluka	99%
14	Sodium hydroxide	NaOH	British Drug House/ British	99%
15	Sulphuric acid	H_2SO_4	British Drug House/ British	98%

2.2 Instruments

Table (2-2) shows the instruments used in this study as well as the companies and places.

Table 2.2 The Instruments Utilized in This Study, as well as Their Models and Manufacturers.

NO	Instrument	Model	Company, Source	Location
1	X–rays Diffraction (XRD)	Lab X XRD 6000 SHIMADZU	Japan	Ministry of Science and Technology
2	Scanning Electron Microscope (SEM)	Thermo fisher Scientific XL30	Germany	AlKhora Company Bagdad
3	Thermal gravimetric analysis (TGA)	SDT Q600 V20.9 Build 20	Japan	Tehran University Iran
4	UV-vis spectrophotometer double beam	shimadzu 1600	JAPAN	Babylon University Department of Chemistry
5	Fourier Transform Infrared (FTIR)	FTIR 8400S Shimadzu	JAPAN	Babylon University Department of Chemistry
6	Centrifuge	Cyan, CL008	Malaysia	Babylon University Department of Chemistry
7	Zeta Potential Analysis (ZPA)	Zeta plus, Brook haven	Germany	Ministry of Sciencesand Technology
8	Oven	Memmert	USA	Babylon University Department of Chemistry
9	pH-Meter	WTW-Inolab PH	Germany	Babylon University Department of Chemistry
10	Sensitive Balance	Sartorius HR-200	Germany	Babylon University Department of Chemistry
11	Magnetic-Stirred Hot Plate	Gallenkamp, England	Germany	Babylon University Department of Chemistry
12	Gemmy orbit shaker	Model VRN-480	Germany	Babylon University Department of Chemistry

2.3. Synthesis of PANI/Nb_2O_5/MnO_2 and PANI/Nb_2O_5/Cr_2O_3 Nanocomposites

Aniline (8g) dissolved in 100 ml of (1M) HCl solution, which is then agitated for an hour before being cooled for a further 30 minutes. Powder (1g of Nb_2O_5 + 1g of MnO_2) is added straight to a solution, by dissolving 14 g of the oxidant solution (APS) in an 80 ml aqueous solution of 1 M HCl, the oxidant solution is synthesized. So, using magnetic stirring and a thermometer[169, 170]. Aniline and metal oxide are combined, and the combination was slowly exposed to the oxidant solution (APS), which is released dropwise from a separating funnel. Adding 10 drops of APS per minute helped maintain the temperature of the polymerization solution process at 1-2 °C, which resulted in the creation of the PANI. The polymerization reaction lasted for six hours and the colour of the arrangement changed gradually from gray to blue to green. The PANI/Nb_2O_5/MnO_2 Nanocomposites is then subjected to cleaning using a Buchner funnel, acetone, 1 L of 1 M HCl and distilled water. The product is then dried for 24 hours at 70 °C in a vacuum oven. The above method was used again to prepared PANI/Nb_2O_5/Cr_2O_3 with the same steps just add 1g of Cr_2O_3 instead of MnO_2 has been illustrated in Figure (2.1).

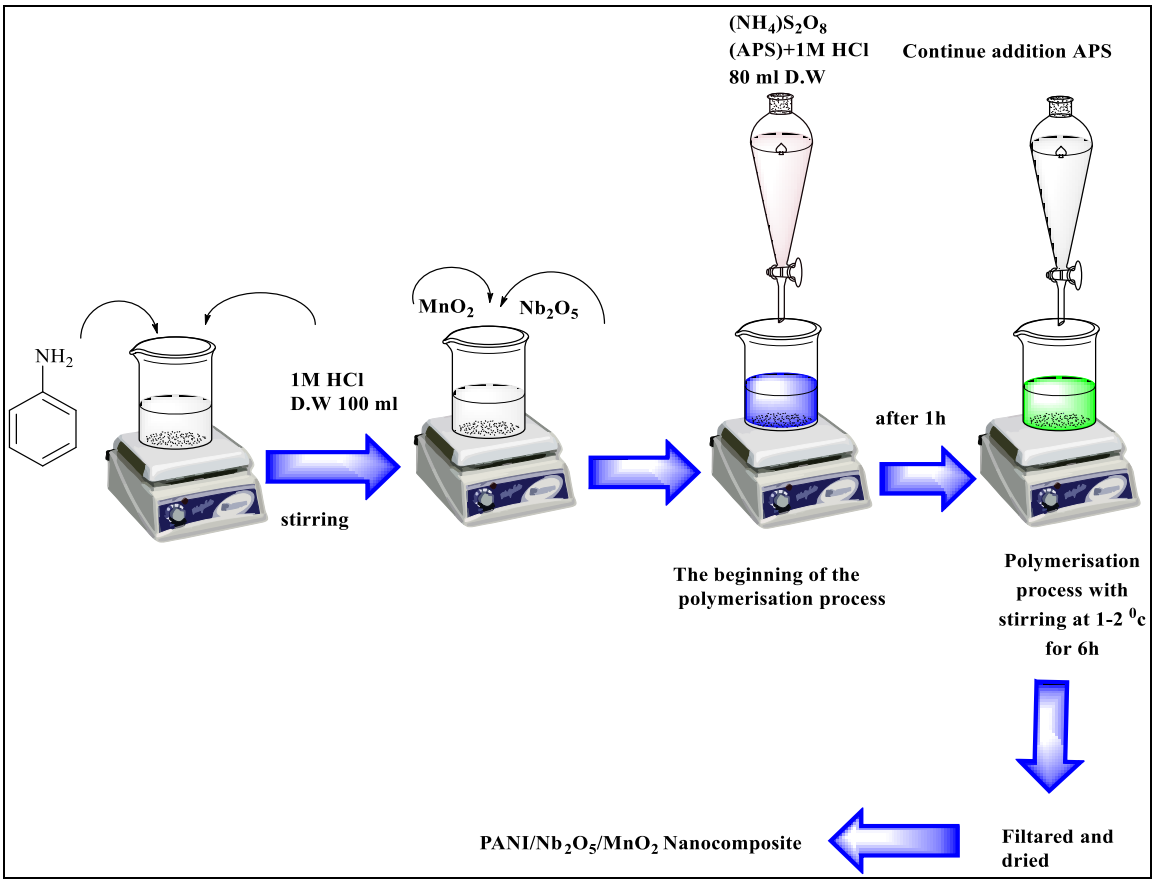

Figure 2. 1. Diagram showing the anticipated interactions between the PANI/Nb_2O_5/MnO_2 and PANI/Nb_2O_5/Cr_2O_3 sample created via in-place oxidative polymerization.

2.4. Synthesis of CS/Nb_2O_5/MnO_2 and CS/Nb_2O_5/ Cr_2O_3 Adsorbent

At the first, the procedure for dissolving 2 g of chitosan in 2% of acetic acid under magnetic starrier for 1 hour at room temperature. Subsequently,1g of Nb_2O_5 and 1g of MnO_2 powder were directly added to the solution, creating a black mixture that was then ultrasonically dispersed for 1hour [171]. The final step involved combining the ultrasonic solution with 0.1 M NaOH (pH =6), and allowing the reaction to occur for 4 hours with magnetic stirring. Using the same method, CS/Nb_2O_5/Cr_2O_3 are made, mirroring the synthesis of CS/Nb_2O_5/MnO_2 nanocomposites. The resulting nanocomposites went through a series of washes by acetone, 1 M HCl solution, distilled water, and a Buchner funnel before it is dried

in a vacuum oven for 24 hours at 90°C. Figure 2.1 depicts the formation of two nanocomposites: CS/Nb_2O_5/MnO_2 and CS/Nb_2O_5/Cr_2O_3.

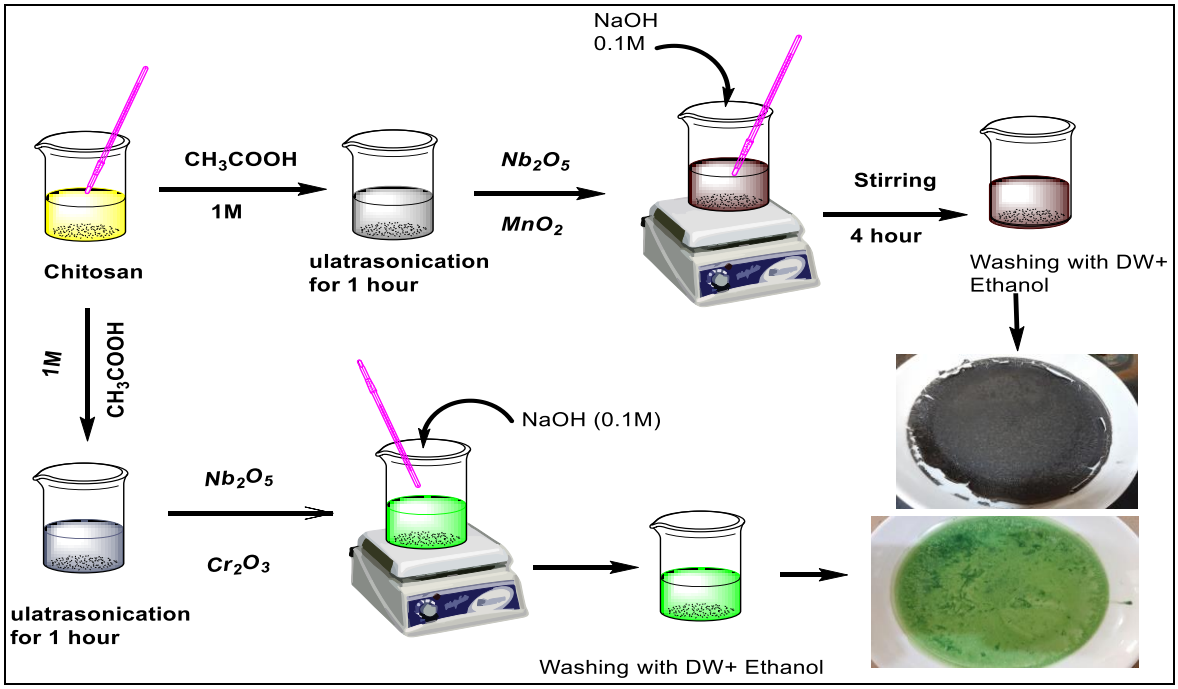

Figure 2.2 Diagram showing the in-situ oxidative polymerization used to create a sample of chitosan with Nb_2O_5, Cr_2O_3, and MnO_2 interactions

2.5. Characterization technology

2.5.1. X-ray Diffraction (XRD)

By employing a (Shimadzu-XR-6000) equipment with a copper target, voltage (40 KV), and current (30 mA), the produced materials are analyzed by X-ray diffraction. Utilizing a receiving slit, scanning is carried out continuously at a rate of 5 degrees per minute (0.3 mm) on the range (2 = 10.000–80.000). The following equation applies Scherrer's equation to XRD data to get the mean crystallite size (D)[172, 173].

$$\mathcal{D} = \frac{k\lambda}{\beta \cos \theta} \qquad \text{…….. (2.1)}$$

D : Size of the crystal is measured in units of nm.

K:The Scherrer constant (0.94) is determined by the crystal structure.

For the X-ray radiation wavelength (0.15406 nm for Cu Kα), λ is the appropriate symbol.

β: is multiplied by (/180) to convert the Full width half maximum (FWHM) to radians.

Θ: (Bragg's angle) is diffraction.

2.5.2. Scanning Electron Microscope (SEM)

Using a focused beam of electrons, a scanning electron microscope (SEM) generates images by scanning a material. This process produces several signals by interacting with sample atoms, providing surface topography and composition information. An image results from combining the detected signal with the beam's position, created as the beam is typically scanned in a raster pattern. The SEM is capable of achieving a resolution greater than 1nm. With the environmental SEM, samples can be observed under varying environmental conditions, including high and low vacuum. From an electron beam, the most commonly detected occurrence is the discharge of second electrons from stimulated atoms.

Scanning the sample and spotting secondary electrons, an illustration depicting the slant of the surface is generated. The quantity of secondary electrons generated is determined by the angle between the beam and the surface. Typically, the sample's plume of secondary electrons is limited to a level surface. However, if the surface is tilted, the plume becomes partly naked, resulting in the release of additional electrons.

The following is a description of the SEM methodology for NP identification; Before analysis, one milligram of the produced Nanocomposites powder is

sputtered with gold to improve the sample's conductivity and resolution. After placing the sample into the SEM S 50, an image was captured.

2.5.3 Fourier transform infrared spectrophotometer (FTIR).

The infrared spectroscopy technique that is most frequently employed is called Fourier transform infrared (FTIR). IR radiation is passed through a substance during IR spectroscopy, with some of it either transmitting or absorbing. The resulting spectrum, which depicts molecule absorption and transmission, serves as the material's molecular fingerprint. Because no two distinct molecule structures produce the same IR spectra, much like a fingerprint, IR spectroscopy is useful for a variety of research. Utilizing the rotations and vibrations of molecules, infrared spectroscopy can detect heat. These activities result in modifications to a molecule's dipole moment. Infrared light from a source strikes the mirror, causing a beam to be produced that travels through the cell. The energy that travels through the sample at each frequency is then measured by the detector, which focuses the radiation and produces a spectrum that plots intensity versus frequency[174, 175]. The FTIR procedure The measurements were as follows: 40–50 mg of the resulting mixture was used to create KBr pellets or disks, which were made from 200 mg of dry KBr and 2 mg of Nanocomposites. KBr was employed as a backdrop for spectrophotometer measurements in the 400–4000 cm^{-1} range. prior to the FTIR scanning process beginning.

2.5.4. Zeta potential analysis (ZPA)

The difference in potential between the stationary fluid layer attached to the dispersed particle and the dispersion medium is referred to as Zeta potential analysis. This potential is a crucial indicator of the stability of colloidal dispersion. The electrostatic attraction between particles carrying the same charge is

proportional to the magnitude of the zeta potential. A robust zeta potential is beneficial to attain stability in a solution or dispersion by preventing larger particles and molecules from agglomerating. However, if the attractive forces dominate the repulsive forces at lower potentials, the dispersion might floc or break. The ministry of sciences and technology utilized analytical methodologies and (Model: 90 zeta Plus Instruments) to determine the zeta potentials of the nanocomposites powders[176]. Colloids with a high zeta potential are electrically stable, whether they are positive or negative. Conversely, colloids that coagulate or flop have a low zeta potential. Measuring at 25 °C and a wavelength of 657 nm, the determinations are conducted.

2.5.5. UV – Vis. Spectrophotometer

Polyaniline, Chitosan, Nb_2O_5, MnO_2, and Cr_2O_3 are studied using a shimadzu1600 UV/VIS spectrophotometer double beam PG. As well as identifying the adsorption process's by products.

2.5.6. Thermo gravimetric Analyzer (TGA)

Thermo gravimetric analysis is a technique for estimating a compound's weight change in proportion to temperature change. It is frequently used to determine the temperature at which solvent residue decomposes, the level of organic and inorganic compounds in a material, and the composition of composites. The analyzer typically comes with a high-precision balance that weighs the sample in a ceramic pan and records the weight change. The analyzer typically comes with a high-precision balance that weighs the sample in a ceramic pan and records the weight change. In addition, nitrogen (N_2) gas must be used to purify the instrument's environment in order to prevent Any undesirable reaction, such as oxidation, occurs. Depending on the type of sample pan, the heating temperature

can range from 55 °C to 1700 °C, and a percentage of It is possible to trace weight reduction against temperature. Consequently, the graph can be used to study a compound's thermal stability.

2.6. Calibration Curve of Dyes

2.6.1.Methyl Orange

By making a series of serial methyl orange dye solution concentrations ranging from 1 to 25 mg/L, the calibration curve for these dyes was conducted. According to figure, the dye solution is scanned from 290 to 793 nm, and the absorbance for these concentrations is measured at the wavelength (463 nm) that is discovered (2-3). Tables (2-3) showed the correlations between absorption and concentration, which are illustrated in figure.

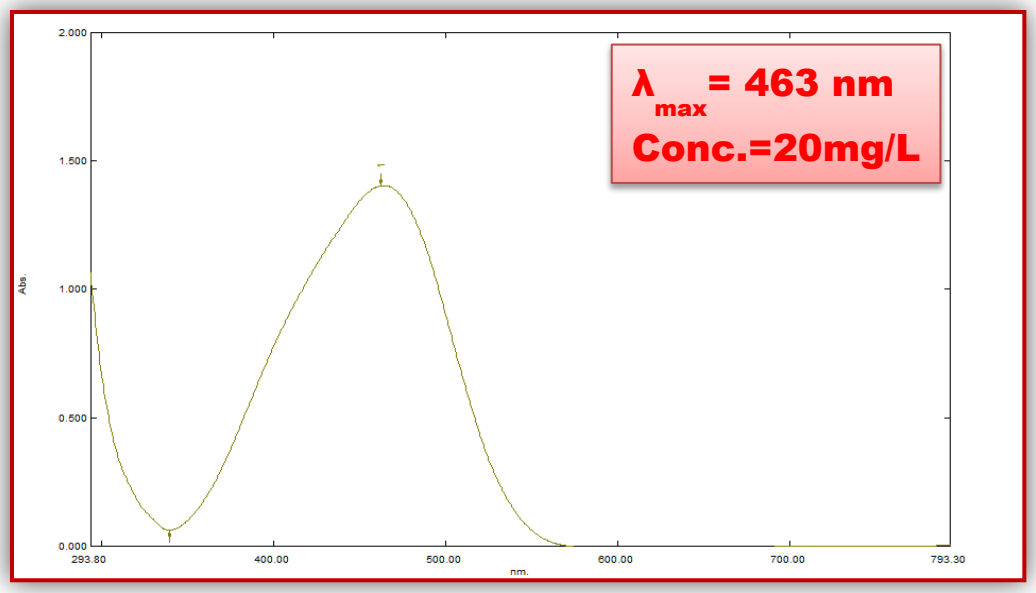

Figure 2.3. UV- Visible spectrum of Methyl Orange dye solution.

Table 2.3. Calibration Curve Data of Methyl orange dye.

Conc. Mg/L	Abs
1	**0.08**
3	**0.17**
5	**0.30**
10	**0.62**
15	**1.00**
20	**1.38**
25	**1.68**

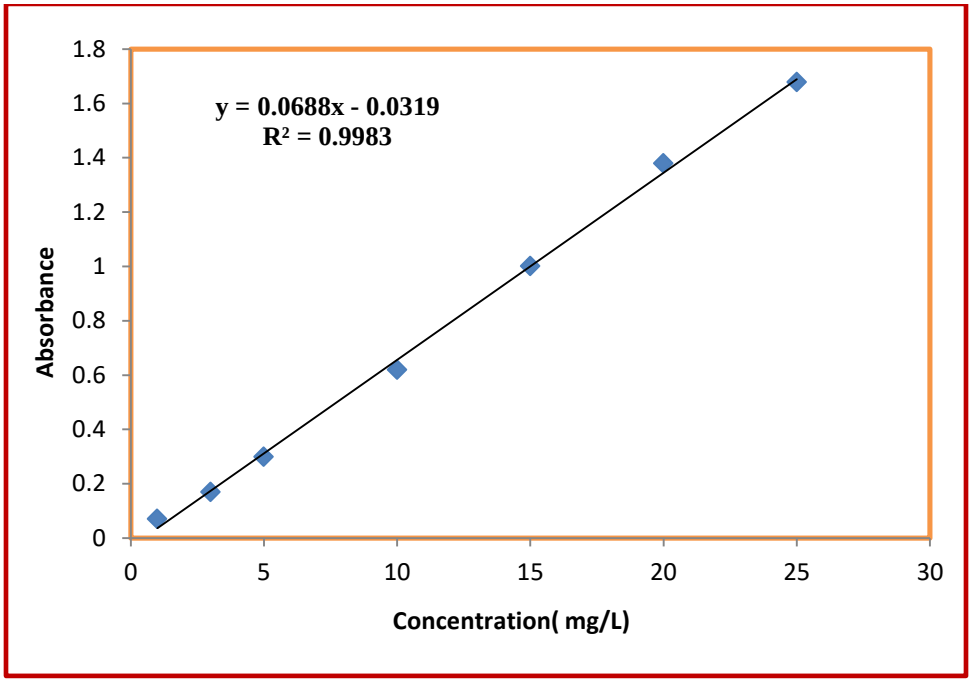

Figure 2.4. Calibration curve of Methyl Orange dye

2.6.2. Bromocresol green

The UV-Vis absorption wavelength of BCG is 615 nm, and the stock solutions are made in double-distilled water. BCG serial solutions with concentrations ranging from (1-25 mg/L) are developed. Figure (2.5)and table (2.4) illustrates the scanning of the dye solution from 313 - 800 nm and the measurement of absorbance at various concentrations (615 nm).

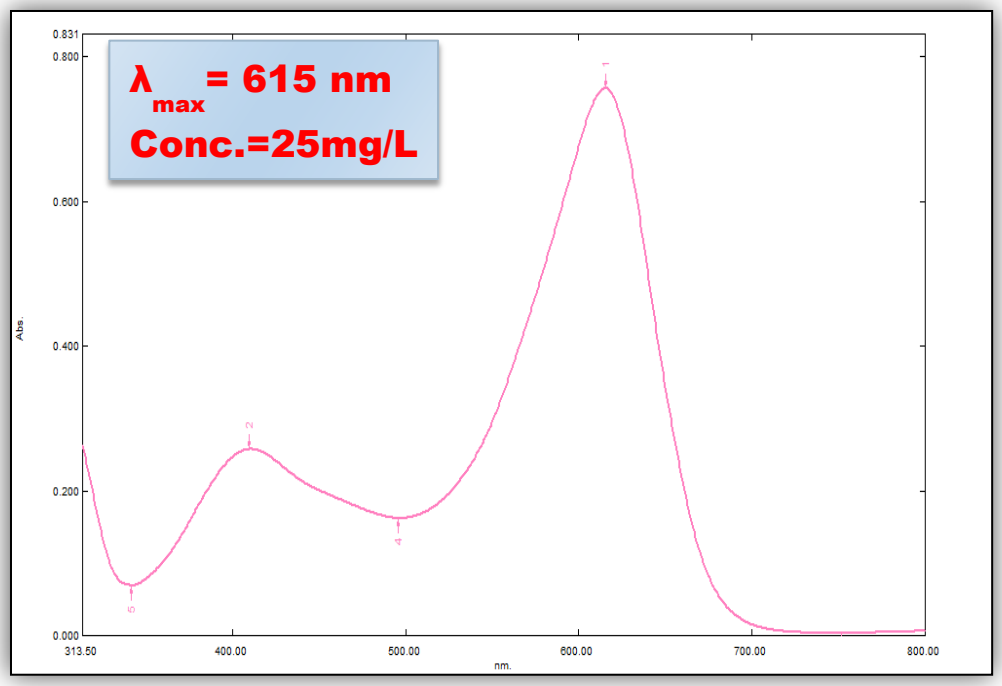

Figure 2.5. UV- Visible spectrum of Bromocresol green day

Table 2.4. Calibration Curve Data of Bromocresol green dye.

Conc. mg/L	Abs
1	**0.09**
5	**0.23**
10	**0.39**
15	**0.51**
20	**0.60**
25	**0.76**

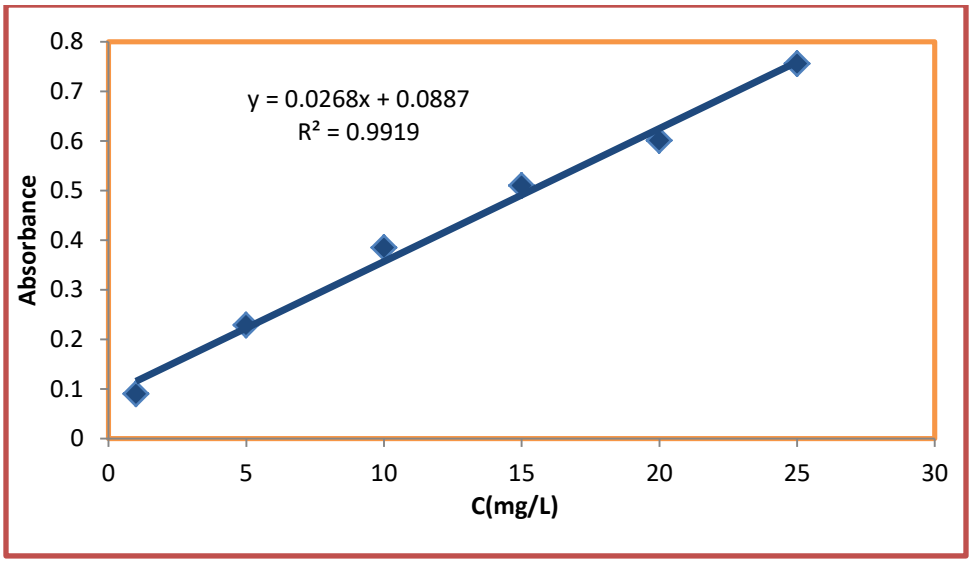

Figure 2.6. Calibration curve of Bromocresol green day

2.6.3. Direct yellow 50

The calibration curve of various Direct yellow 50 concentrations is created through successive dilutions (5-50 mg/L). Figure (2.7) illustrates the scanning of the dye solution from 313 to 800 nm and the measurement of absorbance at various concentrations (403 nm).

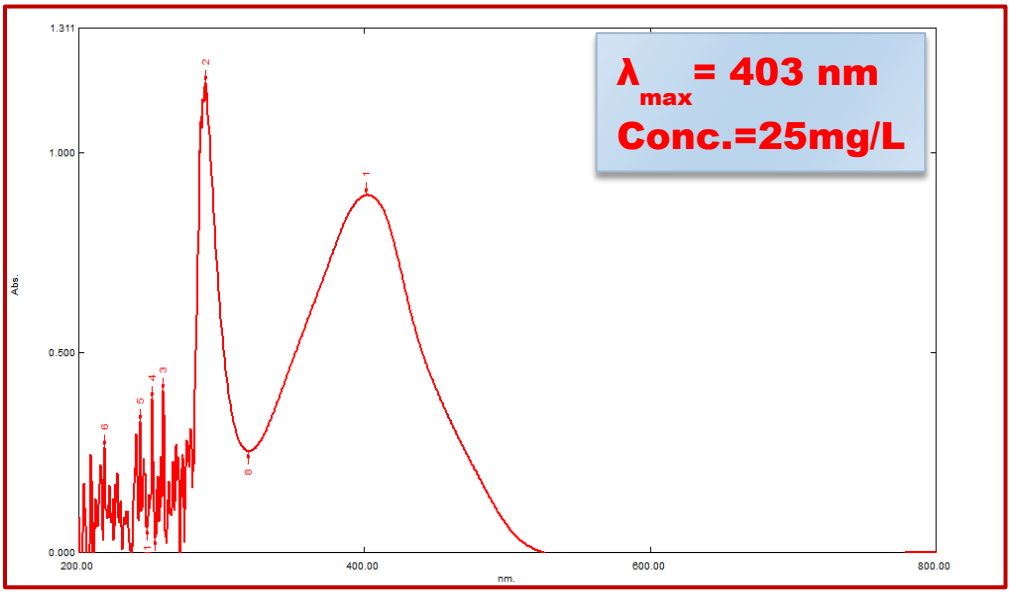

Figure 2.7. UV- Visible spectrum of Direct yellow 50 dye

Table 2.5. Calibration Curve Data of Direct yellow 50 dye.

Conc. mg/L	Abs
1	**0.12**
5	**0.24**
10	**0.382**
20	**0.67**
25	**0.86**
30	**1.07**
50	**1.68**

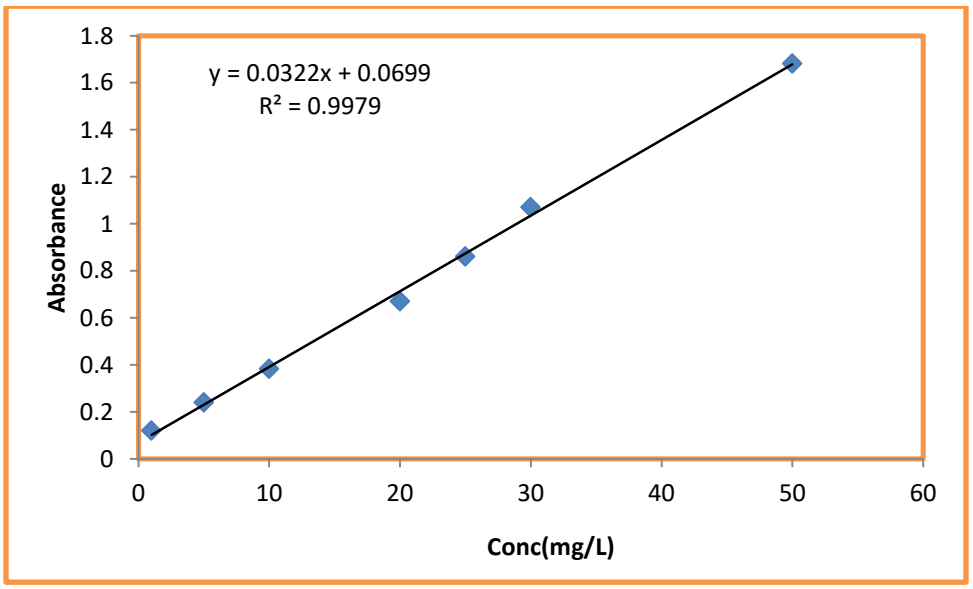

Figure 2.8.The calibration curve of Direct yellow 50 dye

2.7. Batch adsorption experiment and experimental design

The use of PANI, Nb_2O_5, Cr_2O_3, MnO_2, and chitosan Nanocomposites as adsorbents for water and wastewater purification stems from their excellent adsorption capability and large surface area. A comprehensive investigation involving several factors, such as adsorbent dosage, initial concentration of the MO dye, the conduct time, and the solution's pH, is conducted to determine the Nanocomposites' efficacy in adsorbing and removing the MO dye, a typical

organic contaminant found in industrial sewage; MO, BCG, and DY50 dyes are the identified contaminants. To 250 mL conical flasks are utilized to conduct an experiment on equilibrium adsorption of dyes (MO, BCG, and DY50). A constant dosage (mg) of adsorbent is added to the flasks, with initial concentrations of dyes measured in mg/L. To regulate the pH, a pH meter is utilized, with the pH adjusted to a specific value. Equilibrium is ensured by orbital shaking the reactions at a constant speed of 180 rpm for a duration of 60 minutes. The concentrations before and after are determined by using a UV-Vis spectrophotometer (Shimadzu 1600, Japan), with the maximum wavelengths utilized being 463, 615, and 403 nm. Using a variety of methods, it is possible to determine the percentage of dye removal (percent DR), as demonstrated in Equation 2.2:

$$\boldsymbol{Dye\ Removal}\ \% = \frac{(ci-ce)}{ci} \times \mathbf{100} \quad \ldots\ldots\ldots\ldots \quad (2.2)$$

Where C_i is the initial concentration of MO dye in mg/L and C_e is the dyes' equilibrium concentration after adsorption. The adsorption capacity (qe) was calculated using Eq 2.3

$$\boldsymbol{qe = \frac{(ci-ce)v}{m}} \quad \ldots\ldots\ldots\ldots\ldots\ldots\ldots \quad \mathbf{(2.3)}$$

Where: M is the synthetic adsorbent's weight (g), and V is the dye solution's volume (L).

2.8. Isotherms of adsorption

Isotherm models like Temkin, Langmuir, and Freundlich can be used to analyze adsorption data. The equilibrium adsorption isotherm of homogeneous systems can be determined using the Langmuir model by solving the following linear equation[177].

$$\frac{\mathbf{Ce}}{\mathbf{qe}} = \frac{\mathbf{Ce}}{\mathbf{qm}} + \frac{\mathbf{t}}{\mathbf{qmKL}} \ldots\ldots\ldots\ldots (\mathbf{2.4})$$

where

(C_e) The equilibrium concentration and (q_e) adsorption capacity are measured in mg/g and mg/L, respectively. The greatest capacity for metal ion adsorption (mg/g) is known as Q_m.

The adsorption energy ($mg.L^{-1}$) is related to the Langmuir constant (KL).The plot between Ce/qe and Ce was used to compute the isotherm constant.

The oldest equation, the Freundlich adsorption isotherms, illustrates the variety of adsorption sites during use. Freundlich's formula[178]

$$\mathbf{log\ qe} = \mathbf{log\ KF} + \frac{\mathbf{1}}{\mathbf{n}} \mathbf{log}\, ce \ldots\ldots\ldots\ldots (\mathbf{2.5})$$

where KF is an adsorption capacity-related constant.

A chemisorptions n1of a physisorption n>1 process' affinity is defined by the experimental parameter 1n, which is proportional to adsorption intensity. Already mentioned are the q_e and C_e.

warmer Temkin Adsorbent-adsorbate interactions are especially taken into consideration in one section of this isotherm. The model implies that the heat of adsorption, which is a function of temperature, will drop linearly rather than logarithmically with coverage by neglecting extremely low and high concentrations. [179].

$$\mathbf{qe} = \mathbf{A} + \mathbf{B\ log\ Ce} \ldots\ldots\ldots\ldots (\mathbf{2.6})$$

Where:

A represents the Temkin isotherm constant (L/g), and B represents the heat of sorption constant (J/mol). Plots of q_e against C_e were employed to derive the Temkin linear equation..

2.9 Primary experiments for adsorption Methyl Orange

2.9.1 Effect of Adsorbent dosage

Many experiments have been made to knowing the effect of the weight of the catalyst on the adsorption methyl orange (100 ml) with 25 mg/L initial concentration at a temperature of 25 °C and using different quantity of PANI/Nb_2O_5/MnO_2 and PANI/Nb_2O_5/Cr_2O_3 (10 ,20 ,30, 50,100,150) mg.

2.9.2 Effect of Initial MO Concentration

Different concentrations of MO were taken in many experiments (1, 3, 5, 10,15,20,25) mg/L with constant quantity in 100 mL of solution. Also, all the rest conditions are kept constant.

2.9.3 Effect of pH Solution

To determine the effect of pH on the removal of MO dye at various pH solution (2, 3, 5, 7, 8, 9, and 10) as well as the ideal catalyst mass and dye concentration, a number of experiments are conducted for PANI/Nb_2O_5/MnO_2 and PANI/Nb_2O_5/Cr_2O_3.

2.9.4 Effects of conduct time

The catalysts PANI/Nb_2O_5/MnO_2 and PANI/Nb_2O_5/Cr_2O_3 are used to study the adsorption time of the methyl orange dye under constant conditions and at various times (10,20,30,40,50,60)min.

2.10 Primary experiments for adsorption Bromocresol green

2.10.1 Effect of pH level on adsorption procedure

Using a range of pH values (5,6,7,8,9,10,11,12) where the pH is adjusted by adding hydrochloric acid HCl at a concentration of (0.1 $mol.L^{-1}$) to form an acidic

medium and adding sodium hydroxide NaOH at a concentration of (0.1 $mol.L^{-1}$) to form a basic medium, a series of experiments were carried out to determine the best pH at which the best BCG dye removal occurs and following the addition of the catalyst for an hour at a temperature of 25°C and regulating the acidity of the dye solution at a concentration of 10 mg/L.

2.10.2 Effect of Adsorbent dosage

The optimal weight of the prepared $CS/Nb_2O_5/MnO_2$ and $CS/Nb_2O_5/Cr_2O_3$ for dye adsorption was determined through a series of studies by using various weights (25,50,75,100,150,250,350,450,550,650) mg while maintaining the same circumstances.

2.10.3 Effect of Initial BCG Concentration

The optimal BCG dye concentration was determined by a series of studies using several concentrations (1, 3, 5, 10, 15, 20, and 25 mg/L) under the identical conditions..

2.10.4 Effect of Temperature on Removal of BCG Dye

Several trials are conducted at different temperatures (293, 298, 303, 313, 323, and 333 K) in order to determine the optimal temperature for BCG dye adsorption under the conditions specified, and to illustrate the effect of temperature on reaction speed.

2.10.5 Effects of conduct time

With the other conditions held constant, the duration of BCG dye adsorption on the surfaces of the catalysts $CS/Nb_2O_5/MnO_2$ and $CS/Nb_2O_5/Cr_2O_3$ is investigated.

2.11 Primary experiments for adsorption Direct yellow 50

2.11.1 Effect of pH level on adsorption procedure

Using a range of pH values (2,3,4,6,7,9,11), the pH is adjusted by adding sodium hydroxide NaOH at a concentration of (0.1 $mol.L^{-1}$) to form a basic medium and hydrochloric acid HCl at a concentration of (0.1 $mol.L^{-1}$) to form an acidic medium in order to determine the best pH at which the best BCG dye removal occurs. The dye solution's acidity is then adjusted to 15 mg/L, and the catalyst is added for an hour at a temperature of 25 °C.

2.11.2 Effect of adsorbent dosage

The optimal weight of the synthesized CS/Nb_2O_5/MnO_2 and CS/Nb_2O_5/Cr_2O_3 for dye adsorption was determined by a series of studies by using different weights (10,25,50,75,100,150) mg while maintaining the same circumstances.

2.11.3 Effect of Initial DY 50 Concentration

The optimal DY 50 dye concentration is determined by a series of studies using various concentrations (5, 10, 15, 20, 25, and 50 mg/L) under the identical operating conditions.

2.11.4 Effect of Temperature on Removal of DY 50 Dye

To demonstrate how temperatures affect reaction speed, a series of tests are carried out at various temperatures (298, 308, 318, and 328 K) to determine the optimal temperature at which DY 50 dye adsorption occurs while retaining the same conditions.

2.11.5 Effect of conduct Time

The adsorption time of DY 50 dye on the surface of the catalyst CS/Nb_2O_5/MnO_2 and CS/Nb_2O_5/Cr_2O_3 was studied with the other conditions constant and with different times (10,20,30,40,50,60,90,120)min.

Chapter 3

Results and Discussion

3.1 Characterization of the Synthesized Nanocomposites

With an objective towards characterizing polyaniline/Nb_2O_5, MnO_2, Cr_2O_3, and Chitosan/$Nb_2O_5$with MnO_2 or Cr_2O_3, diverse analytical tools such as FT-IR (Fourier-transform technique), SEM (scanning electron microscopy), ZPA (Zeta potential analysis), XRD (X-ray diffraction), and UV-Visible spectroscopy are used.

3.1.1 FTIR stands for Fourier-transform Infrared Spectroscopy.

3.1.1.1 PANI/Nb_2O_5/MnO_2 and PANI/Nb_2O_5/Cr_2O_3

In the 400–4000 cm^{-1} region, Figures (3.1) and (3.2) show FT-IR peaks for constructed of PANI/Nb_2O_5/Cr_2O_3 and PANI/Nb_2O_5/MnO_2 Nanocomposites, respectively. It is evident that the peak at 3740, cm^{-1}, which is caused by the aromatic amines' N-H stretching, is present in all PANI samples[170]. The aromatic ring's C-H stretch is within the range of 2933,3039 cm^{-1}.The peak at 1550 cm^{-1} is suggestive of the quinoid rings even if the peaks at 1423 and 1464 cm^{-1} are related to the C=C stretching of the benzenoid rings. At 1550 cm^{-1}[180], the C=N stretch hits its peak. Varied maximum values ranging from 1097 cm^{-1} to1236 cm^{-1} [181] are detected in the C-H out-of-plane (o/p) bending vibration. The wide bands of PANI/Nb_2O_5/MnO_2 are discovered between 489 and 792 cm^{-1}. Despite top peak intensities being present in PANI/Nb_2O_5/Cr_2O_3 and PANI/Nb_2O_5/MnO_2, the results indicated that the surface of PANI interacted with Nb-O, Cr-O, and Mn-O. PANI/Nb also revealed the presence of quinoid and benzenoid rings.[182].

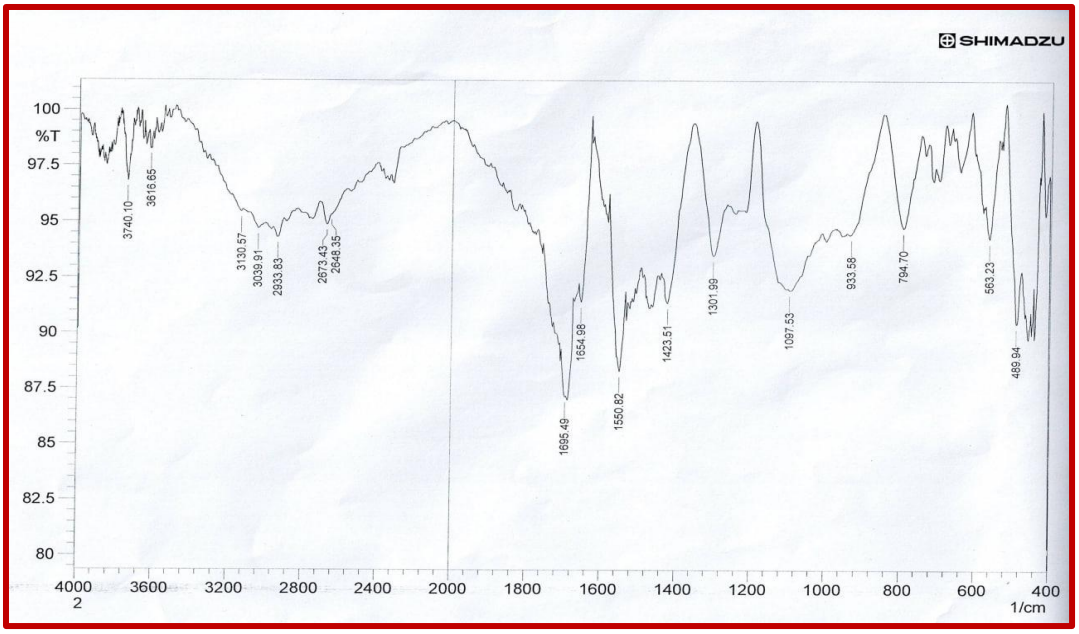

Figure 3.1 FT-IR spectra for PANI/Nb_2O_5/MnO_2.

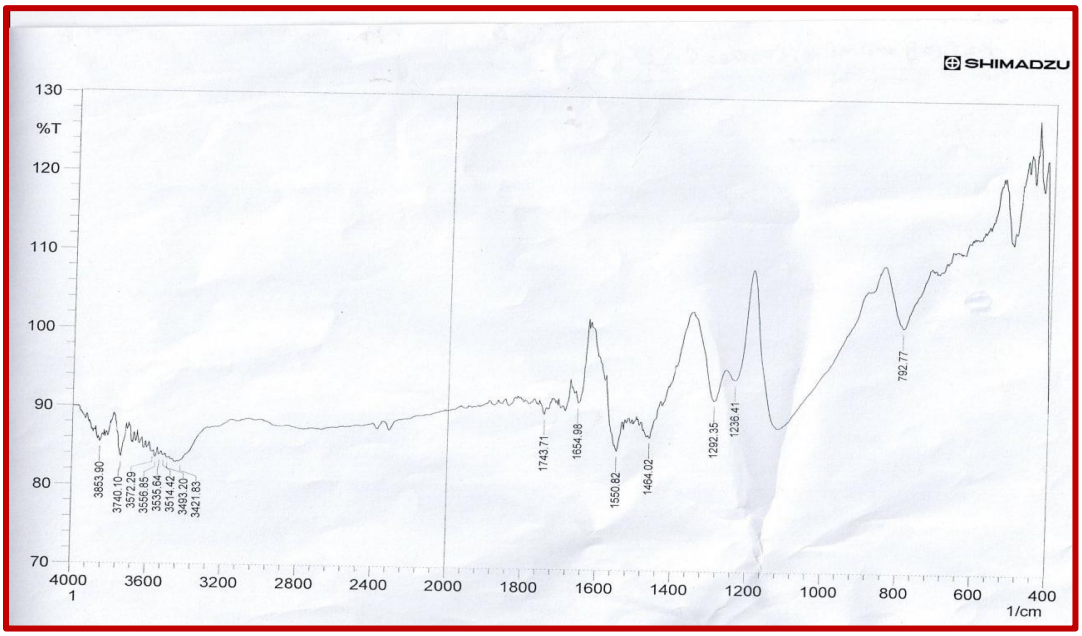

Figure 3.2 FT-IR spectra for PANI/Nb_2O_5/ Cr_2O_3

3.1.1.2 Chitosan/Nb_2O_5/MnO_2 and Chitosan/Nb_2O_5/Cr_2O_3

For constructed of CS/Nb_2O_5/Cr_2O_3 and CS/Nb_2O_5/MnO_2 nanocomposites, respectively, Figures (3.3) and (3.4) show FTIR peaks in the 400–4000 cm^{-1} range. that all chitosan samples exhibit the peak at 1152,1020 cm^{-1}, which results from the

saccharide moiety[183-185]. additionally to the stretching vibration of CH at 2921 cm^{-1}. Distinctive peaks are present in the spectra of CS-Nb_2O_5/MnO_2 and CS-Nb_2O_5/Cr_2O_3, showcasing metal oxide and CS (chitosan) peaks. The amide stretching vibration was pointed out by the peak at 1557 cm^{-1}, whereas NH_2 bending vibration is indicated by the peak at 1637 cm-1. The OH and NH_2 stretching vibration is linked to a strong band at 3420 cm^{-1}. Additionally, wide peaks ranging from 1339-1412 cm^{-1} are caused by M-O-M deformation vibration. M-OH and M-O bending vibration led to the presence of peaks in the 807-413 cm^{-1} range.

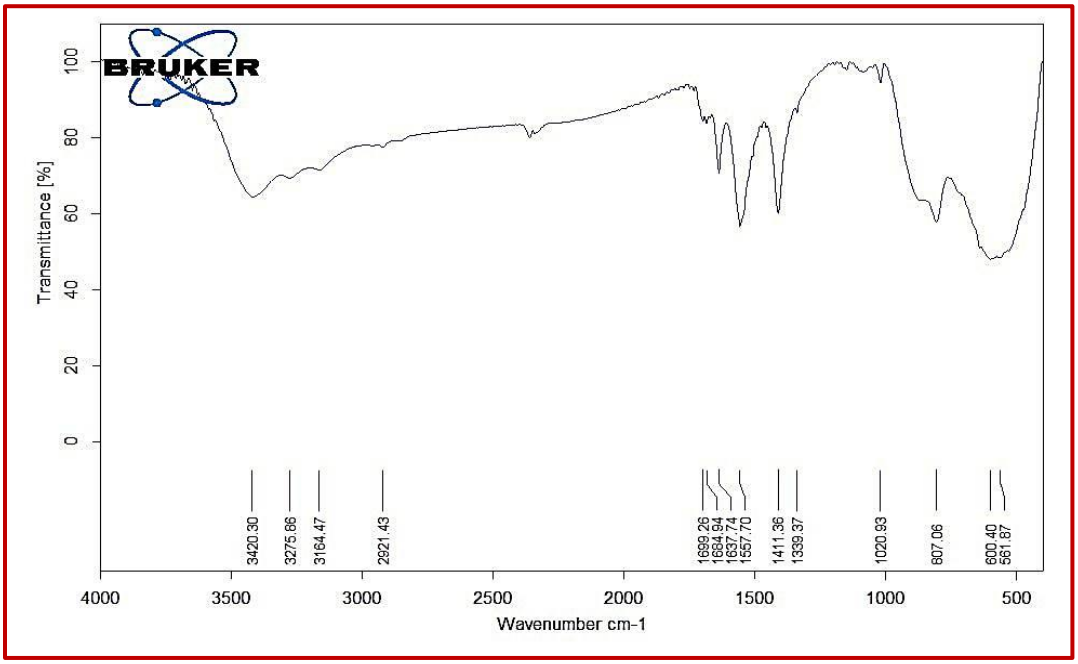

Figure 3.3. FTIR spectra for CS /Nb_2O_5/MnO_2 .

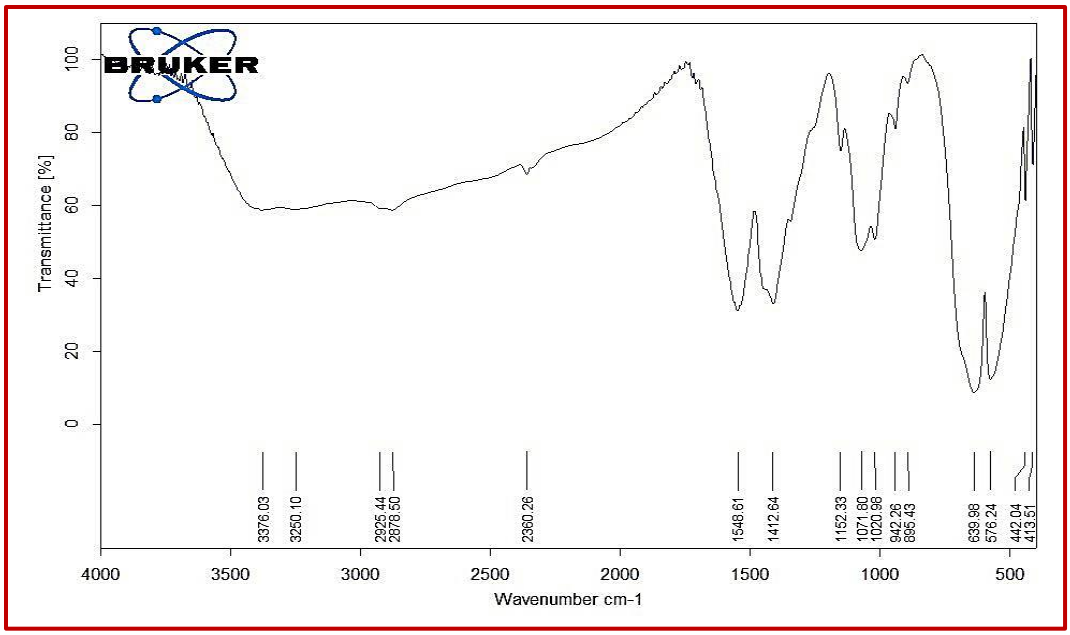

Figure 3.4. FTIR spectra for CS/Nb_2O_5/Cr_2O_3 .

3.1.2 X-ray Diffraction Pattern (XRD)

3.1.2.1 PANI/Nb_2O_5/MnO_2 and PANI/Nb_2O_5/Cr_2O_3

Further attributes of the PANI/Nb_2O_5/Cr_2O_3 and PANI/Nb_2O_5/MnO_2 structures were investigated by means of X-beam difraction (XRD), as displayed in Figures (3.5) and (3.6) to look at the crystallinity and undefined organization present in these examples [187]. the wide peaks are seen at 2θ = 9.65°, 15.65°, 20.6° ,25.35°,44.2°,64.55° and 77.65°. These pinnacles confrmed that formless construction is available PANI/Nb_2O_5/MnO_2 in the lattice[162, 188]. while The PANI/Nb_2O_5/Cr_2O_3 Nanocomposites XRD tops noticed are basically indistinguishable from the PANI precious stone planes 2θ = 9.2°, 15.2°, 21.25° and 25.7°,44.35°,64.55° and 77.7°. separately, showing that the metal oxides have adsorption interactions of a nanocrystalline type. (Nb_2O_5 and additionally MnO_2,Cr_2O_3) and PANI network This suggests that the PANI was collaborating with Nb_2O_5, Cr_2O_3 and MnO_2 in great precious stone construction. These outcomes (i.e., XRD), close FTIR results have demonstrated that the surface-based

polymerization of the aniline monomer is successful of the Nb_2O_5, Cr_2O_3 and MnO_2 nanoparticles[189, 190].

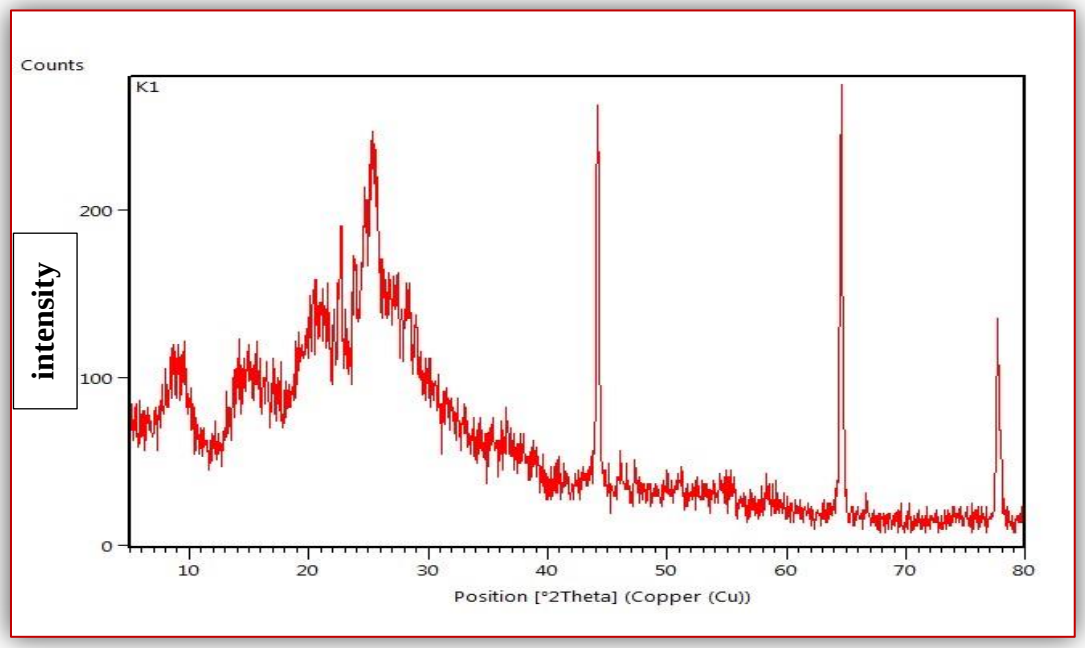

Figure 3.5. XRD spectra for PANI/Nb_2O_5/MnO_2

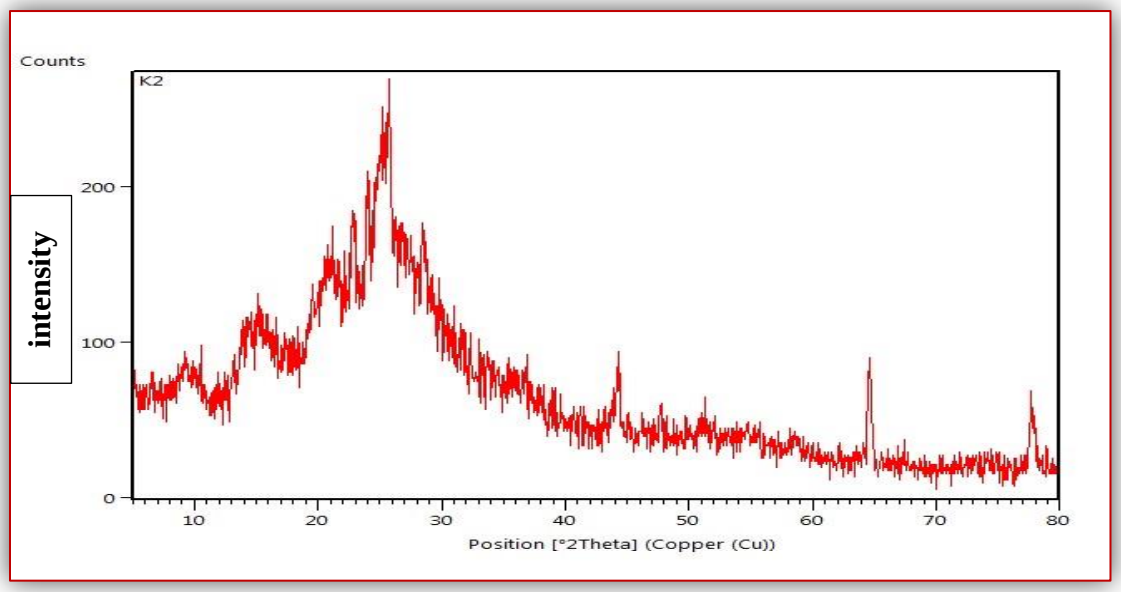

Figure 3.6. XRD spectra for PANI/Nb_2O_5/Cr_2O_3 .

3.1.2.2 Chitosan/Nb_2O_5/MnO_2 and Chitosan/Nb_2O_5/Cr_2O_3

The XRD examination can provide information on the creation of chitosan's semi-crystalline structure, crystalline chitosan-Nb_2O_5/MnO_2, and crystalline chitosan-Nb_2O_5/Cr_2O_3 structures, as displayed in Figrues(3.7 and 3.8). the all sharp peaks were seen at 2θ = 11.7°, 22.2°, 24.5° ,43.2°,50.6°,60.55° and 76.65°. These pinnacles confirmed that formless construction was available CS/Nb_2O_5/MnO_2 in the lattice[191] while The CS/Nb_2O_5/Cr_2O_3 Nanocomposites XRD tops noticed are basically indistinguishable from the Chitosan precious stone planes 2θ = 11.78°, 22.4°, 24,4° 33.4°,36°,41.3°,50.05°,54.7°, 72.8° and 76.7°. separately, showing that there are adsorption associations between the metal oxides, some of a nanocrystalline structure (Nb_2O_5 and additionally MnO_2,Cr_2O_3) and chitosan network This suggests that the chitosan is collaborating with Nb_2O_5, Cr_2O_3 and MnO_2 in great precious stone construction. The successful polymerization of chitosan on the outer layer of nanoparticles Nb_2O_5, Cr_2O_3, and MnO_2 is supported by the results from XRD and FTIR measurements[192] [193].

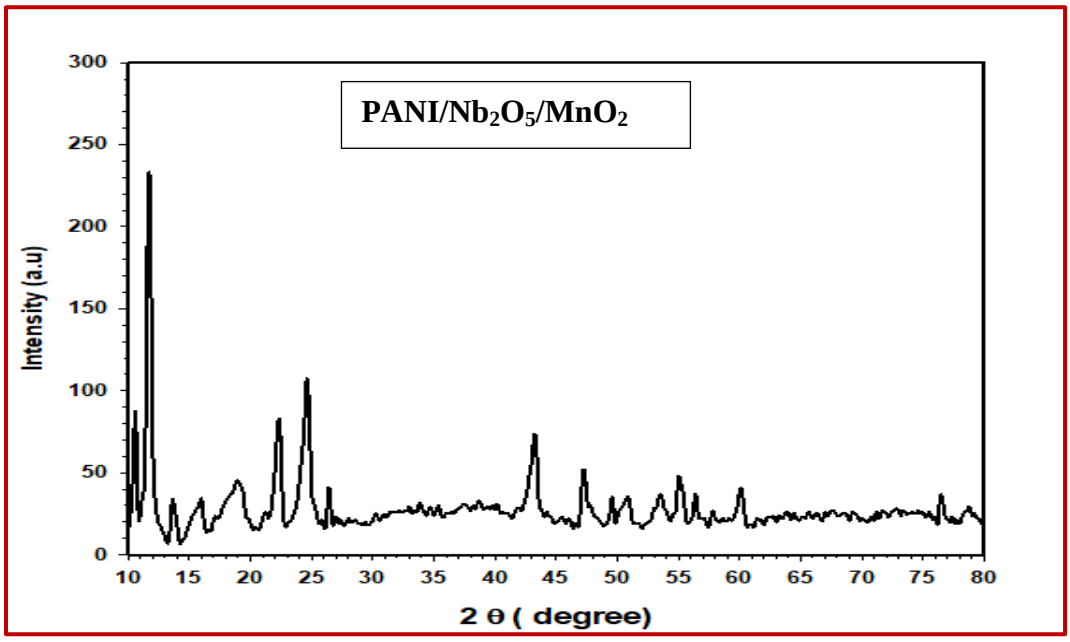

Figure 3.7.XRD spectra for the CS/Nb_2O_5/MnO_2 Nanocomposites

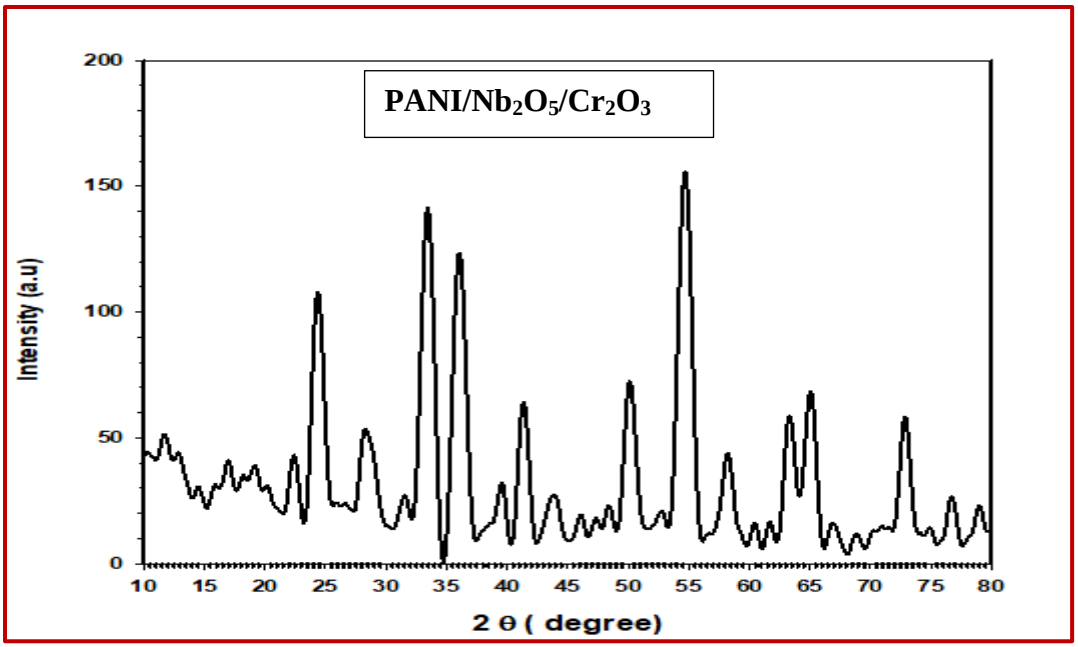

Figure 3.8. XRD spectra for CS/Nb_2O_5/Cr_2O_3 Nanocomposites

3.1.3 Scanning Electron Microscopy (SEM)

3.1.3.1 PANI/Nb_2O_5/MnO_2 and PANI/Nb_2O_5/Cr_2O_3

The surface morphologies of artificial metal oxides/PANI nanocomposites is investigated via FE-SEM as shown in Figures(3.9,3.10) it can be seen that the morphology of. Nb_2O_5,Cr_2O_3 and MnO_2 The majority of nanoparticles had spherical shapes and had sizes of around 30–68 nm. The metal oxide nanoparticles in the PANI/Nb_2O_5/MnO_2 and PANI/Nb_2O_5/Cr_2O_3 nanocomposites both had the same form and are flawlessly coated with thin polymer chains during the aggregation process [194, 195]. assuming that the PANI/Nb_2O_5/Cr_2O_3 and PANI/Nb_2O_5/MnO_2 Nanocomposites surface and size morphologies differed significantly. According to the XRD results, the chain diameter of the polymer nanocomposite ranged between 31-69 nm, changing the crystal growth's direction during adsorption. The doping of metal oxide nanoparticles in the polyaniline matrix was shown using FE-SEM.

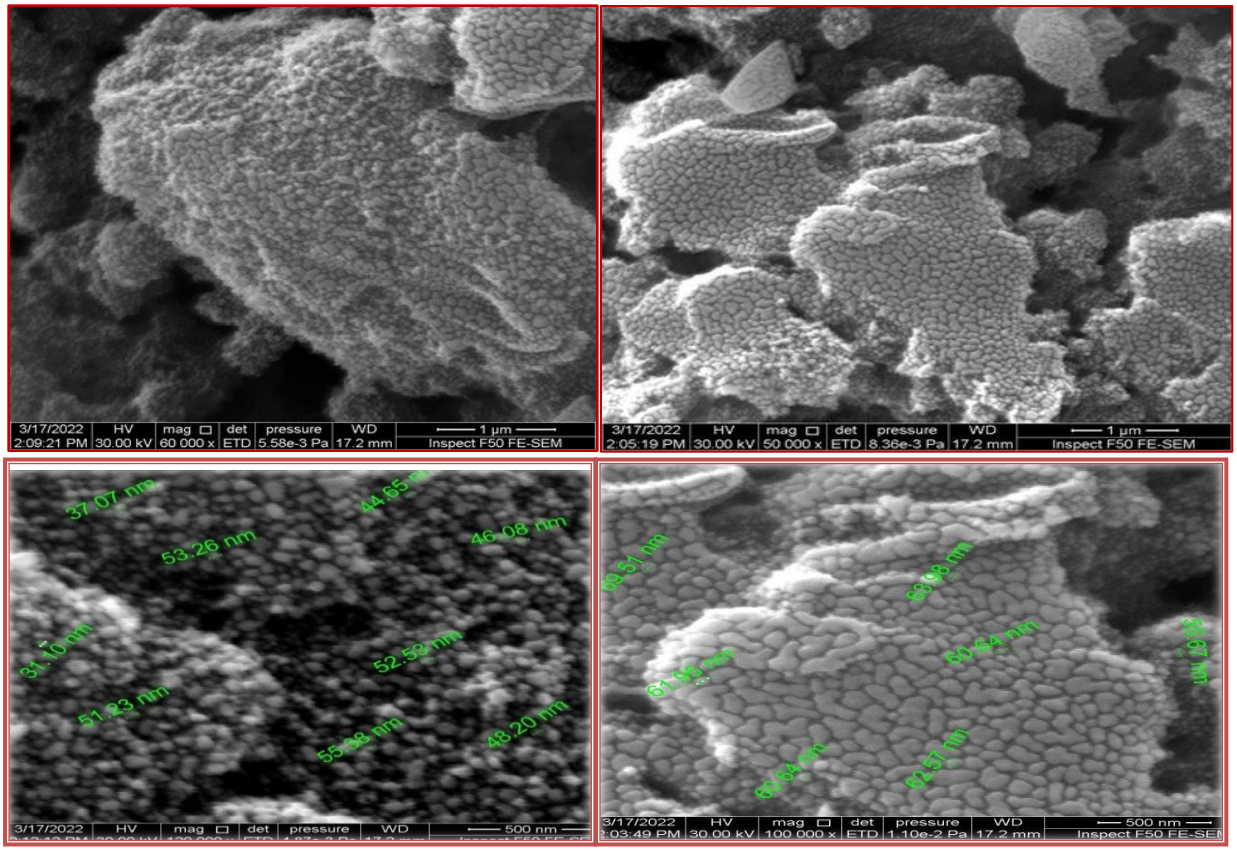

Figure 3.9 FE-SEM spectra for PANI/Nb_2O_5/MnO_2

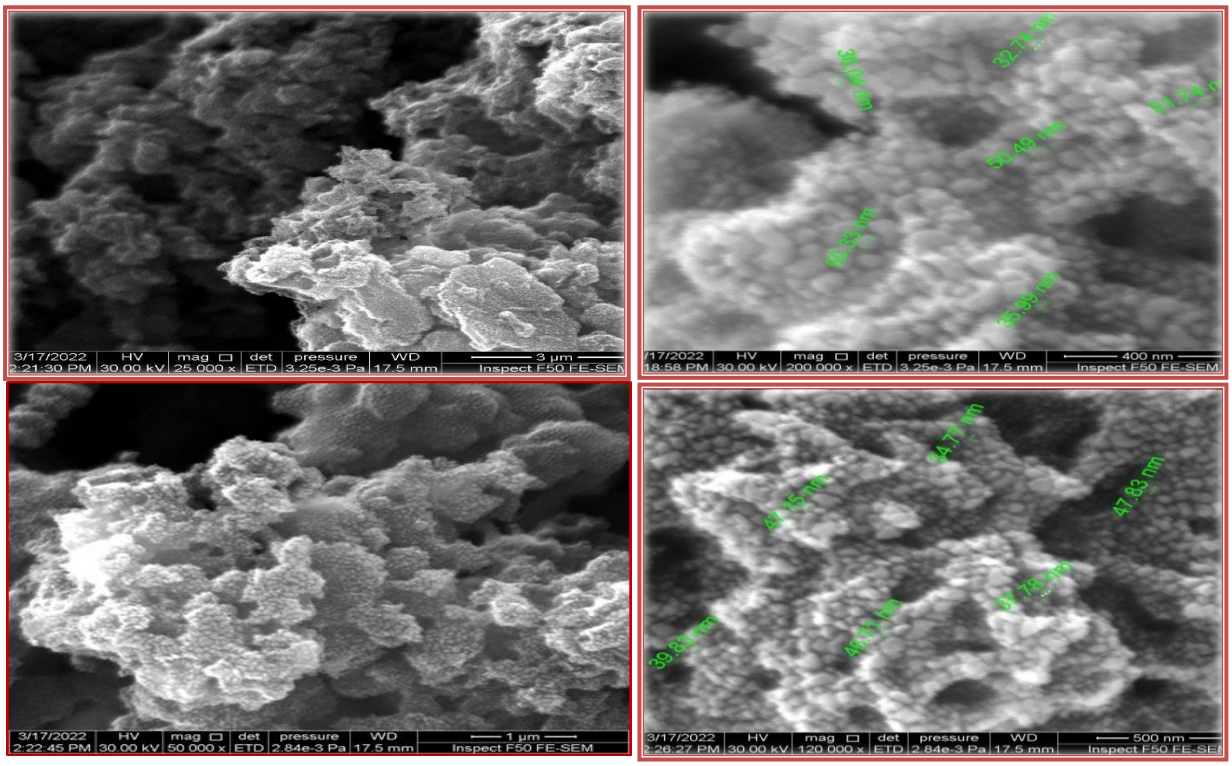

Figure 3.10 FE-SEM spectra for PANI/Nb_2O_5/Cr_2O_3

3.1.3.2 SEM for Chitosan/Nb_2O_5/MnO_2 and Chitosan/Nb_2O_5/Cr_2O_3

The distribution of metal oxides and the morphology of the nanocomposite Chitosan-Nb_2O_5/MnO_2 and chitosan-Nb_2O_5/Cr_2O_3 nanocomposite SEM images are shown in Figure (3.11 and 3.12). SEM image show the instrument characteristics, accelerating voltage, spot size, magnification, and working distance. The concentration of salt, the amount of chitosan in the solution, the temperature, and the solution's pH all have an impact on the shape and particle size of Nb_2O_5, MnO_2 and Cr_2O_3 [196]. The SEM image show the presence of some sort of agglomeration-type structure. The clearly apparent black and white patches on the nanocomposites surface.

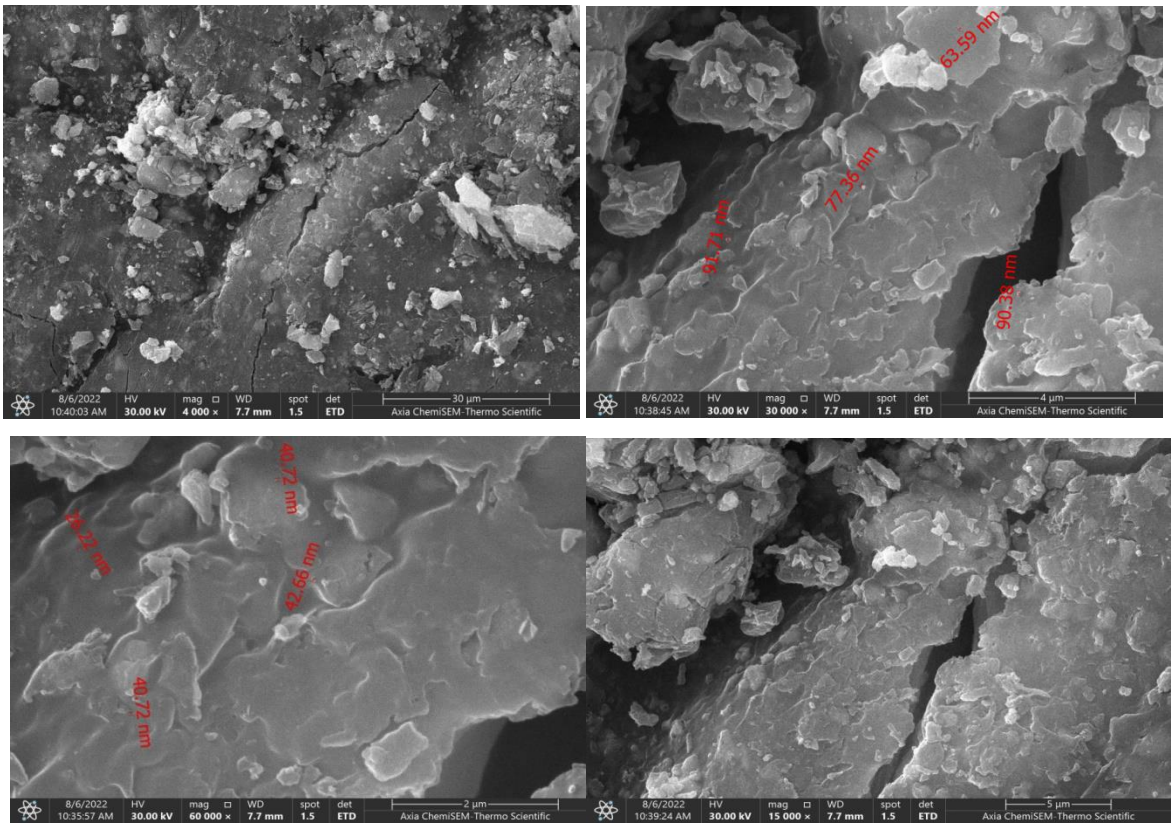

Figure 3.11. SEM images spectra for CS/Nb_2O_5/MnO_2 Nanocomposites

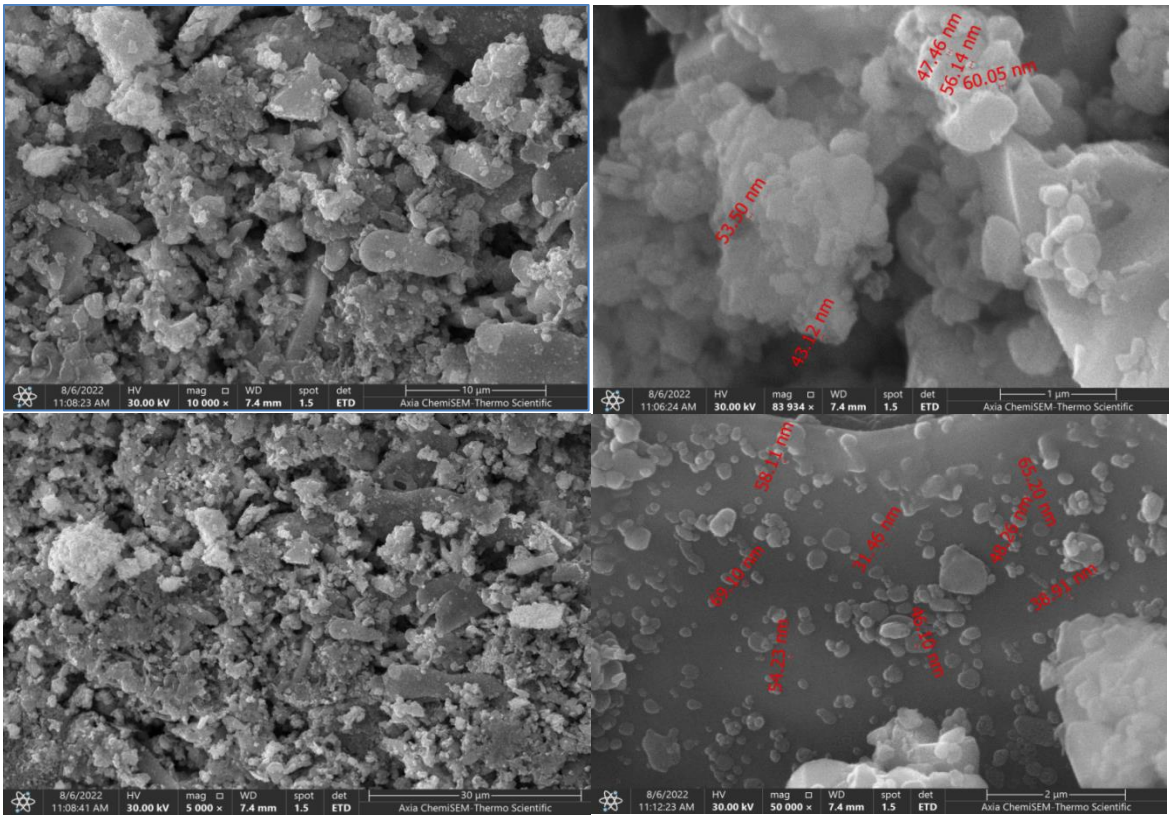

Figure 3.12. SEM images of CS/Nb_2O_5/Cr_2O_3 Nanocomposites

3.1.4 Zeta Potential Analysis (ZPA)

3.1.4.1 PANI/Nb_2O_5/MnO_2 and PANI/Nb_2O_5/Cr_2O_3

At a zeta potential of 27.66 mV and a mobility of 2.16 v/cm, the pH was measured at 7.4. The introduction of 20 ml of KCl had two effects: a decrease in zeta potential and an increase in particle size. The largest particle size was observed at the isoelectric point of pH 10.2. Basically, maintaining a stable pH level is crucial in understanding and adjusting (PANI/Nb_2O_5/MnO_2) suspensions. Zeta potential refers to the electric potential developed by the particle surface charge, which can be either positive or negative depending on the chemistry of the particle. The likely physical stability of a formulation (PANI/Nb_2O_5/Cr_2O_3) can be determined by measuring the strength of attraction between like-charged particles through the zeta potential. Particle size and mobility played a role in this

assessment, with a recorded mobility of 2.75 (v/cm), Zeta potential of 35.22 mV, and pH of 7.4. However, pH is not a negligible variable as its decrease caused the zeta potential to rise.

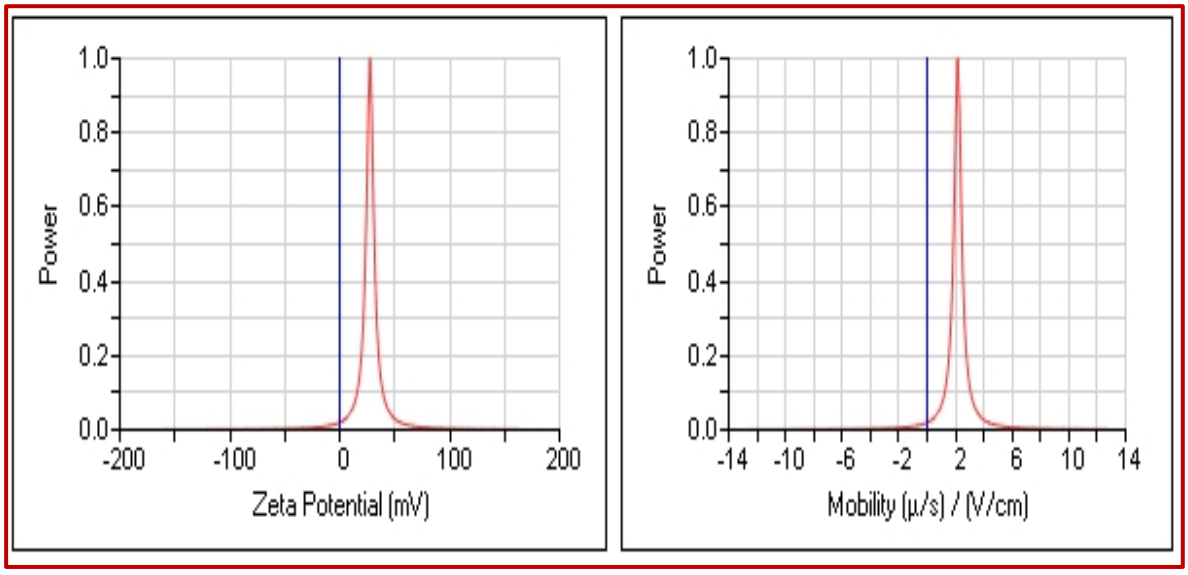

Figure 3.13. Zeta potential curves for PANI/Nb_2O_5/MnO_2

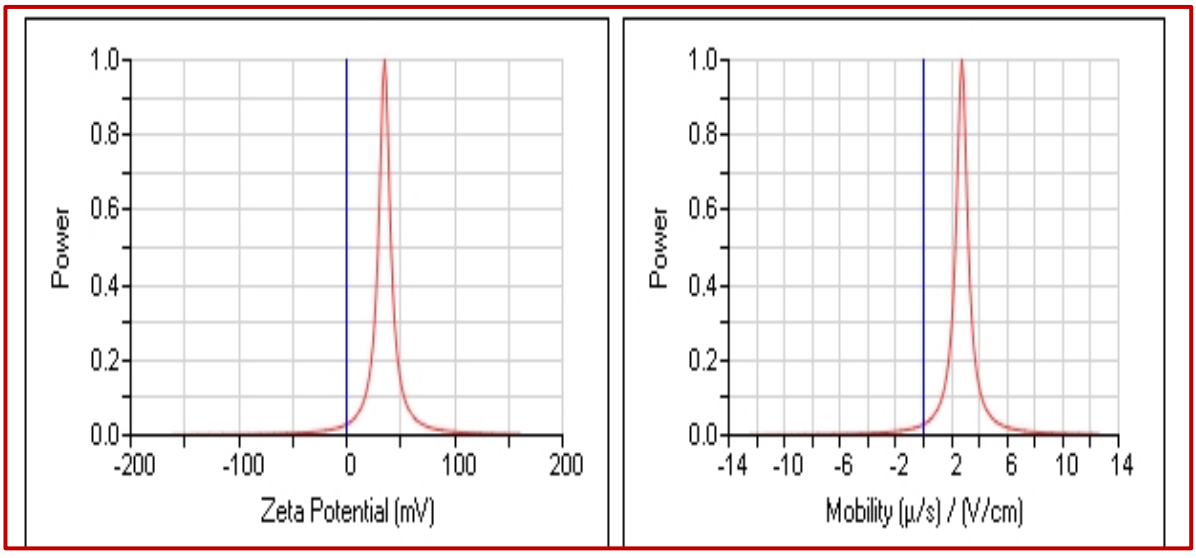

Figure 3.14. Zeta potential curves for PANI/Nb_2O_5/Cr_2O_3

3.1.4.2 Chitosan/Nb_2O_5/MnO_2 and Chitosan/Nb_2O_5/Cr_2O_3

The possibility of physical stability in a formulation is determined by its zeta potential, a measure of the electric potential generated by a charge on a particle surface- either positive or negative depending on particle chemistry. Similar charges on particles are kept apart by repulsion forces, preventing particle agglomeration during storage. Consequently, the zeta potential also assesses the intensity of attraction between like-charged particles in the formulation. The zeta potential alterations are depicted in figure 3.15 and 3.16. Moreover, particle size. The zeta potential is 19.38 mV, the pH is 7.3, and it appears that the pH has an impact. As pH value decreases, the zeta potential rises. Like other employed characterization techniques, the zeta potential of the dispersion of CS/Nb_2O_5/Cr_2O_3 depends on the pH value as shown in Figure (3.15). When the pH rises past the isoelectric point, which is at pH = 5.6, the zeta potential is positive for pH values under 5.5 and negative for pH values above that. The interaction between water ions with nanoparticles determines the zeta-potential.

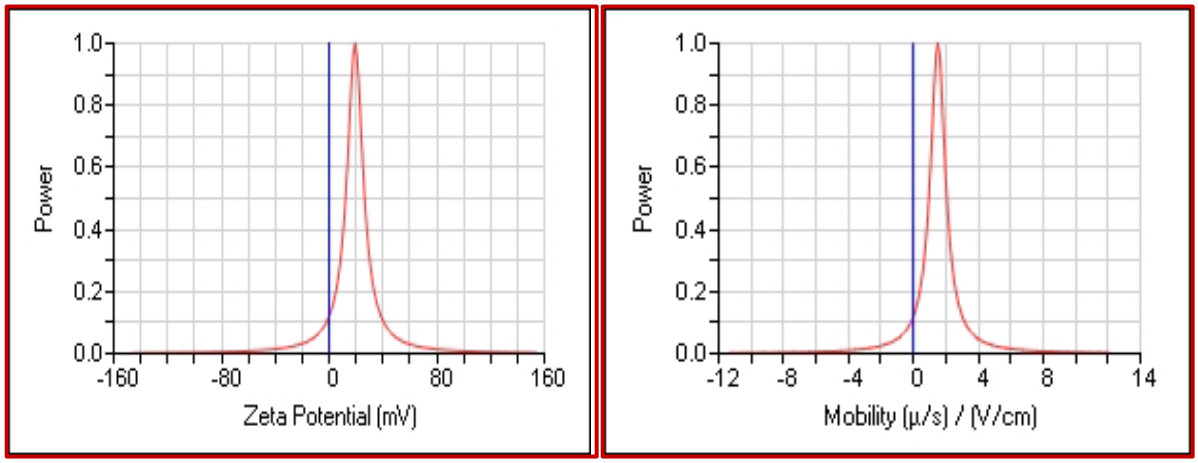

Figure 3.15. Zeta potential curves for CS/Nb_2O_5/Cr_2O_3.

This is due to negatively charged molecules on surfaces repelling negatively charged nanoparticles. However, other researchers believe that there are just a few cationic spots on cell surfaces that can adsorb and bind to negatively charged

particles. They postulated that the numerous negatively charged domains on the cell surface act as an attractor, causing negatively charged NPs to congregate (agglomerate) when they bind to cationic sites. Additionally, the bound NPs diminish the charge density on the cell surface, which might make it easier for other free NPs to bind.

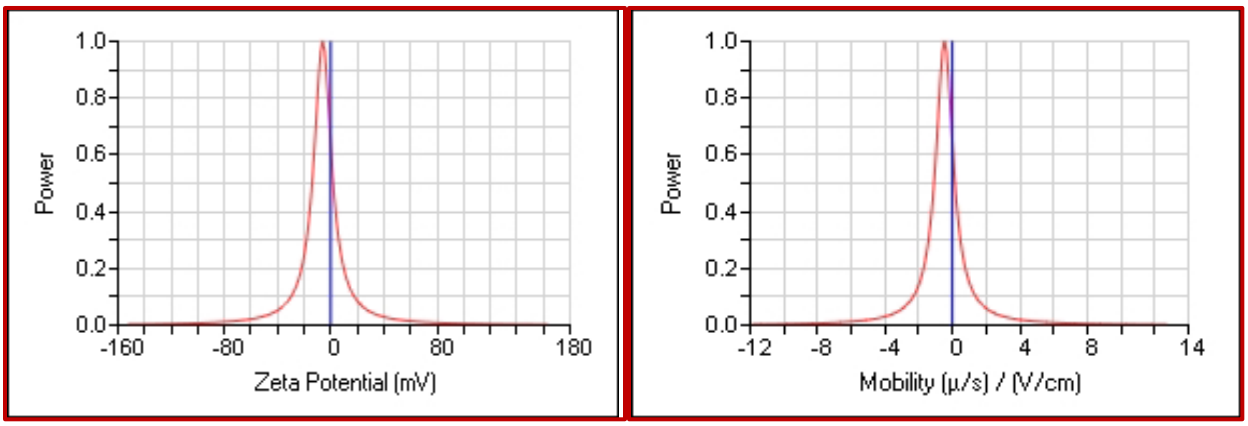

Figure 3.16. Zeta potential curves for CS/Nb_2O_5/MnO_2.

3.1.5 Thermo gravimetric Analyzer (TGA)

3.1.5.1 PANI/Nb_2O_5/MnO_2 and PANI/Nb_2O_5/Cr_2O_3

One of the traditional techniques in this context is thermogravimetric analysis, which analyzes the weight change of a sample as a function of temperature, observes the degradation of polymers, and quantifies the amount of water and other volatile materials lost during the process. Figures (3.17 and 3.18)reveal that the samples exhibit weight loss in three distinct stages; this discovery is consistent with data from past investigations[199, 200]. The initial weight loss is due to the removal of moisture absorbed on the surface and in the polymer lattice. PANI/Nb_2O_5/MnO_2 shows a naturally occurring weight loss between 50 and 100°C, while PANI/Nb_2O_5/Cr_2O_3 shows a weight loss between 63 and 100°C. In the case of PANI/Nb_2O_5/MnO_2, the loss of dopant anions occurs in the second stage between 200 and 450 °C. In contrast, weight loss is observed for

PANI/Nb_2O_5/Cr_2O_3 in the second stage between 220 and 500 °C, which may also be related to the loss of dopant anion (HCl). The PANI/Nb_2O_5/MnO_2 Nanocomposites showed a rapid third-stage weight loss between 520 and 900 °C, while the PANI/Nb_2O_5/Cr_2O_3 Nanocomposites did not. These results demonstrate the increased thermal stability of PANI/Nb_2O_5/MnO_2 and PANI/Nb_2O_5/Cr_2O_3 nanocomposites after contacting Nb_2O_5, Cr_2O_3 and MnO_2 nanoparticles with PANI compared to homopolymer (PANI), as confirmed by FTIR and XRD This point is tested in the previous sections.

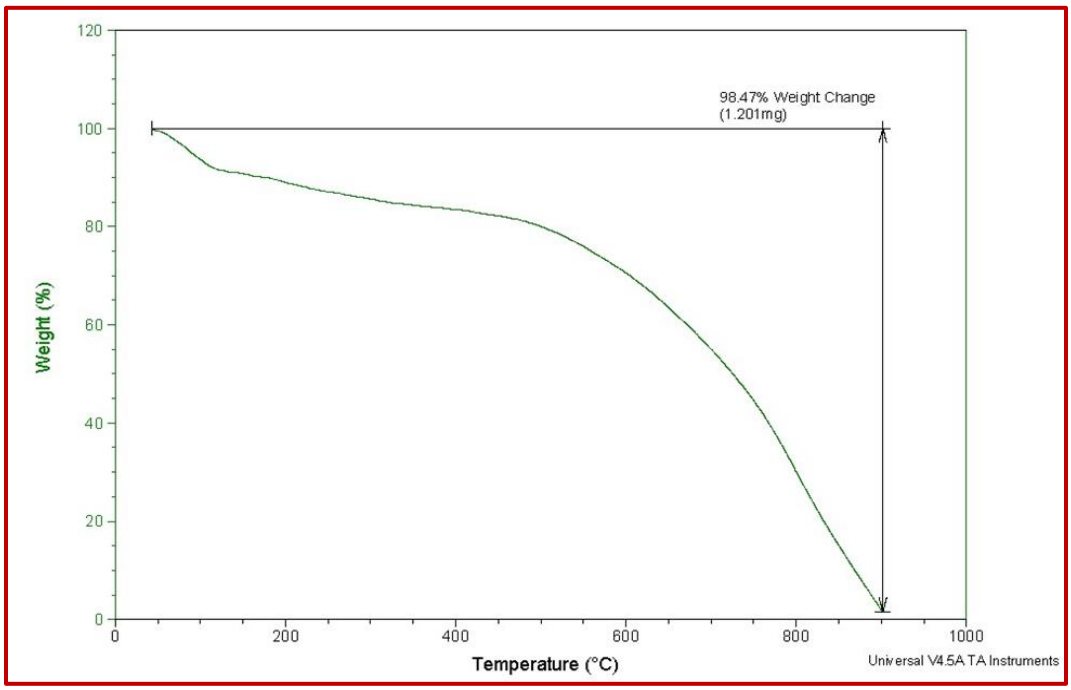

Figure 3.17. TGA curves for PANI/Nb_2O_5/MnO_2 Nanocomposites

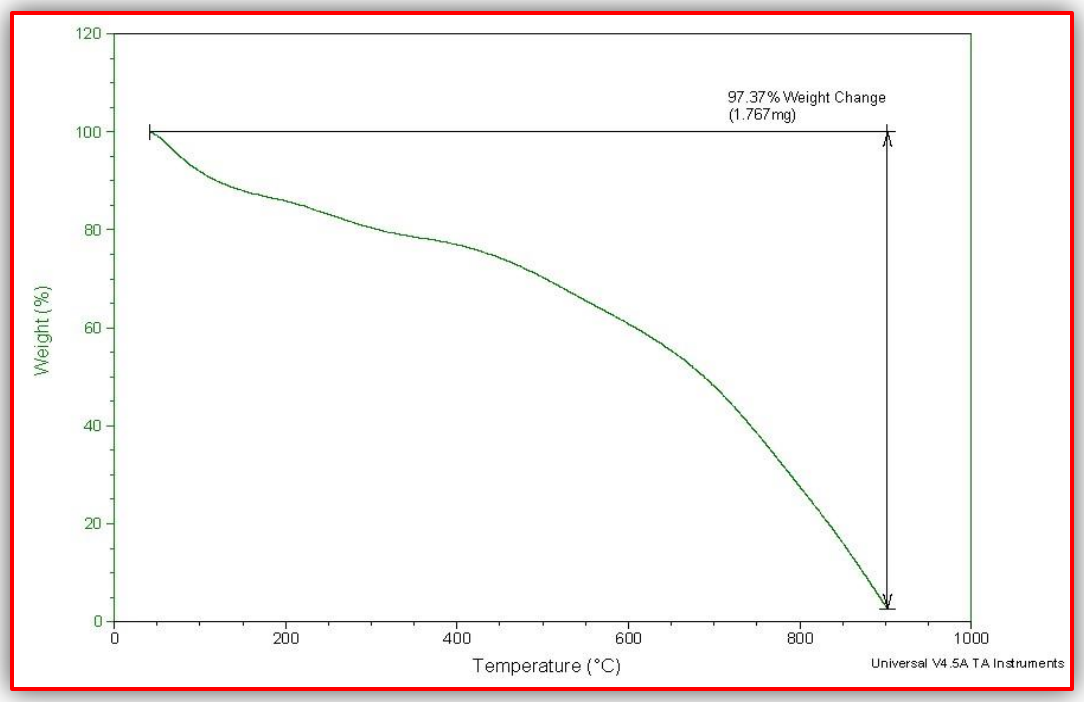

Figure 3.18. TGA curves for PANI/Nb_2O_5/Cr_2O_3 Nanocomposites

3.1.5.2 Chitosan/Nb_2O_5/MnO_2 and Chitosan/Nb_2O_5/Cr_2O_3

As shown in Figures 3.19 and 3.20, the thermal stability of the original CS/Nb_2O_5/MnO_2 and CS/Nb_2O_5/Cr_2O_3 nanocomposites are examined by analyzing TGA from 40 to 900°C. As previously reported, the CS/Nb_2O_5/MnO_2 exhibits weight loss in three stages. The first step began at temperatures between 40 and 100 °C as a result of the elimination of water, and the second stage began at 120 to 390 °C in connection with the deacetylation and depolymerization of chitosan[201, 202]. Final weight loss starts above 410°C, is ascribed to the degradation of the polymer chain. and dissociation chemical interaction of Nb_2O_5 and MnO_2 or Cr_2O_3 nanoparticles with chitosan. The TGA experiments of CS/Nb_2O_5/Cr_2O_3 performed as well to verify their thermal stability The loss of a water molecule and any volatile components between 40 and 135 is considered the first step. The deacetylation and depolymerization of chitosan during the second stage resulted in

unexpected and significant weight loss at 140-350°C. Final weight loss starts above 450°C, is ascribed to the degradation of the polymer chain and dissociation chemical interaction of Nb_2O_5 and Cr_2O_3 nanoparticles with chitosan[203].

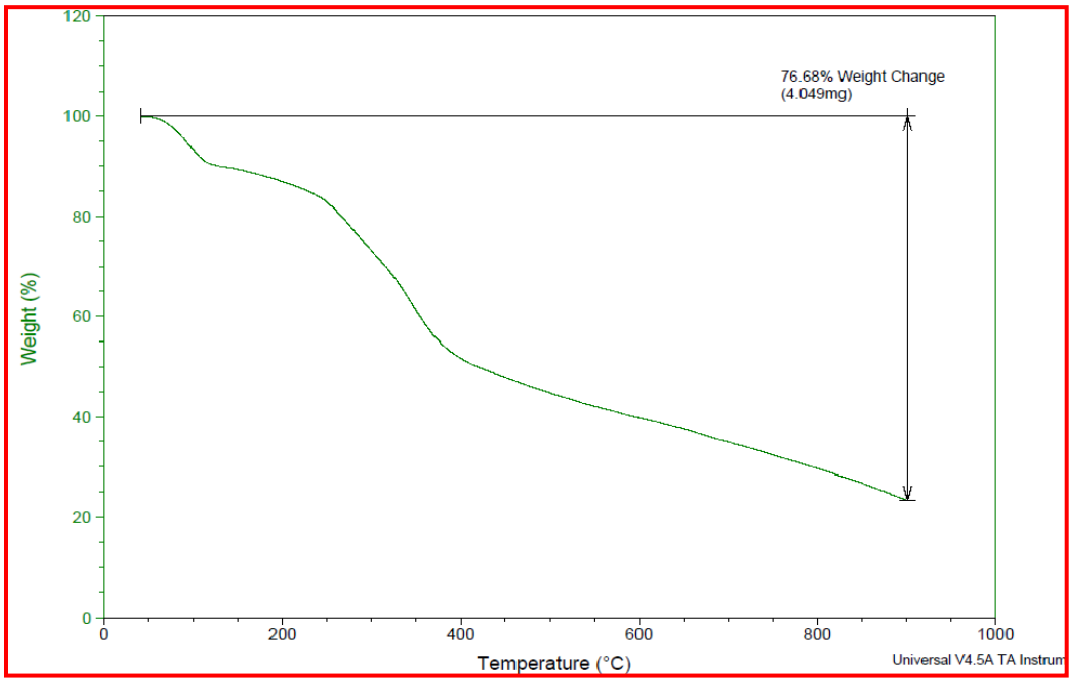

Figure 3.19.TGA curves for CS/Nb_2O_5/MnO_2 Nanocomposites

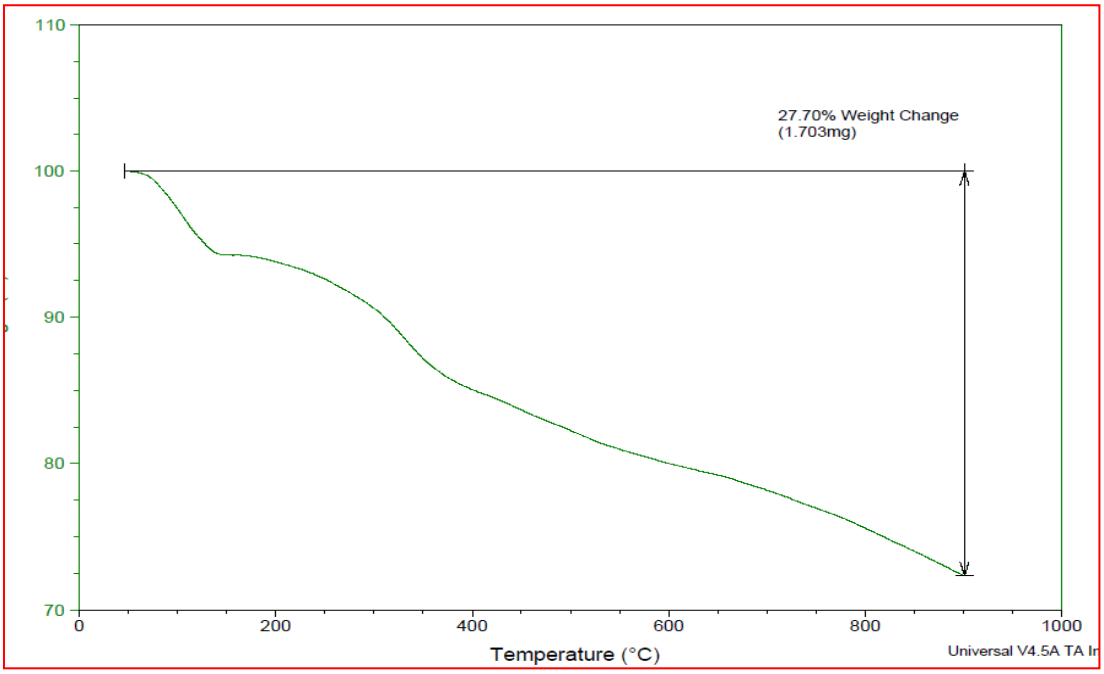

Figure 3.20.TGA curves for CS/Nb_2O_5/Cr_2O_3 Nanocomposites

Applications

Part 1:Adsorpion of methyl orange by using PANI/Nb_2O_5/MnO_2 and PANI/Nb_2O_5/Cr_2O_3

3.2 Adsorption Experiment for methyl orange

The contact time , initial concentration of the MO dye solution, the solution's pH, and the dosage of the adsorbent are the factors that could affect the adsorption characteristics of MO dye on PANI/Nb_2O_5/MnO_2 and PANI/Nb_2O_5/Cr_2O_3. These factor effects on the sample adsorption behaviour are examined, and the findings are discussed in the sections below.

3.2.1 Effect of Adsorbent dosage

In removal examinations, PANI/Nb_2O_5/Cr_2O_3 and PANI/Nb_2O_5/MnO_2 are tested at various adsorbent dosages. Each dose ranged from 10 to 150 mg. A summary of how each adsorbent dose affected the efficiency of removal is shown in Figure 3.21. With constant other conduction (pH = 5.3, Conc. = 15 mg/L, T = 298 K), the efficacy of MO dye removal was significantly improved by increasing PANI/Nb_2O_5/Cr_2O_3 and PANI/Nb_2O_5/MnO_2 from (10 – 50) mg. The initial removal rates for PANI/Nb_2O_5/Cr_2O_3, which were 77%, and PANI/Nb_2O_5/MnO_2, which were 70%, gradually increased until they were, respectively, 87% and 88.5%. It's possible that as adsorbent dosage was increased, more active sites became available, improving the achievement of equilibrium at the 50,100 mg dosage for this experiment. Consequently, for this experiment. As a result, for all future trials, the 50,100 mg adsorbent dosage were selected.

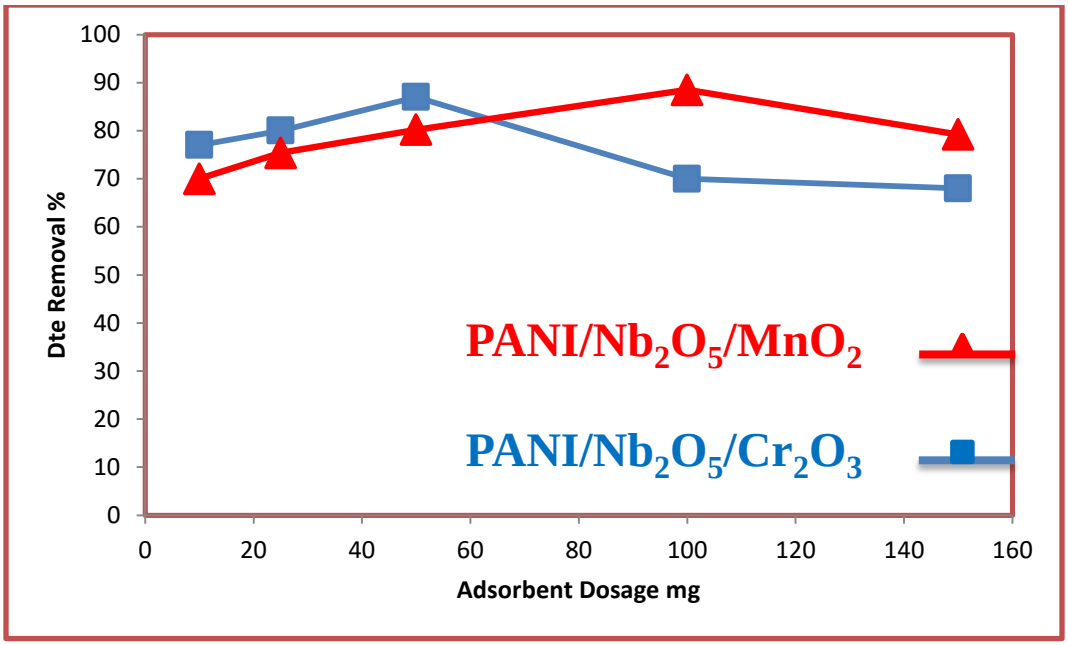

Figure 3.21. Effect of adsorbent dosage to the removal of MO dye

3.2. Effect of Differences in Initial MO Dye Concentrations on the Removal Process

As shown in Fig(3.22), the removal efficiency of PANI/Nb_2O_5/Cr_2O_3 and PANI/Nb_2O_5/MnO_2 was investigated using a variety of initial MO dye concentrations ranging from (1 – 25) mg/L at a fixed 50 mg of PANI/Nb_2O_5/Cr_2O_3 and 100 mg of PANI/Nb_2O_5/MnO_2. This graph shows that as the original concentration of MO dye was increased. Accordingly, When the original MO dye concentration is decrease, the removal effectiveness by the PANI/Nb_2O_5/Cr_2O_3 nanocomposite was high, demonstrating that each of the adsorbents and the MO dye molecules interacted strongly even at low beginning concentrations [204]. Additionally, because to the larger surface area and strong electrostatic interactions, PANI/Nb_2O_5/Cr_2O_3 and PANI/Nb_2O_5/MnO_2 nanocomposite are two possible explanations for the These products effectively remove a high percentage of MO dye.A porosity of the adjusted PANI/Nb_2O_5/Cr_2O_3 and PANI/Nb_2O_5/MnO_2 nanocomposite.

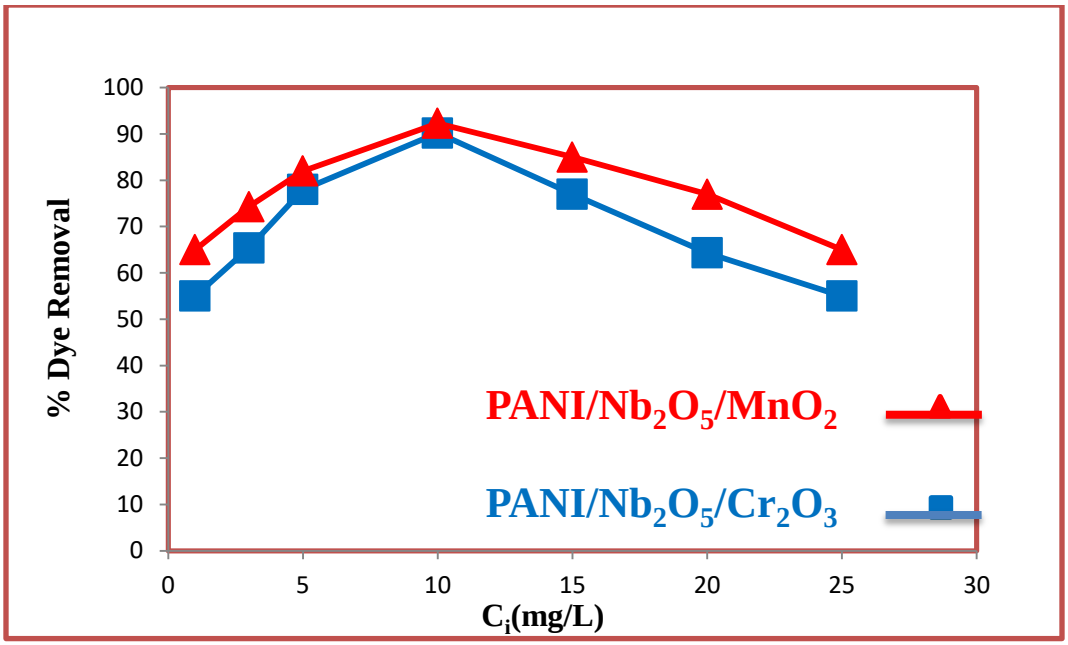

Figure 3.22. Effect of initial concentration of MO dye on removal process

3.2.3 Effect of pH on Removal of MO Dye

Figure (3.23) illustrates how pH affects the proportion of MO dye removed by nanocomposite materials made of PANI/Nb_2O5/Cr_2O_3 and PANI/Nb_2O_5/MnO_2. Additionally investigated are the initial and final (equilibrium) pHs. It is clear that, at all chosen beginning pHs, the PANI/Nb_2O_5/MnO_2 nanocomposite outperformed PANI/Nb_2O_3/Cr_2O_3 in the removal of MO dye from aqueous solution (from 2 - 10). 0.1 M HCl or 0.1 M NaOH were used to regulate the pH during an experiment, and a pH meter was used to record the results. The orbital shaking speed, quantity of both adsorbents, and solution temperature were all altered while the starting MO dye concentration was held constant at 25 mg/L, 300 rpm, 50,100 mg, and 298 K. The findings of all the best studies pointed to the following PANI/Nb_2O_5/Cr_2O_3 adsorbents performed better at pH 9 and PANI/Nb_2O_5/MnO_2 adsorbents at pH 7, respectively. Based on an estimated pKa value of MO.As a result, it becomes protonated at the initial pH values of 2 and 3 (pH is less than the pKa of MO), where it is primarily present in anionic form. Additionally, the presence of basic

amine groups causes PANI to build a positive charge on its conductive backbone in an acidic media. Consequently, at initial acidic pH values, there was a significant degree the removal rates of adsorbents were a result of electrostatic attraction between the positively charged PANI strength and protonated MO dye molecules. PANI/Nb_2O_5/Cr_2O_3 nanocomposites for MO dye removal to decline [205, 206]. The preferred initial pH range was(2 to 8), with neutral being the best value (about 94.20 %PANI/Nb_2O_5/Cr_2O_3 and 95.37 % nanocomposites). This was because at neutral pH, The MO would primarily take the anionic form, increasing the number of electrostatic interactions between the MO dye and PANI/Nb_2O_5/Cr_2O_3 and PANI/Nb_2O_5/MnO_2 adsorbents.

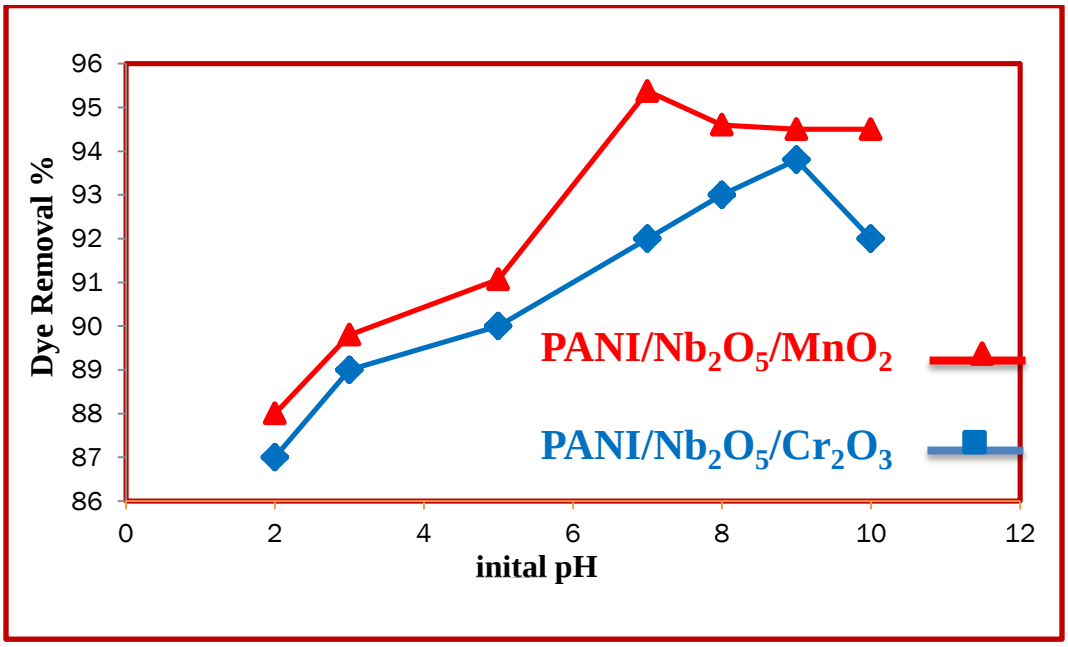

Figure 3.23. Effect of pH on removal of MO Dye

3.2.4 Effect of Adsorption Time

Another important factor in the color removal process is the adsorption time. Through a series of adsorption experiments with adsorption times between 10 and 120 minutes, impact of adsorption duration on MO dye's adhesion to the PANI/Nb_2O_5/Cr_2O_3 and PANI/Nb_2O_5/MnO_2 adsorbents were investigated. The

results are shown in Figure (3.24). For each of the adsorbents, it is obvious that the removal rate of MO dye increases from 10 to 60 min and then stays constant from 60 min to 120 min. Thus, following detour shaking for 60 min, the MO dye adsorption equilibrium is attained. It should be noted, however, that the rate of MO dye removal was extremely rapid during the first 10 min, during which time the MO dye molecules were adsorbent to around 94.2% of the PANI/Nb_2O_5/Cr_2O_3 and 97.75 % by the PANI/Nb_2O_5/MnO_2 adsorbents, before slowly and gradually increasing until equilibrium was reached at roughly 60 min. Because there were several active sites available for MO dye molecules on both adsorbents' surfaces [207]. the initial rapid removal of MO dye was explained. The number of active sites that could be removed decreased over time as the removal time rose, and the pushing force decreased, resulting in a slow removal rate. As a result, the optimal adsorption time for subsequent research was chosen to be 60 minutes.

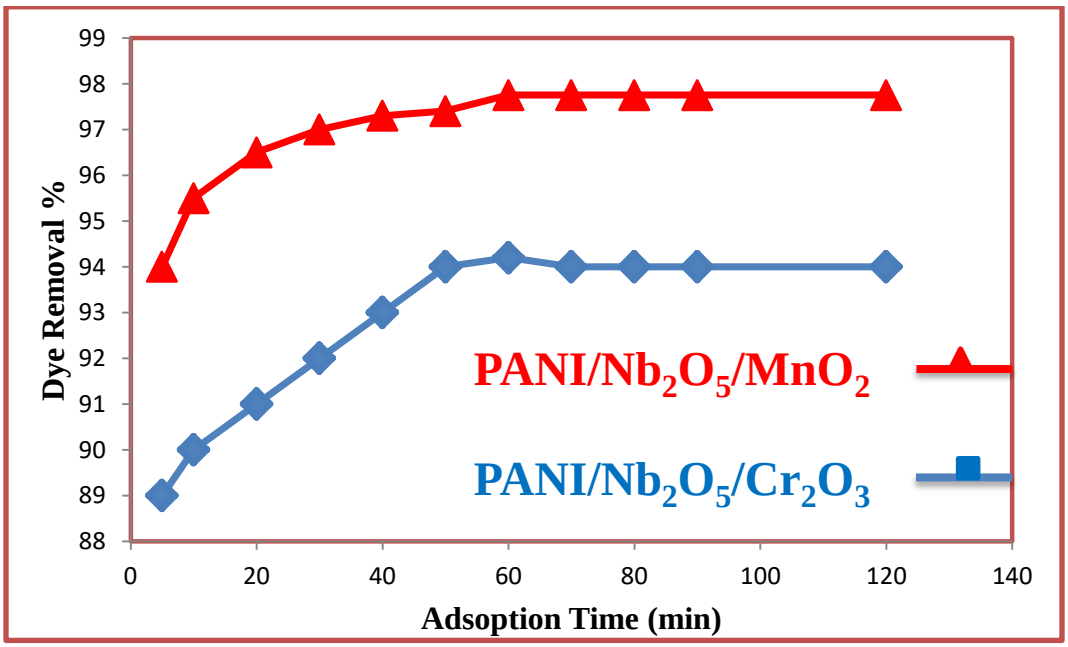

Figure 3.24. Effect of Adsorption time on removal of MO Dye

3.4 Adsorption isotherms for methyl orange

When utilized with 100 mL solutions of MO dye at room temperature (298 K), it is discovered experimentally that the PANI/Nb_2O_5/Cr_2O_3 and PANI/Nb_2O_5/MnO_2 adsorbents' adsorption capacities are optimal at pH 9 or pH 7, respectively (Figure 3.25a). The PANI/Nb_2O_5/Cr_2O_3 and PANI/Nb_2O_5/MnO_2 materials' maximum adsorption capacities This figure shows that the adsorbents have similar amounts, 148 mg/g and 84 mg/g, respectively. To analyze the adsorption data and determine the maximum adsorption capacity (q_m) for the appropriate adsorbent, three fundamental isotherm models specifically the Langmuir, Freundlich, and Temkin models are applied[208]. The curves for the isotherm parameters for the linearized equation for MO dye removal at 298 K. Table (3.1) lists the three equations for the isotherm models of adsorption at room temperature along with their maximum adsorption capacities (q_m), correlation coefficients (R^2), and other information. The Langmuir model was based on a number of assumptions, including the adsorbate's monolayer adsorption on an even surface of the adsorbent. In order to achieve adsorption, chemisorption also takes place at predetermined homogeneous sites inside the adsorbent. In Eq. (3.1), the Langmuir equation is presented [74, 209].

$$\frac{\mathbf{Ce}}{\mathbf{qe}} = \frac{\mathbf{Ce}}{\mathbf{qm}} + \frac{\mathbf{t}}{\mathbf{qmKL}} \ldots\ldots\ldots\ldots (\mathbf{3.1})$$

Where: qm and qe are the maximum and empirical adsorption capacities of the MO dye, respectively, expressed in q_e mg/g and C_e, respectively. is the quantity of MO dye that is remaining in the solution following the adsorption procedure, and KL is the Langmuir constant (L/ mg). C_e/q_e against C_e is plotted to evaluate the adsorption capability. In Figure 3.24b

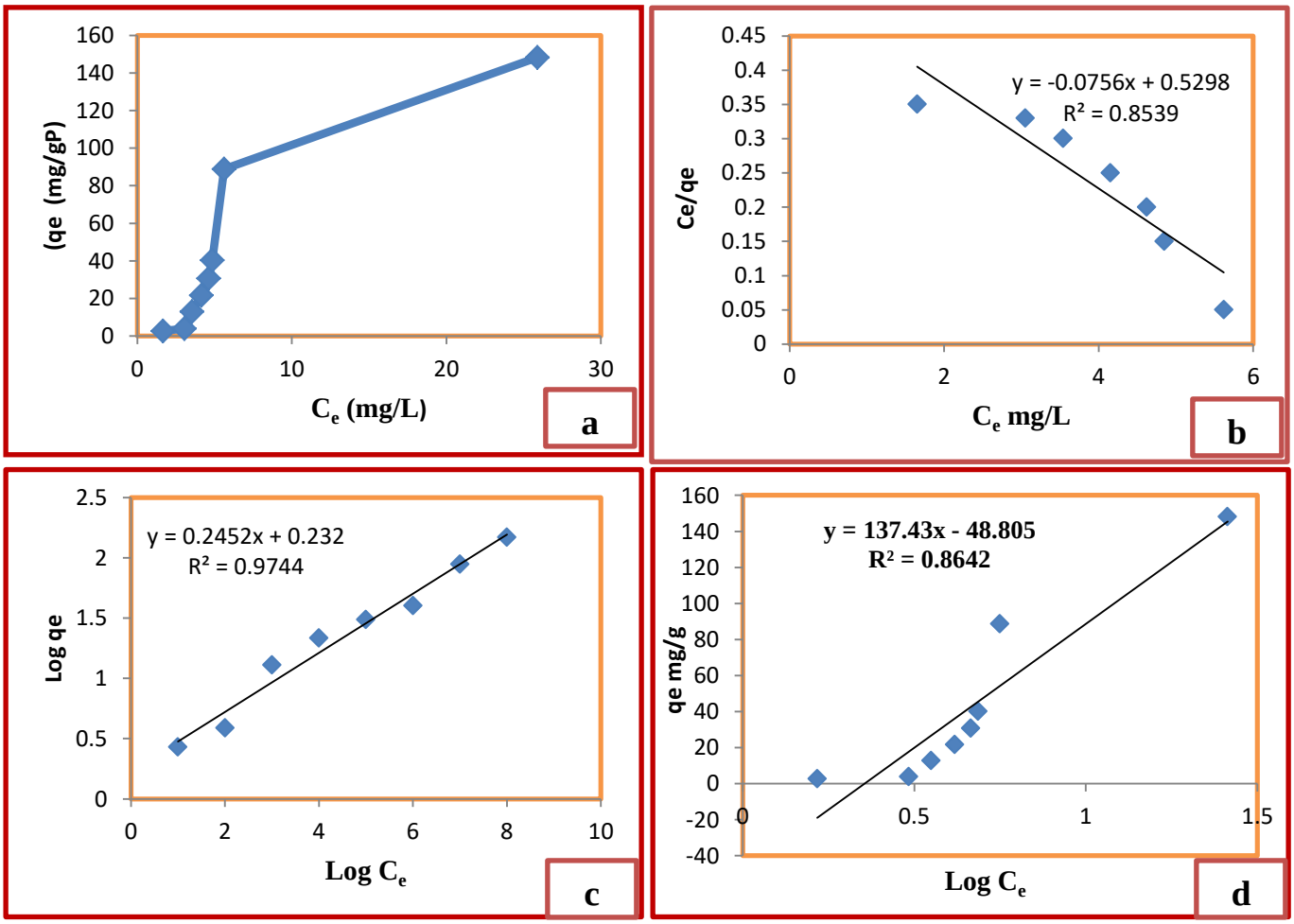

Figure 3.25a Adsorption isotherms of MO onto PANI/Nb_2O_5/Cr_2O_3 adsorbents (conditons: pH 9; dosage=50 mg; volume=100 mL; time=60 min; temperature=298 K); fitting the adsorption isotherm curves of MO dye of adsorbents: b Langmuir isotherm model, c Freundlich isotherm model, and d Temkin isotherm.

where qm and KL are estimated using the gradient and intercept of this (straight) line, respectively. In order to match multilayer adsorption onto a heterogeneous surface, the Freundlich model is utilized, and the supposed adsorption mechanism is physisorption, which is brought on by van der Waals interactions. The Freundlich equation is given by Eq. (3.2) [210].

$$\log qe = \log KF + \frac{1}{n} \log ce \quad \ldots\ldots\ldots (3.2)$$

Freundlich constant (K_F), adsorption capacity (mg/g), and heterogeneity factor (n), which denotes the bond distribution, are all defined in Eq. (3.1). The Freundlich linear equation is identified by plotting log q_e versus log C_e. The intercept and slope of this linear connection are then used to compute K_F and n with accuracy (Figure 3.24c). The Temkin equation is given in equation (3.3), and the Temkin isotherm model relies heavily on the heterogeneous surface energy and non-uniform distribution of sorption heat on adsorbents. [211].

$$\mathbf{qe} = \mathbf{A} + \mathbf{B}\,\mathbf{log}\,\mathbf{Ce} \ldots\ldots\ldots (\mathbf{3.3})$$

Where:

The heat of sorption constant (J/mol) and the Temkin isotherm constant (L/g) are the two constants, respectively. The Temkin linear equation is obtained by plotting q_e against log C_e (Figure 3.24d). The values of B and A are provided by the gradient and intercept of the straight line, respectively.. The Langmuir, Freundlich, and Temkin models' estimated parameters are provided in)The experimental equilibrium capacities (qe) and coefficients of determination (R^2) for the fit of the experimental data to the three isotherms show that the Freundlich isotherm appears to best describe the adsorption of MO dye against Polyaniline/Nb_2O_5/Cr_2O_3 and PANI/Nb_2O_5/MnO_2 adsorbents. This suggests that the adsorption mechanism is multilayer in nature and that the polyaniline/Nb_2O_5/Cr_2O_3 and polyaniline/Nb_2O_5/MnO_2 adsorbents both exhibit significant MO dye adsorption sites. [212].

Table 3.1. Adsorption Langmuir, Freundlich, and Temkin model isotherm parameters for MO dye by PANI/Nb_2O_5/Cr_2O_3 and PANI/Nb_2O_5/MnO_2

Isotherms	Parameters	PNAI/Nb_2O_5/Cr_2O_3	PNAI/Nb_2O_5/MnO_2
Langmuir	**Q_m**	**142**	**115**
	K_L	**0.18**	**0.45**
	R^2	**0.8895**	**0.915**
Freundlich	**K_F**	**1.8**	**3.02**
	n	**4**	**2.37**
	R^2	**0.974**	**0.94**
Temkin	**A**	**137**	**33.2**
	B	**48**	**2.38**
	R^2	**0.864**	**0.966**

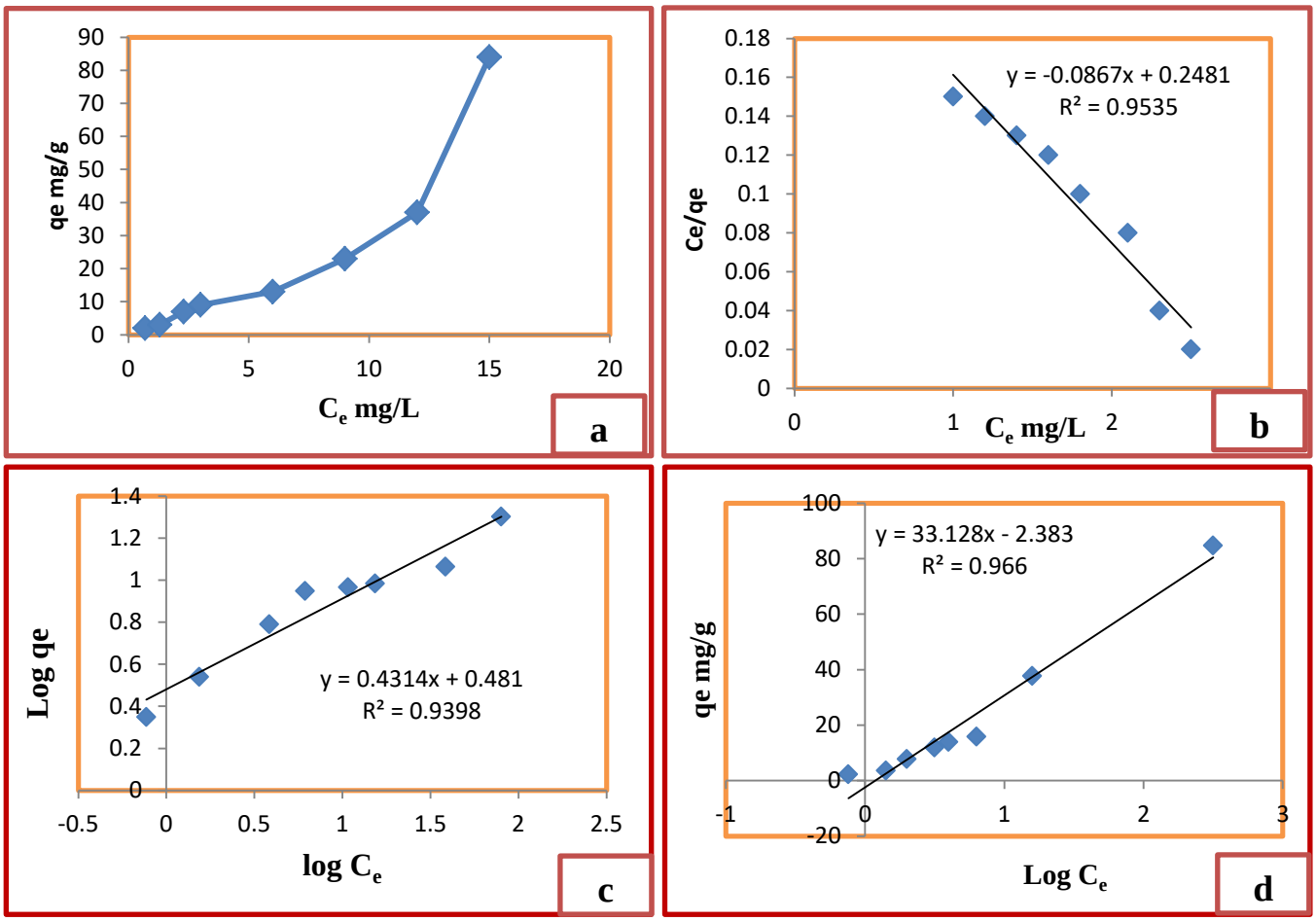

Figure 3.26. a Adsorption isotherms of MO onto PANI/Nb_2O_5/MnO_2 adsorbents (conditions: PH 7; dosage=100 mg; V=100 mL; time=60 min; T=298 K); fitting the adsorption isotherm curves of MO dye of adsorbents: b Langmuir isotherm model, c Freundlich isotherm model; d Temkin isotherm model

3.5 Suggested Mechanism for methyl orange dye Decolorization

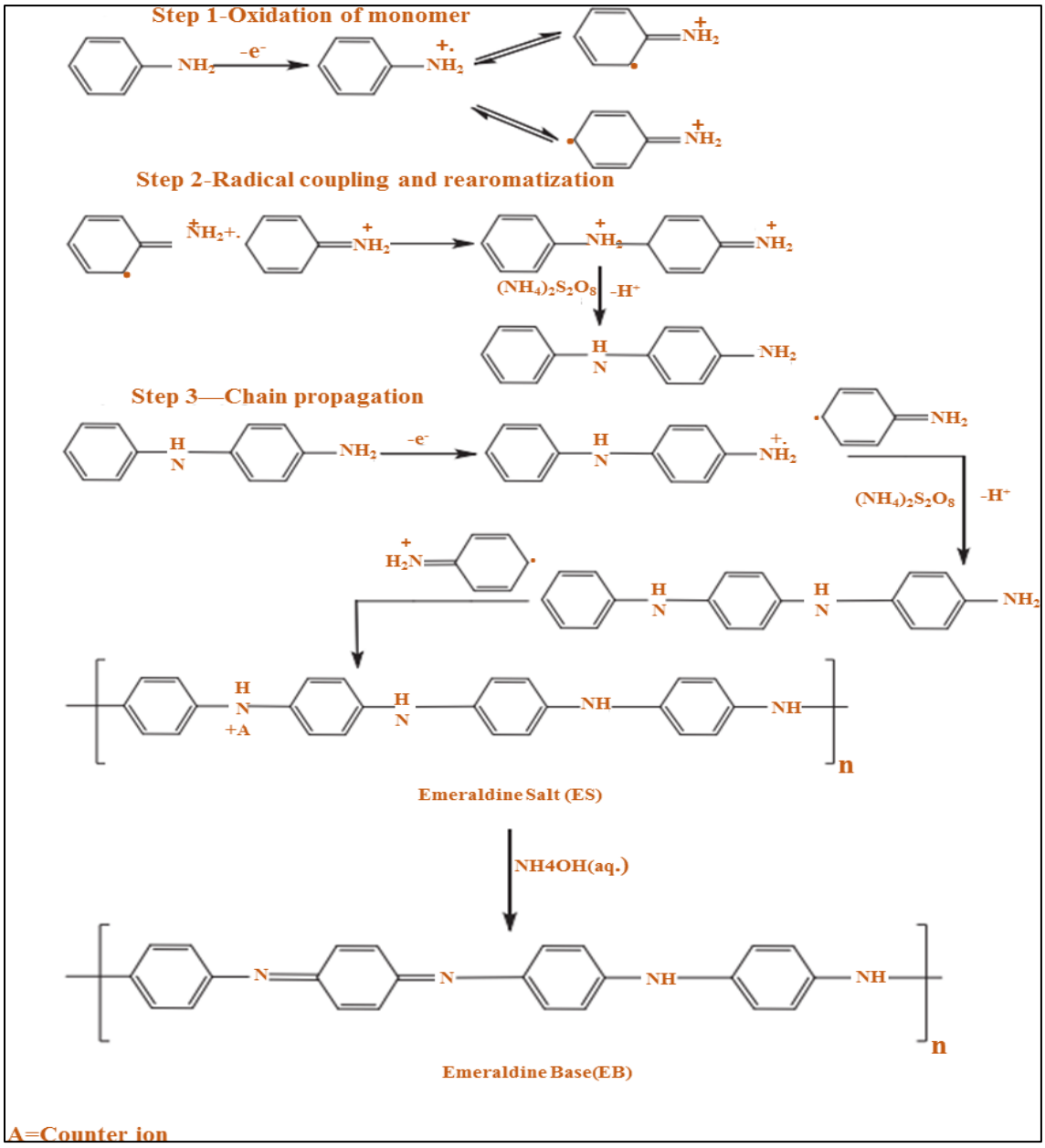

Figure 3.27. PANI with oxidative polymerization of aniline

(a) **(b)**

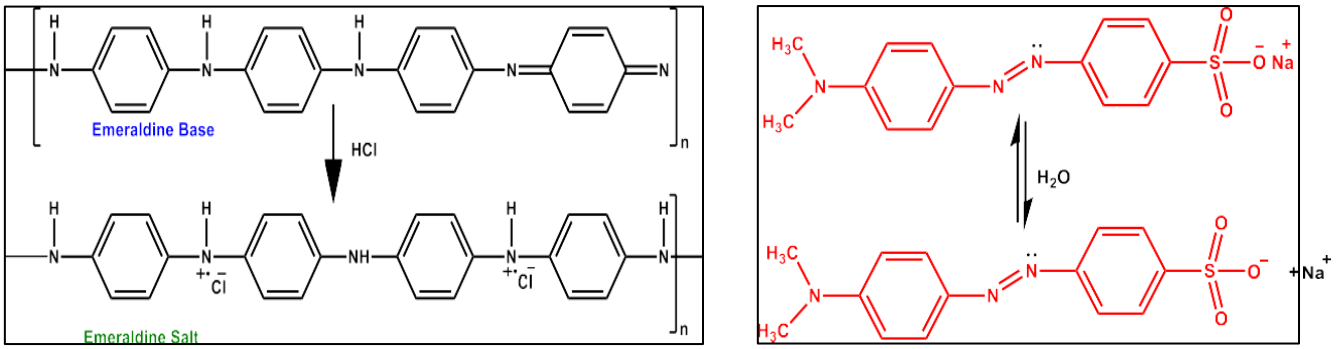

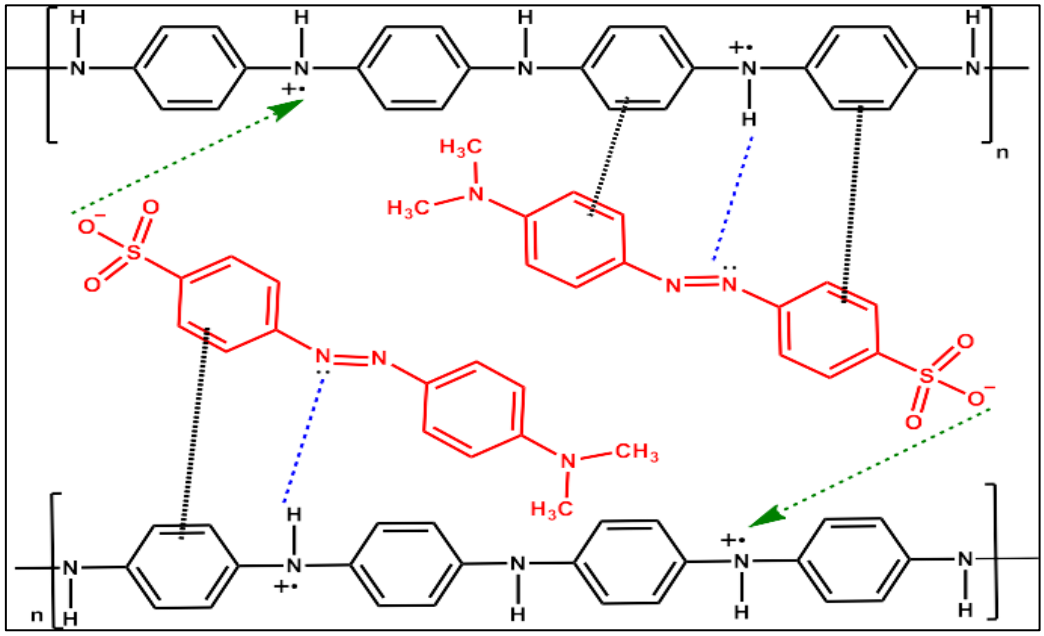

(c)

Electrostatic interaction

…… π-π interaction

…… Hydrogen bonding

Figure 3.28 a Chemical structure of PANI, b dissociation of MO in aqueous solution, and c mechanism for the adsorption of the anionic MO dye onto the emeraldine salt of the PANI nanocomposite

Part 2: Adsorption of bromocresol green by using $CS/Nb_2O_5/MnO_2$ and $CS/Nb_2O_5/Cr_2O_3$

3.6 Adsorption Experiment for bromocresol green

The contact time, initial concentration of the BCG solution, the solution's pH, and the dosage of the adsorbent are the factors that could affect the adsorption characteristics of BCG on For $CS/Nb_2O_5/MnO_2$ and $CS/Nb_2O_5/Cr_2O_3$. These factors' effects on the samples' adsorption behaviour are examined, and the findings are discussed in the sections below.

3.6.1 Effect of pH on BCG dye Removal

The pH level of a sample has a significant impact on the nature, surface characteristics, and ionization/dissociation of the adsorbate molecule in question. When utilizing nanocomposites materials such as $CS/Nb_2O_5/Cr_2O_3$ and $CS/Nb_2O_5/MnO_2$, the absorption of BCG is heavily influenced by the pH range of 5–12.0, with a better dye removal being observed at acidic pH levels due to electrostatic interaction between the dye and nanocomposites [213]. To regulate pH during experiments, 0.1 M HCl or 0.1 M NaOH is employed and the pH meter records the results. The concentration of BCG dye remained constant at 5 mg/L, 300 rpm, 100 mg, and 298 K for $CS/Nb_2O_5/MnO_2$, and at 10 mg/L, 300 rpm, 250mg, and 298 K for $CS/Nb_2O_5/Cr_2O_3$. The pH played a significant role in the adsorption efficiency of both compounds, with $CS/Nb_2O_5/MnO_2$ reaching its highest efficacy at pH 7 (approximately 81.86 %) and $CS/Nb_2O_5/Cr_2O_3$ at pH 10 (around 67.4 %). As the pH levels rose above 12, the efficacy of both compounds began to decline. Figure (3.29) visually displays this trend. At baseline pH levels above 7, the adsorbent surface underwent debutination and rejected OH ions, which decreased the adsorption capacity [39,40]. However, at lower pH levels, the

amino group on the surface of chitosan is able to attract hydroxonium ions from the solution and enhance the adsorption capacity [214]. Nevertheless, in acidic or basic solutions, the adsorption capacity decreased due to the competition for adsorption sites between the dye and excess H+ and OH ions.

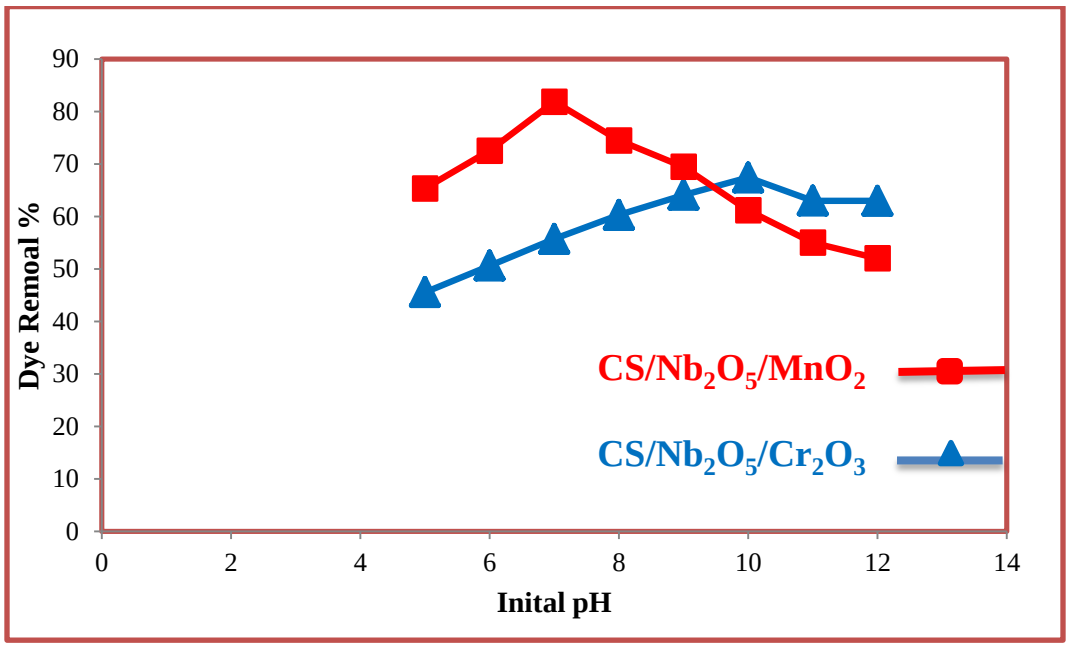

Figure 3.29. Effect of pH on BCG dye removal

3.6.2 Effect of adsorbent dosage

Removal tests employing different dosages of $CS/Nb_2O_5/Cr_2O_3$ and $CS/Nb_2O_5/MnO_2$, ranging from 25 to 650 mg, are conducted to investigate the effects of adsorbent dosage on BCG dye clearance. The impact of adsorbent dose on removal efficacy is shown for each in Figure (3.30). It is demonstrated that raising the adsorbent dosage for $CS/Nb_2O_5/Cr_2O_3$ from 100 to 550 mg and for $CS/Nb_2O_5/MnO_2$ from 25 to 150 mg significantly boosted the removal efficacy of the BCG dye from 67.4 to 78.4% and 81.86 to 90.65 %, respectively. This may be because more active sites became available when the adsorbent dosage was raised, and eventually, at a dosage of 550, 150mg, the associated equilibrium is established. In light of this, an adsorbent dosage of 550,150 mg for

$CS/Nb_2O_5/Cr_2O_3$ and $CS/Nb_2O_5/MnO_2$ respectively are chosen for other experiments.

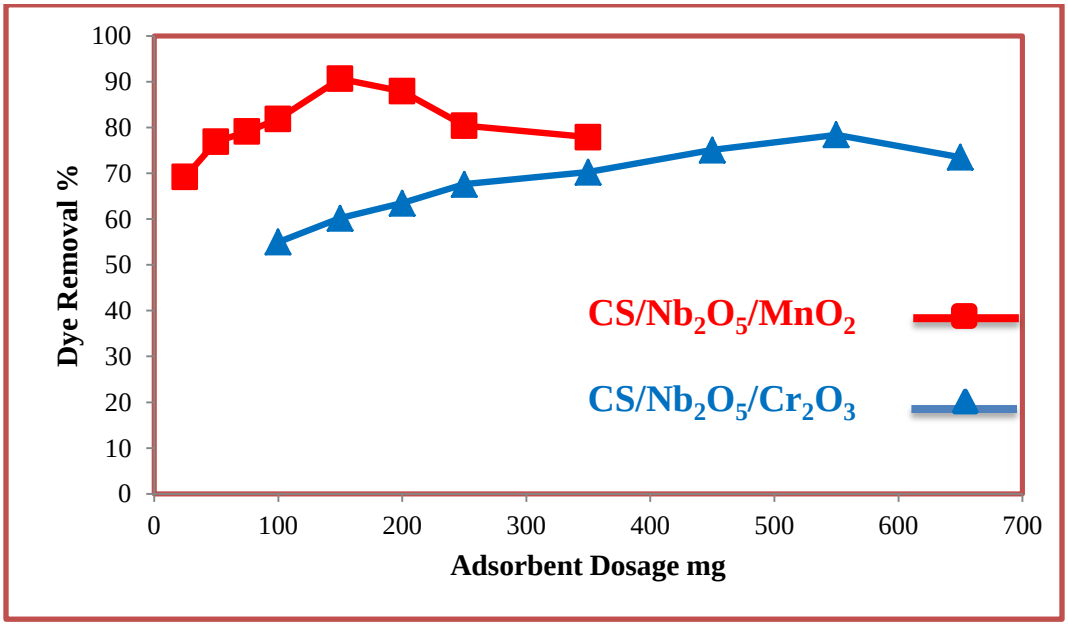

Figure 3.30. Effect of adsorbent dosage on the removal of BCG dye

3.6.3 Influence of differences in removal process of BCG dye initial concentration

As shown in Figure (3.31), the initial dye concentration has a considerable impact on the adsorption potentials of the adsorbents. Both the $CS/Nb_2O_5/Cr_2O_3$ and $CS/Nb_2O_5/MnO_2$ systems are used in this experiment, and the BCG concentrations varied from 1 to 25 mg/L. The adsorbent dosage, time interval, pH, and temperature are all kept constant at 550, 150 g, 30 min, pH=10,7, and 298 K, respectively. The percentage of BCG that is adsorbed diminishes as BCG concentration decrease because there are not enough surface sites to accommodate the dye's concentration.. Additionally, it can be linked to the fact that the accessible solutes are absorbed more quickly when the BCG concentration is lower [215]. Additionally, the high percentage of MO dye removal by $CS/Nb_2O_5/Cr_2O_3$ and $CS/Nb_2O_5/MnO_2$ nanocomposites materials may be explained by their stronger

electrostatic interactions as well as their higher surface areas. The modified $CS/Nb_2O_5/Cr_2O_3$ and $CS/Nb_2O_5/MnO_2$ Nanocomposites porosity.

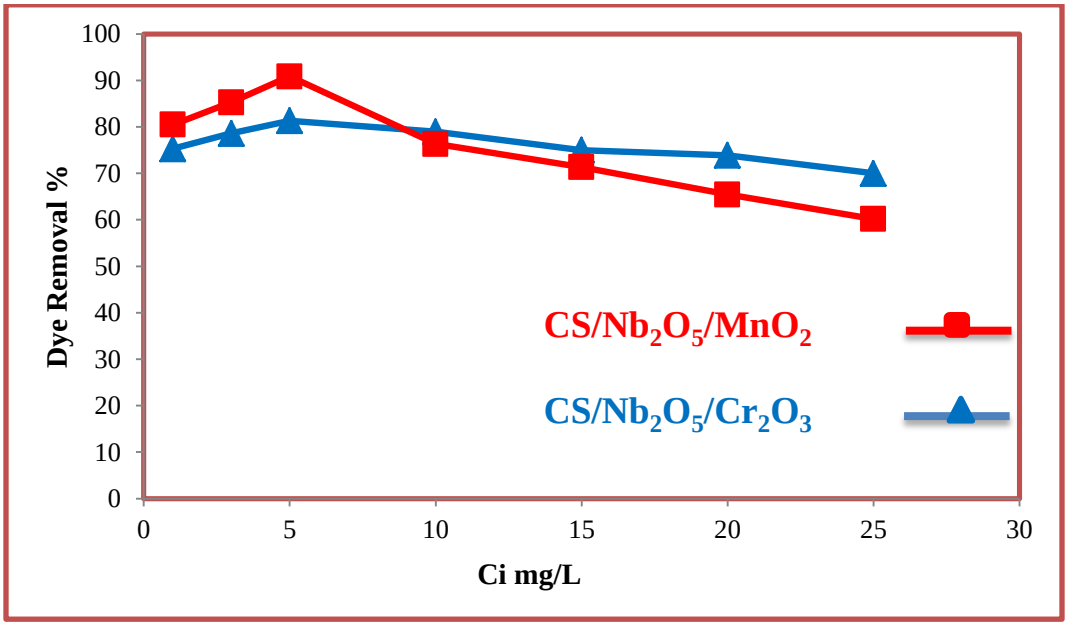

Figure 3.31. Effect of initial concentration of MO dye on removal process

3.6.4 Effect of Temperature on BCG Dye Removal

One of the most important aspects in determining the type of the adsorption process is the effect of temperature on adsorption. Figure (3.32) illustrates the relationship between temperature and BCG adsorption, which is studied at a temperature range of 293-333K with fixed other conduction (550 mg, 5 mg/L, and pH 10 for 30 min for $CS/Nb_2O_5/Cr_2O_3$, and (150 mg, 5 mg/L, and pH 7 for 30 min for $CS/Nb_2O_5/MnO_2$, respectively). For $CS/Nb_2O_5/Cr_2O_3$, bromocresol green dye is rapidly adsorbed from 298 to 323 K, whereas slow adsorption from 323 to 333 K produced the highest clearance percentages (88.5% at 313 K). although the ideal conditions for both adsorption and dye removal are at 298 K (removal percentage 90.65% for $CS/Nb_2O_5/MnO_2$ [216]. The capacity of the adsorbent to adsorb a particular molecule in equilibrium can fluctuate depending on temperature. The adsorption of the dye reduces with rising temperature, indicating an exothermic

adsorption process, whereas a fall in temperature indicates an endothermic adsorption reaction. In addition to the low temperature of the species that are adsorbed and the limited number of active sites, the physical connection between both organic compounds, including dyes and the active sites of adsorption, reduced with rising temperature.[217, 218].

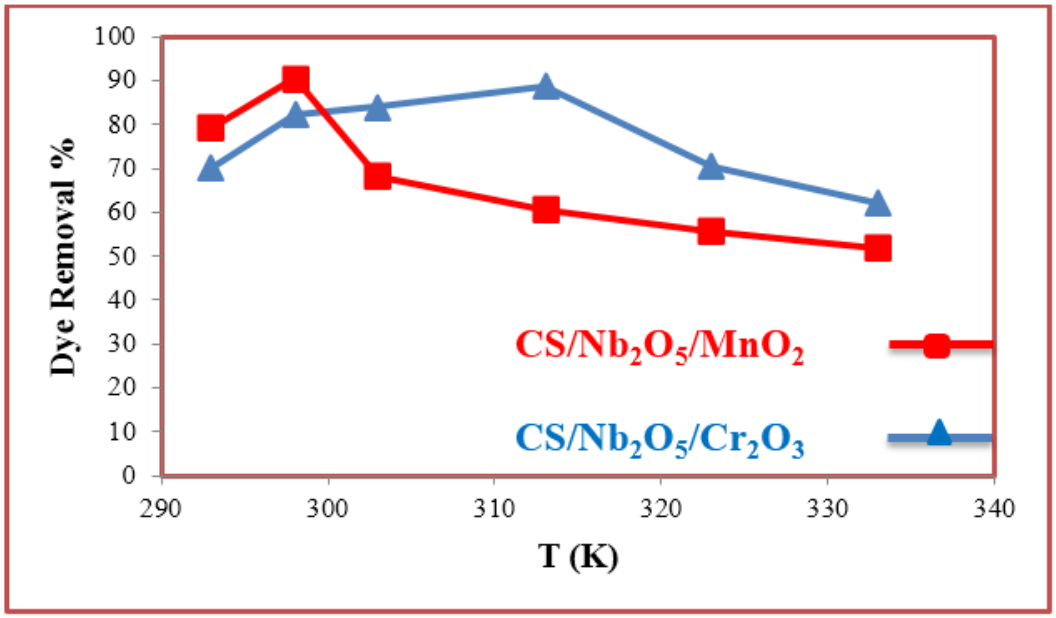

Figure 3.32. Effect of Temperature of BCG dye on removal process.

3.6.5 Effect of equilibrium Time

Another important the adsorption time is a factor in the color removal process. The effects of adsorption time on the adsorption of BCG dye onto various surfaces were examined in a series of experiments with adsorption times between 10 and 120 minutes. the $CS/Nb_2O_5/Cr_2O_3$ and $CS/Nb_2O_5/MnO_2$ adsorbents were investigated. The outcomes are displayed in Figure(3.33). At the beginning of the adsorption phase, a sharp increase in the percentage adsorbed was seen. This is because there were a lot of positively charged surfaces on the adsorbent at first, which enhanced the concentration gradient and the adsorption process' driving force. After 10 minutes, equilibrium concentration was reached. that the rate of

BCG dye removal was extremely rapid during the first 10 min, during which time approximately 88.5% of the BCG dye molecules were adsorbed by the $CS/Nb_2O_5/Cr_2O_3$ and 90.65% by the $CS/Nb_2O_5/MnO_2$ adsorbents. Due to the existence of additional adsorption sites and a high solution concentration, the anions in BCG quickly interacted with the chitosan during the initial contact time, resulting in this high rate of adsorption [219].

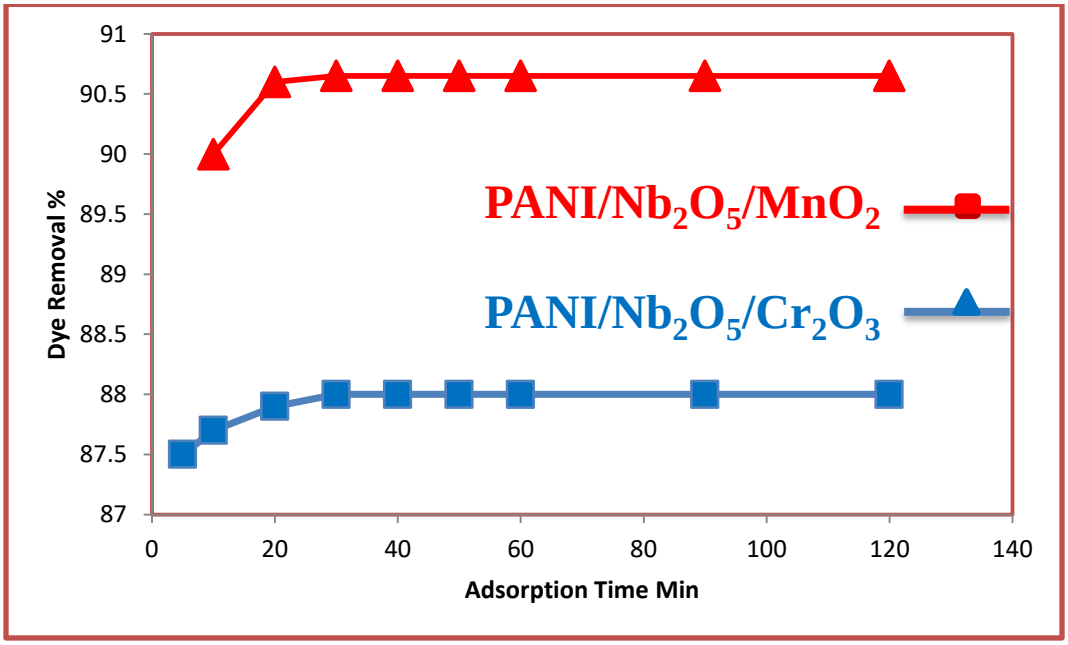

Figure 3.33. Effect of Adsorption time on removal of BCG dye.

3.7 Recyclability Study for $CS/Nb_2O_5/MnO_2$ and $CS/Nb_2O_5/Cr_2O_3$

The $CS/Nb_2O_5/MnO_2$ and $CS/Nb_2O_5/Cr_2O_3$ nanocomposite's excellent recyclability suggests that the method may actually be useful for water purification. Under the ideal conditions described below, the recyclability was tested for 4 consecutive BCG dye adsorption-desorption cycles. For $CS/Nb_2O_5/Cr_2O_3$: pH 10; dosage: 550 mg; volume: 100 mL; time: 30 min; temperature: 313 K; and for $CS/Nb_2O_5/MnO_2$: PH 7; dosage: 150 mg; volume: 100 mL; time: 30 min; temperature: 298 K. The consumed quantity was magnetized out

of the aqueous solution, rinsed with ethanol and deionized water, dried at 75 °C for four hours, and then put back into use for the following cycle of BCG dye adsorption. After then, it was discovered that the adsorption efficiency for the $CS/Nb_2O_5/MnO_2$ and $CS/Nb_2O_5/Cr_2O_3$ mixtures had both decreased from 90.65% to 82% and from 88.55% to 80.1%, respectively. As shown in the Figure (3.34)

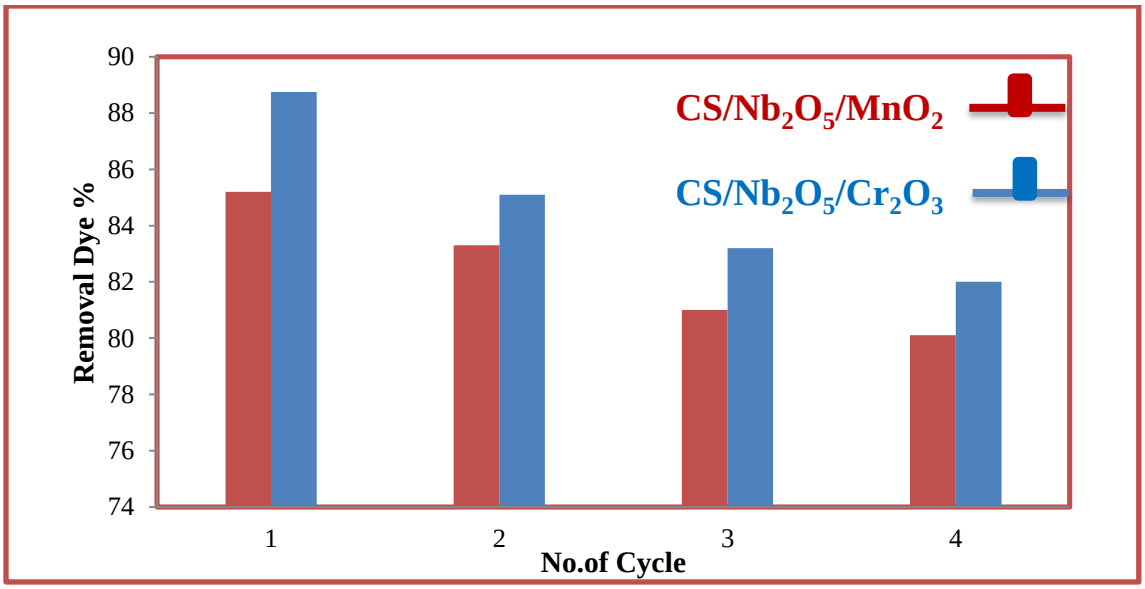

Figure 3.34. Number of adsorption-desorption cycles of $CS/Nb_2O_5/MnO_2$ and $CS/Nb_2O_5/Cr_2O_3$ MO dyes (Conditions: pH 7.10; Dose = 150,550 mg; Ci = 5 mg/L; V = 100 ml; Time = 10 min; T = 298.313 K).

3.8 Adsorption isotherms for bromocresol green

From experimentation using 100 mL solutions of BCG dye ranging from 5-150 mg/L at ambient temperature (298 K), it is observed that pH levels of 10 and 7 are optimal for the $CS/Nb_2O_5/Cr_2O_3$ and $CS/Nb_2O_5/MnO_2$ adsorbents, respectively. In terms of adsorption capacity, the $CS/Nb_2O_5/Cr_2O_3$ and $CS/Nb_2O_5/MnO_2$ adsorbents demonstrated maximum capacities of 43 mg/g and 93 mg/g, respectively, as shown in the presented Figure 3.35a. To determine the maximum adsorption capacity (qm) for the appropriate adsorbent, data analysis and application of three fundamental isotherm models (Langmuir, Freundlich, and Temkin) were performed. [220, 221]. Figure 3.35b reveals the graphs that depict the linearized

equation isotherm parameters for BCG dye removal at a temperature of 298 K. In Table (3.2), can find the three equations for the isotherm models of adsorption at room temperature, along with crucial information such as their maximum adsorption capacities (q_m), correlation coefficients (R^2). One of the many assumptions made by the Langmuir model is that a monolayer of adsorbate would stick to the homogenous surface of the adsorbent[164]. There is a list of all the Langmuir, Freundlich, and Temmken equations in paragraph (3.35c).

Provided by the gradient and intercept of the straight line are the values of A and B. In Table (3.2), there is a list of the parameters estimated for the Langmuir, Temkin, and Freundlich models. Based on the experimental equilibrium capacities (qe) and coefficients of determination (R^2), it appears that the Freundlich isotherm is the most suitable for describing the adsorption of BCG dye onto PANI/Nb_2O_5/Cr_2O_3 and CS/Nb_2O_5/MnO_2 adsorbents since it has higher R^2 values (0.9903 and 0.9434) and better fits the data. The potent BCG dye adsorption sites of the CS/Nb_2O_5/MnO_2 and CS/Nb_2O_5/Cr_2O_3 adsorbents indicate a multilayer adsorption mechanism.

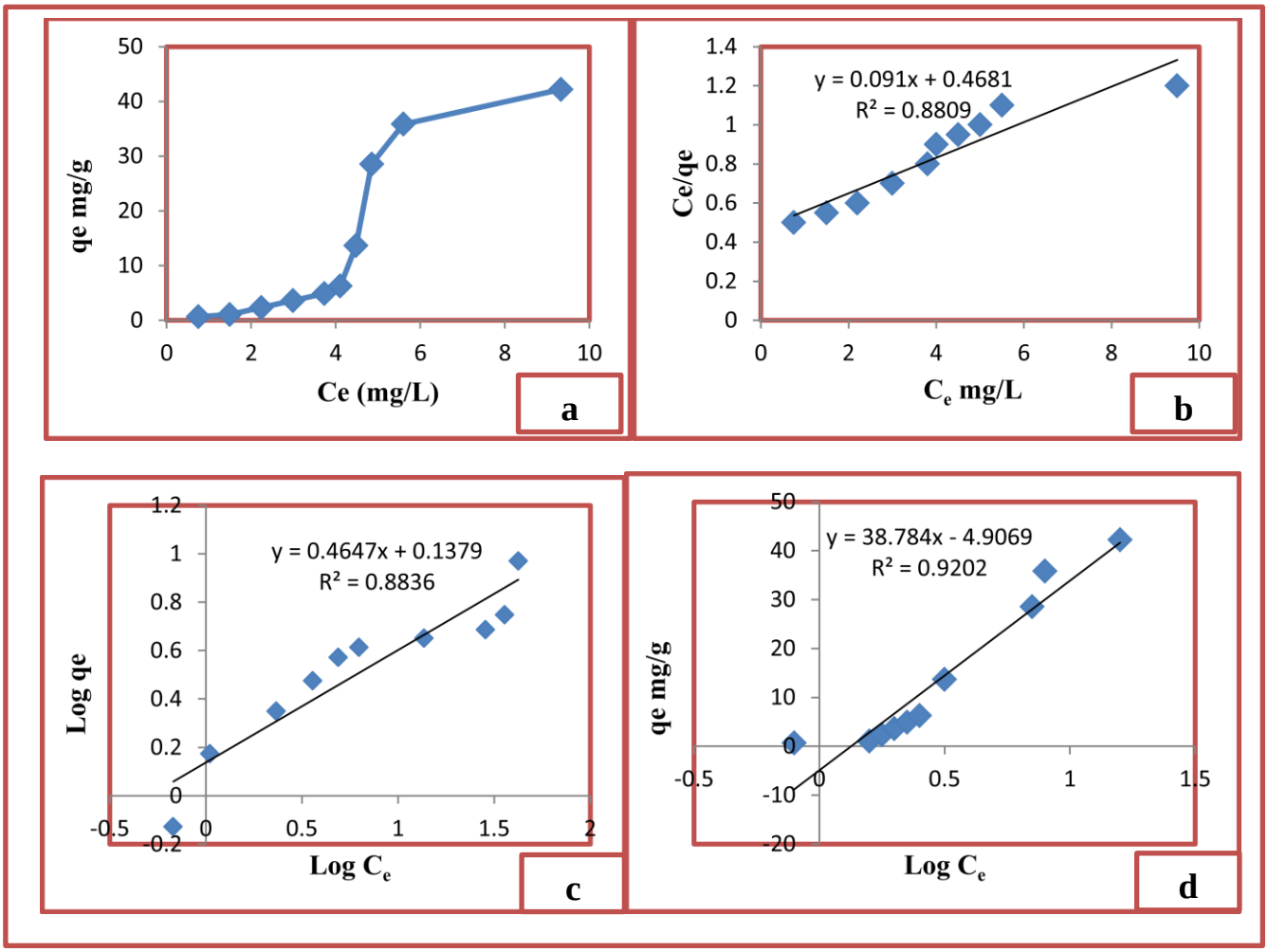

Figure 3.35. a Adsorption isotherm of BCG on CS/Nb_2O_5/Cr_2O_3 adsorbent (conditions: pH 10; dose=550 mg; V=100 ml; time=10 min; T=313 K); Together: b Langmuir isotherm model, c Freundlich isotherm model; d Temkin isotherm model.

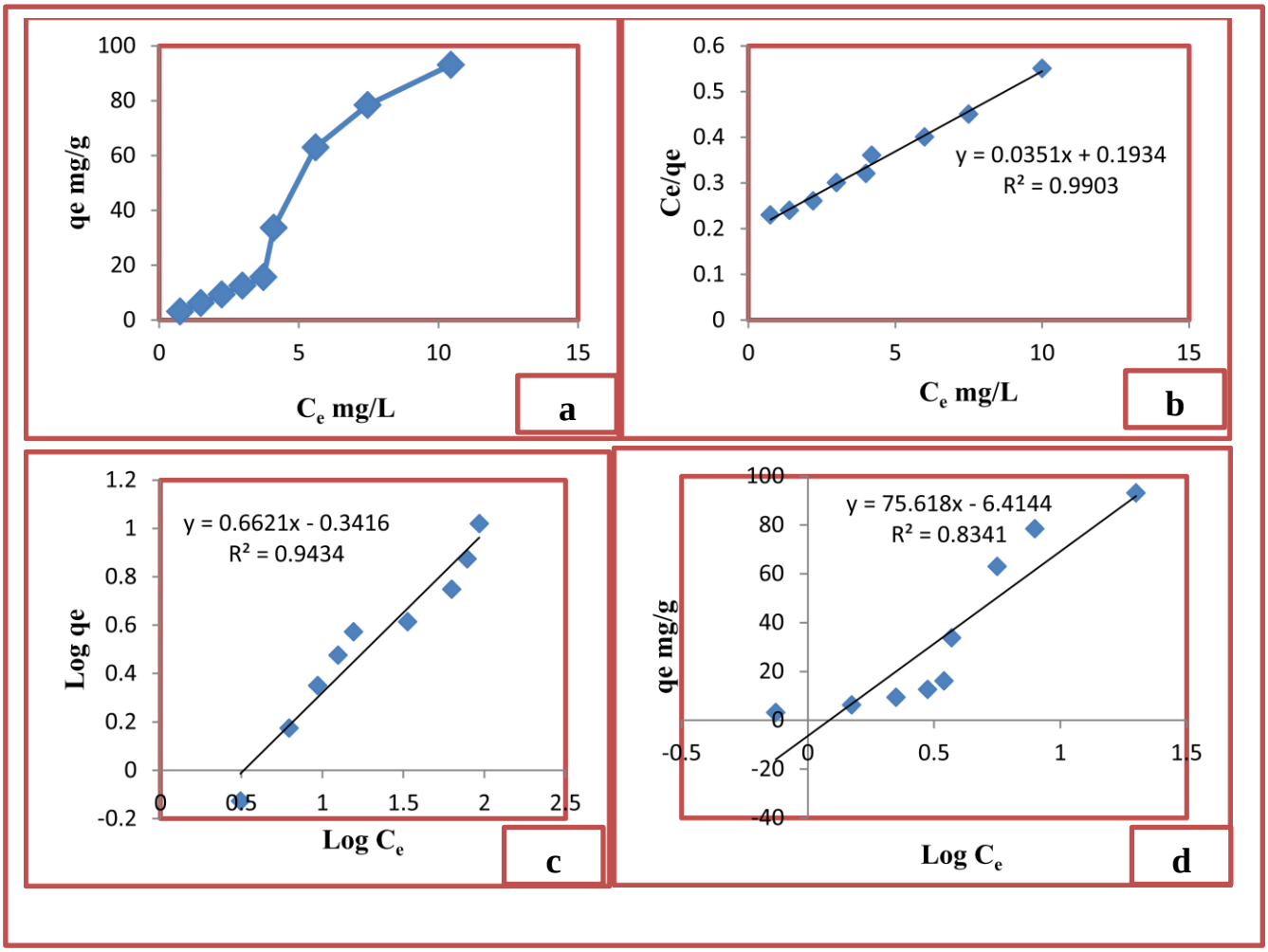

Figure 3.36. a. Adsorption isotherm of BCG on CS/Nb_2O_5/MnO_2 adsorbent (conditions: pH 7; dose=150 mg; V=100 ml; time=10 min; T=298 K); adsorption isotherm curve fitting of adsorbent BCG dye : b Langmuir isotherm model, c Freundlich isotherm model; d Temkin isotherm model.

Table 3.2. Adsorption isotherm characteristics of the Langmuir, Freundlich, and Temkin models for BCG dye by $CS/Nb_2O_5/Cr_2O_3$ and $CS/Nb_2O_5/MnO_2$

Isotherms	Parameters	$CS/Nb_2O_5/Cr_2O_3$	$CS/Nb_2O_5/MnO_2$
Langmuir	Q_m	20.2	33.3
	K_L	0.11	0.16
	R^2	0.8809	0.9903
Freundlich	K_F	1.37	2.19
	n	2.1	1.5
	R^2	0.8836	0.9434
Temkin	A	38.7	75.6
	B	4.9	6.4
	R^2	0.9202	0.8341

3.9 Suggested Mechanism for bromocresol green Decolorization

(a)

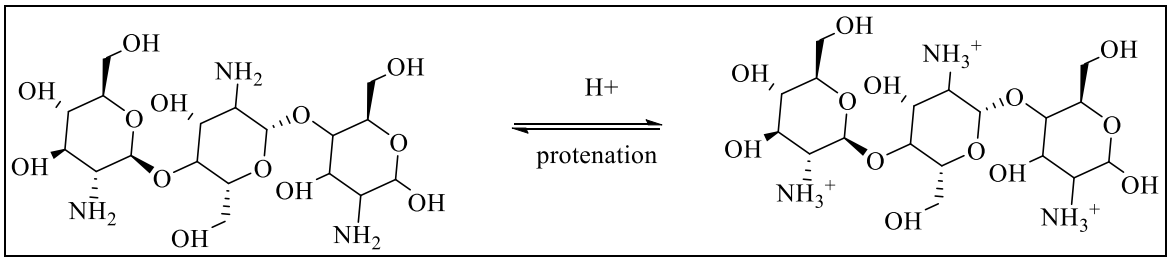

(b)

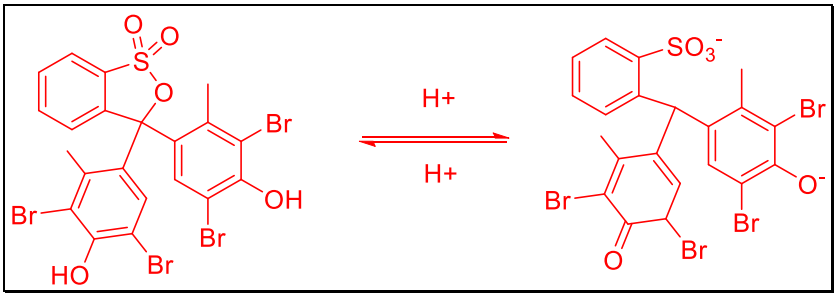

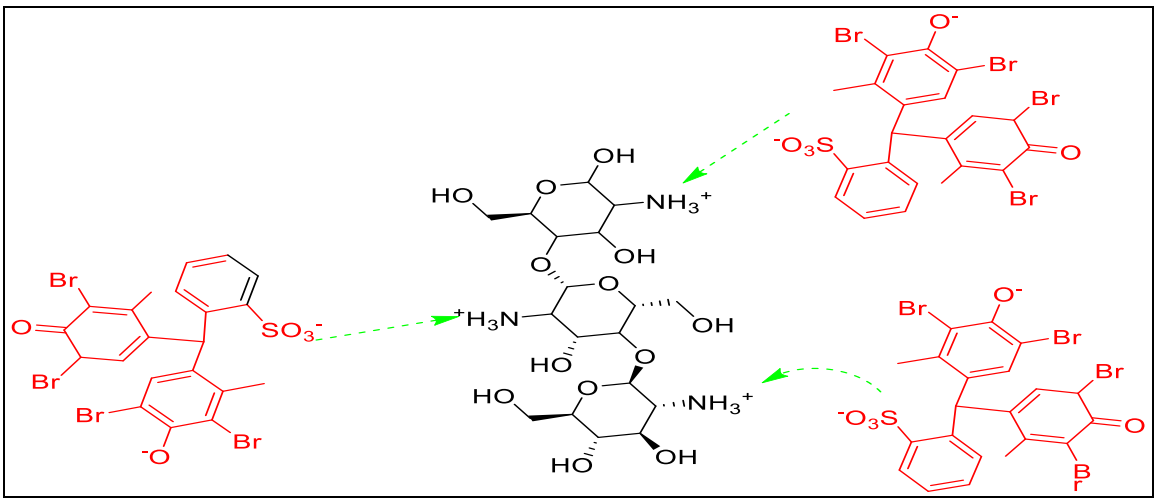

Electrostatic interaction

Figure 3.37 a Chemical structure of CS, b Dissociation of BCG in aqueous solution, and c Mechanism of anionic BCG dye adsorption onto emeraldine salt of CS Nanocomposites

Part 3: Adsorption of Direct yellow 50 by using $CS/Nb_2O_5/MnO_2$ and $CS/Nb_2O_5/Cr_2O_3$

3.10 Adsorption Experiment for direct yellow 50

The contact time, initial concentration of BCG solution, the solution's pH, and the dosage of the adsorbent are the factors that could have an impact on the adsorption characteristics of DY 50 on For $CS/Nb_2O_5/MnO_2$ and $CS/Nb_2O_5/Cr_2O_3$. These factors' effects on the samples' adsorption behaviour are examined, and the findings are discussed in the sections below.

3.10.1 Effect of pH on DY 50 dye Removal

The chemistry of the DY50 solution and the surface charge of the adsorbent. $CS/Nb_2O_5/MnO_2$ and $CS/Nb_2O_5/Cr_2O_3$ absorbed more DY50 as the pH level rose. At pH values between 3.0 and 4, the maximum level of adsorption (84.3%) and (81.76) was observed. The use of chitosan as an adsorbent was discovered to have an ideal pH range between 3 and 6 according to earlier research [222]. The adsorbent utilized was capable of removing DY50 at a consistent rate throughout a range of pH levels, as shown in Figure (3.38). Two inferences can be drawn from the results. Initially, an aqueous solution dissolves DY50 dye resulting in the dissociation of sulfonate groups (R - SO_3Na) from the dye and the anionic dye ion addition. Second, the dye is successfully removed from the adsorbent by electrostatic attraction between the direct yellow 50 ions and the surface. The adsorption was reduced when the dye was increased [223]. The competition between the OH ions in the aqueous solution and the DY50 anions was what caused the alteration.

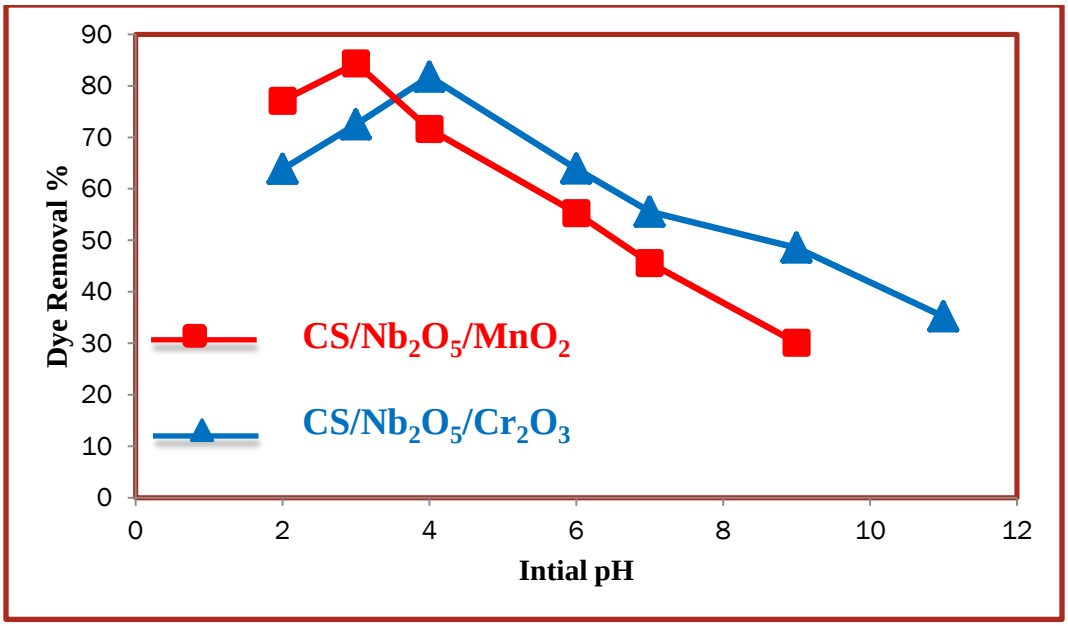

Figure 3.38. Effect of pH on DY 50 dye removal

3.10.2 Effect of adsorbent dose

To determine the adsorption rate of the DY50, the dose test was also carried out in the study. Variations in sorbet dosage ranged from 10-150 mg. Only at mass of 50 mg for $CS/Nb_2O_5/MnO_2$ and 25 mg for $CS/Nb_2O_5/Cr_2O_3$ did dye removal take place, at rates of 89.7% and 85.2%, respectively. A graphic representation of the effect of adsorbent dose on DY50 values was created. demonstrated, as depicted in Figure(3.39). Even though the DY50 removal rate was improved, a further increase in the adsorbent dosage had no discernible effect on the rate of adsorption but did enhance the availability of adsorption sites. This may be brought on by the overlap of adsorption sites, leading to a lengthening of the diffusion channel[224, 225]. The outcomes of this experiment are consistent with those of earlier research.

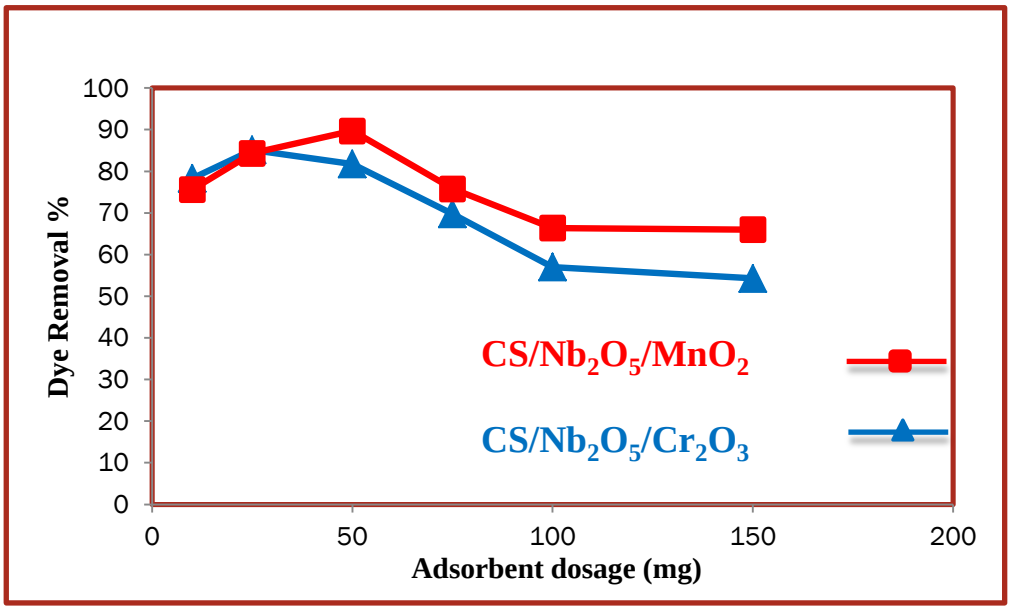

Figure 3.39. Effect of adsorbent dose on DY 50 dye removal

3.10.3 Effect of differences in the initial concentration of the DY50 dye on the removal process

the intensity of the dye's binding to $CS/Nb_2O_5/MnO_2$ and $CS/Nb_2O_5/Cr_2O_3$ increases as the DY50 concentration in the starting material increases. At low concentrations, the dye's initial volume of molecular weight on the accessible adsorption sites is decreased. The dye molecules assimilated additional sites for adsorption as a result. The initial DY50 concentration had an effect on the adsorption rate, and this in turn affected the sorbent's capacity to adsorb[226, 227]. The effect is caused by an increase in the concentration gradient that led to an equal increase in the initial concentration of DY50. However, at high concentrations of starting dye, fewer sites for adsorption are present because the concentration of the dye molecules increased more significantly[228, 229]. The DY50 concentrations for this trial ranged from (5 to 50) mg/L. At concentrations of 25 mg/L for $CS/Nb_2O_5/MnO_2$ and 20 mg/L for $CS/Nb_2O_5/Cr_2O_3$, dye removal occurred, with rates of 97.5% and 95.42%, respectively. The process of protonation increased the degree of anionic dye binding. The initial concentration's

effect is illustrated in the Figure below (3.40). The explanation lies in the relationship between the quantity of dye molecules and the number of available adsorption sites. When the concentration of dye molecules is low, the ratio of the original dye molecules to the adsorption sites is also low. This leads to an increase in the number of open sites for the dye molecules, which results in a higher rate of removal. However, when the concentration of dye molecules is high, the initial number of available adsorption sites is low. This decreases the number of available sites and, in turn, reduces the number of molecules that can be removed. To enhance the ability of anion dye to adsorb onto chitosan, protons are added. This resulted in a significant increase in the adsorption capacity.[230].

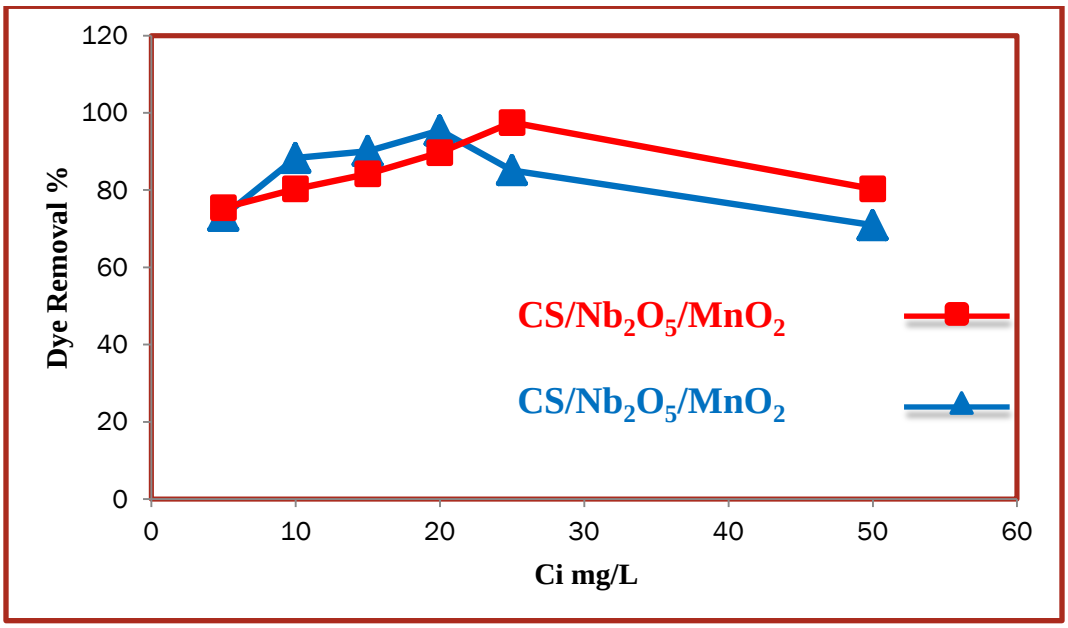

Figure 3.40. Effect of the DY 50 dye's initial concentration on the removal process

3.10.4 Effect of Temperature on Removal of DY50 Dye

Temperature impacts on $CS/Nb_2O_5/MnO_2$ and $CS/Nb_2O_5/Cr_2O_3$ adsorption of DY50 at pH values of 3 and 4, respectively. The removal of DY50 was investigated at four different temperatures (298, 308, 318, and 328 K). Temperature affected the adsorption process, i.e., a change in temperature might

alter the adsorbent's equilibrium ability to adsorb a particular molecule. Because the adsorption mechanism is exothermic, an increase in temperature reduces the dye's adsorption, whereas a drop in Its endothermic nature is shown in Figure (3.41) by temperature. In addition to the low temperature of the adsorbed species and the limited number of accessible active sites, the physical connection between both organic compounds, including dyes and the active sites of adsorption, reduced with rising temperature [231, 232].

The impact of temperature is little, though. This behavior is in line with, where the authors discovered that a change in the temperature of wastewater may not have an impact on the removal of pigments. As a result, temperature has a different impact on adsorption, changing the amplitude of the adsorption equilibrium to adsorb particular compounds.

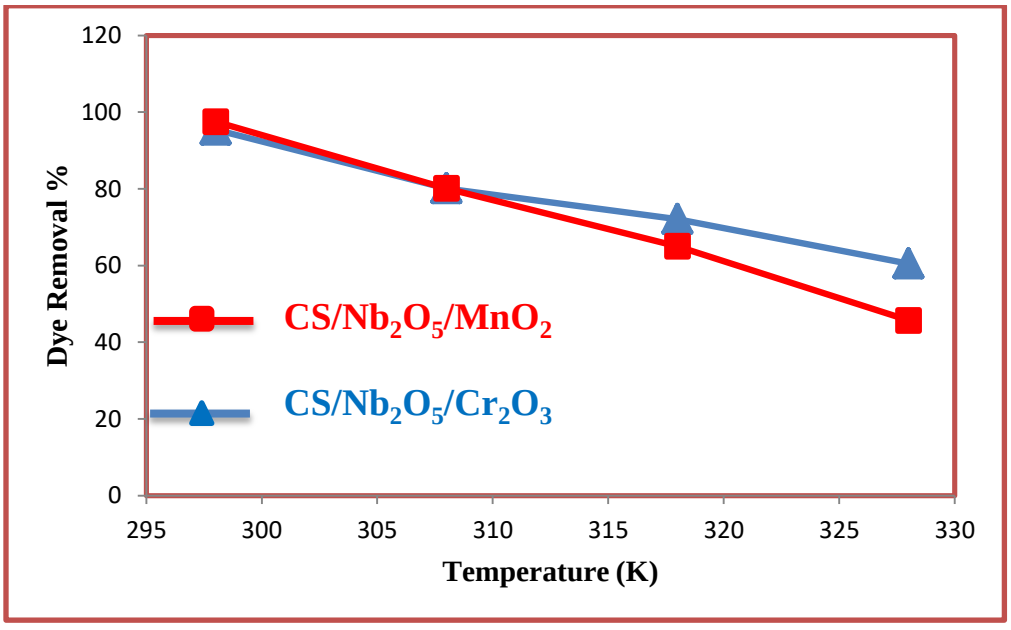

Figure 3.41. Effect of Temperature of DY 50 dye on removal process

3.10.5 Effect of adsorption time

The impact of contact duration on the adsorption of DY50 was investigated using a contact time range of 10 to 120 min, (25,20) mg/L of dye solution, pH of 3,4 298 K temperature, and 25,50 mg of adsorbent dose. As shown in Figure (3.42), there was a rapid rise in the percentage of DY50 adsorbed in $CS/Nb_2O_5/MnO_2$ and $CS/Nb_2O_5/Cr_2O_3$ from 10 to 30 minutes in comparison to other contact times. Many adsorption sites and a high solution concentration are responsible for the rapid force of interaction between the anions in DY 50 and the individual $CS/Nb_2O_5/MnO_2$ and $CS/Nb_2O_5/Cr_2O_3$ during the initial contact time [233].

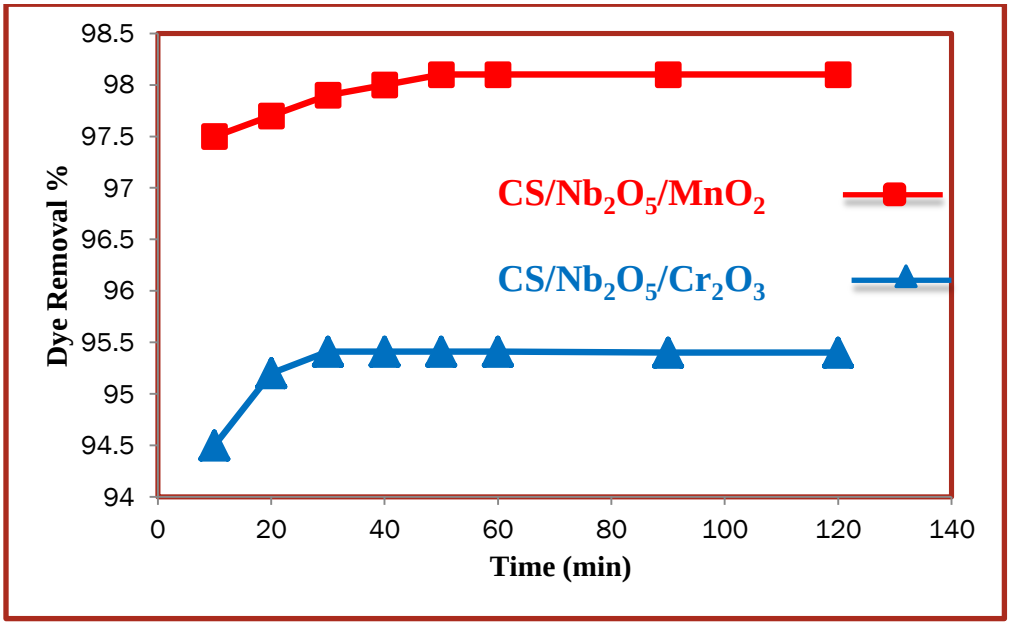

Figure 3.42. Effect of adsorption time on DY 50 dye removal

3.11 Recyclability Study for $CS/Nb_2O_5/MnO_2$ and $CS/Nb_2O_5/Cr_2O_3$

The excellent recyclability of the Nanocomposites $CS/Nb_2O_5/MnO_2$ and $CS/Nb_2O_5/Cr_2O_3$ suggests that this approach may indeed be useful for water purification. The recyclability tests are performed for 4 consecutive DY50 dye adsorption-desorption cycles under the ideal conditions described below. For

$CS/Nb_2O_5/Cr_2O_3$: pH 4; Dose: 25 mg; Volume: 100ml; Time: 30 minutes; Temperature: 298K; For $CS/Nb_2O_5/MnO_2$: pH 3; minutes; temperature: 298 K. The spent volume is magnetized from the aqueous solution, rinsed with ethanol and deionized water, dried at 75 °C for 4 h, and reused for the following cycle of DY50 dye adsorption. It is then found that the adsorption efficiencies of the mixtures $CS/Nb_2O_5/MnO_2$ and $CS/Nb_2O_5/Cr_2O_3$ decreased from 98.1% to 92.5% and from 95.41% to 87.1%, respectively. As shown in Figure (3.43).

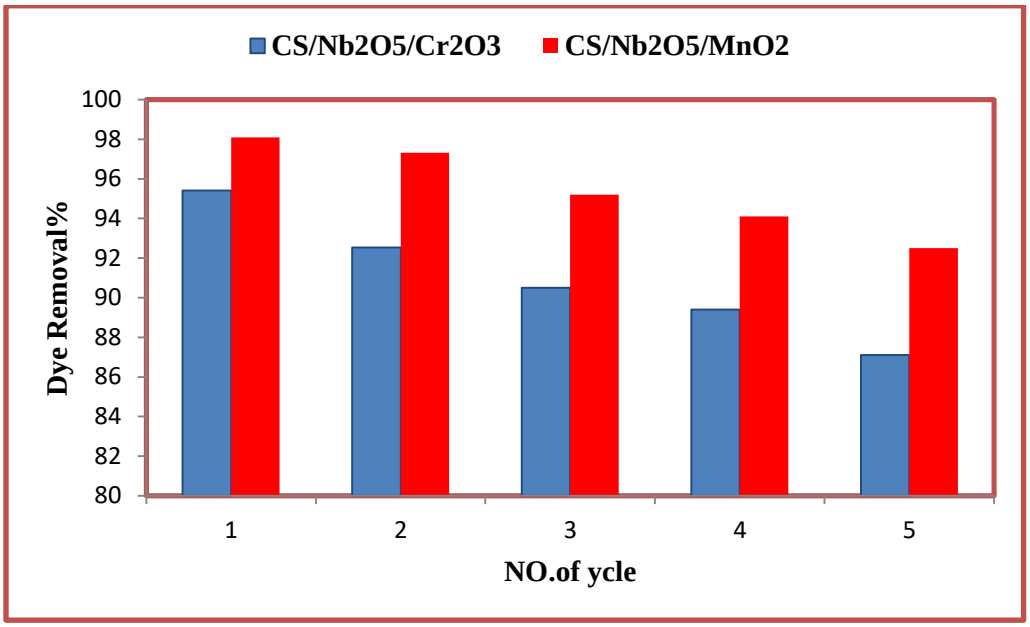

Figure 3.43 Number of adsorption-desorption cycles of $CS/Nb_2O_3/MnO_2$ and $CS/Nb_2O_5/Cr_2O_3$ dyes DY 50 (Condition: pH3,4; Dose = 50.25 mg; Ci = 20.25 mg/L; V = 100 ml; Time = 30 min; T = 298K).

3.12 Adsorption isotherms for direct yellow 50

At 298 K, it is observed through experimentation that the $CS/Nb_2O_5/MnO_2$ and $CS/Nb_2O_5/Cr_2O_3$ adsorbents had optimal adsorption capacities at pH 4 and pH 3, respectively, when used with 100 mL solutions of DY50 dye with concentrations between 5 to 150 mg/L. The highest adsorption capacities for the $CS/Nb_2O_5/Cr_2O_3$ and $CS/Nb_2O_5/MnO_2$ adsorbents measured 351.5 mg/g and 200.6 mg/g, respectively, as depicted in a Figure (3.44a). In order to calculate the maximum

adsorption capacity (q_m) of the appropriate adsorbent, data was studied by implementing the Langmuir, Freundlich, and Temkin models.[220, 221]. Figure (3.44b) displays the linearized equation isotherm parameters for the elimination of DY50 dye at 298 K. Correspondingly, Table (3.3) features the three equations for the isotherm models of adsorption at room temperature, inclusive of their maximum adsorption capacities (qm), correlation coefficients (R^2), and other key data. The assumptions that are taken into account by the Langmuir model encompassed the adherence of the adsorbate to the adsorbent as a monolayer on a homogeneous surface..[164]. Provided in paragraph (3.44C) are the Langmuir, Freundlich, and Temmken equations, which have been rearranged and some of the text sporadically removed in order to make it more unique and interesting to read. The parameters required for the Langmuir, Freundlich, and Temkin models can be found in Table (3.3) .The values for B and A can be determined from the straight line's gradient and intercept, respectively. Upon examination of the coefficients of determination (R^2) for the fit of the experimental data to the three isotherms, it was determined that the Freundlich isotherm is the best model for the adsorption of BCG dye onto PANI/Nb_2O_5/Cr_2O_3 and CS/Nb_2O_5/MnO_2 adsorbents. This conclusion is reinforced by the greater R^2 (0.9927 and 0.9661) and experimental equilibrium capacities (qe) observed for the Freundlich isotherm. The CS/Nb_2O_5/Cr_2O_3 and CS/Nb_2O_5/MnO_2 adsorbents appear to have ample spots for DY50 dye adsorption, hinting at a complex, multilayer adsorption mechanism.

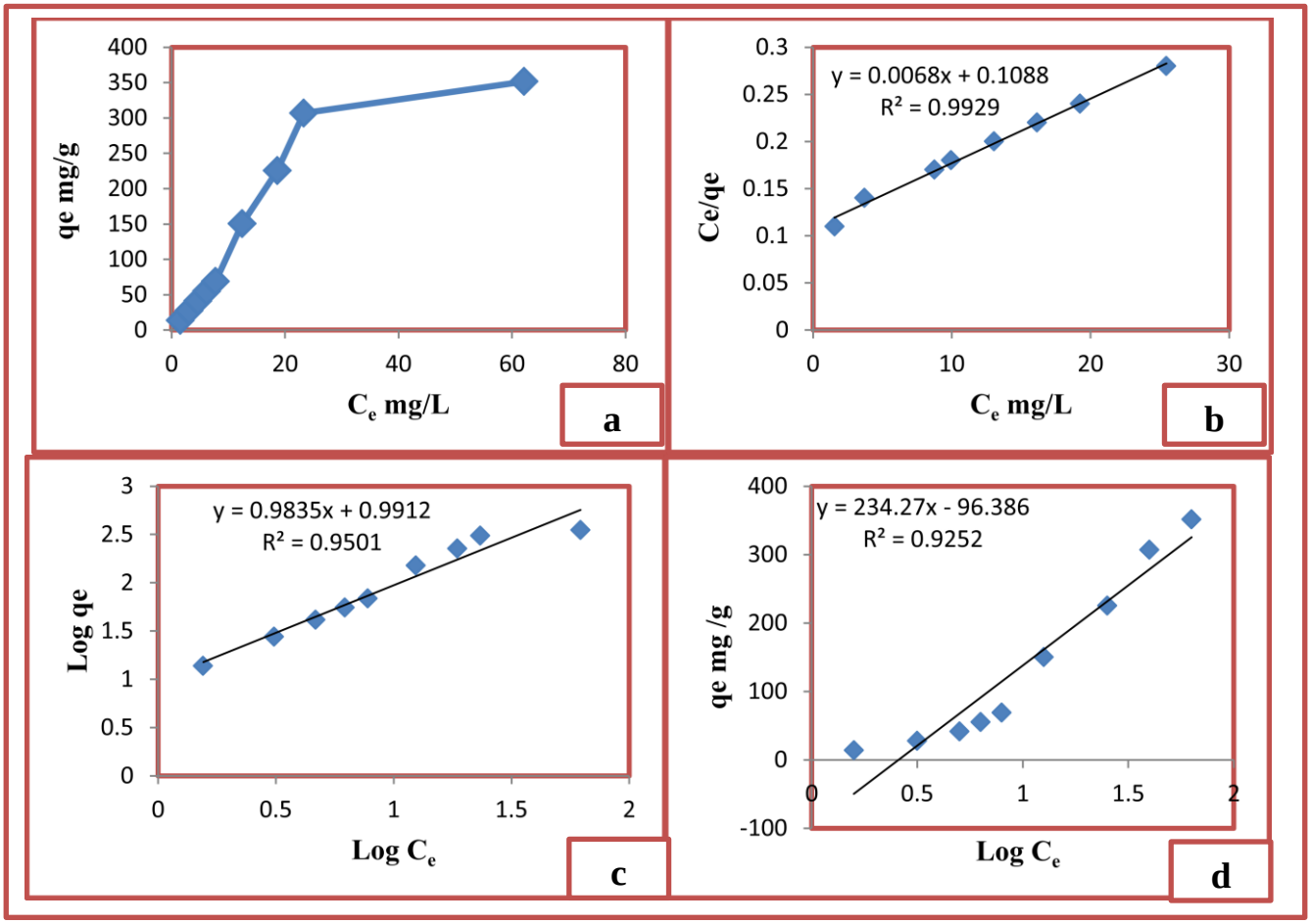

Figure 3.44. a Adsorption isotherm of DY 50 on CS/Nb_2O_5/Cr_2O_3 adsorbent (conditions: pH 4; dose=25 mg; V=100 ml; time=30 min; T=298 K); adsorption isotherm of adsorbent for DY dye Curve fitting: b Langmuir isotherm model, c Freundlich isotherm model; d Temkin isotherm.

Table 3.3. Adsorption Langmuir, Freundlich and Temkin model isotherm parameters for CS/Nb_2O_5/Cr_2O_3 and CS/Nb_2O_5/MnO_2 dyes DY50

4. Isotherms	3. Parameters	2. CS/Nb_2O_5/Cr_2O_3	1. CS/Nb_2O_5/MnO_2
8. 9. Langmuir	7. Q_m	6. 166.6	**5. 250**
	12. K_L	0.055 .11	**0.04 .10**
	15. R^2	0.9929 .14	**0.9584 .13**
19. 20. Freundlich	18. K_F	17. 9.8	**16. 12.8**
	23. n	1.02 .22	**1.4 .21**
	26. R^2	0.9501 .25	**0.9661 .24**
30. 31. Temkin	29. A	28. 234	**27. 90.6**
	34. B	33. 96	**32. 1.2**
	37. R^2	0.9252 .36	**0.9324 .35**

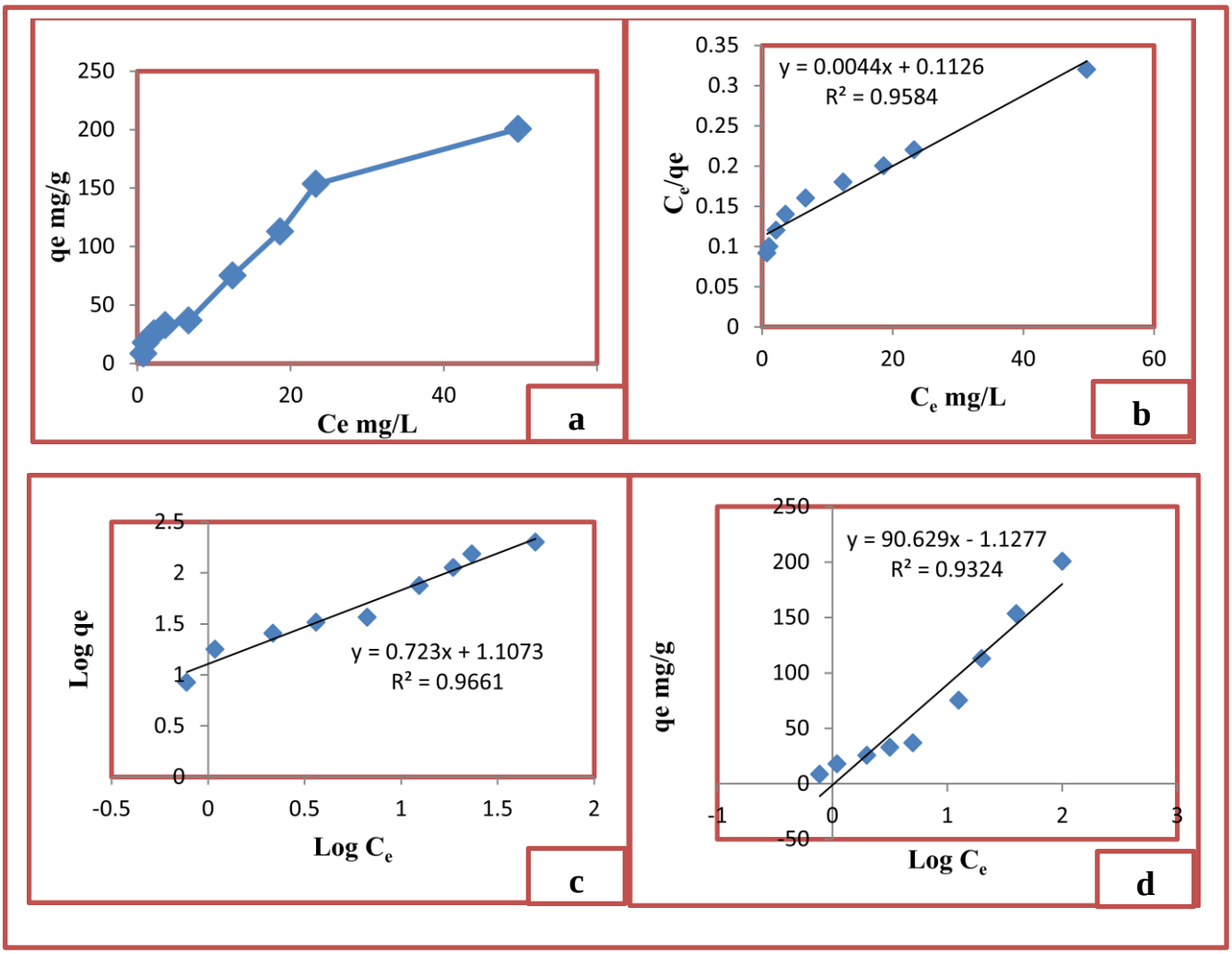

Figure 3.45. a Adsorption isotherm of DY 50 on CS/Nb_2O_5/MnO_2 adsorbent (conditions: pH 3; dose=50 mg; V=100 ml; time=30 min; T=298 K); adsorption of DY dye by adsorbent Isotherm curve fitting: b Langmuir isotherm model, c Freundlich isotherm model; d Temkin isotherm model.

3.13 Suggested Mechanism for direct yellow 50 Decolorization

(a)

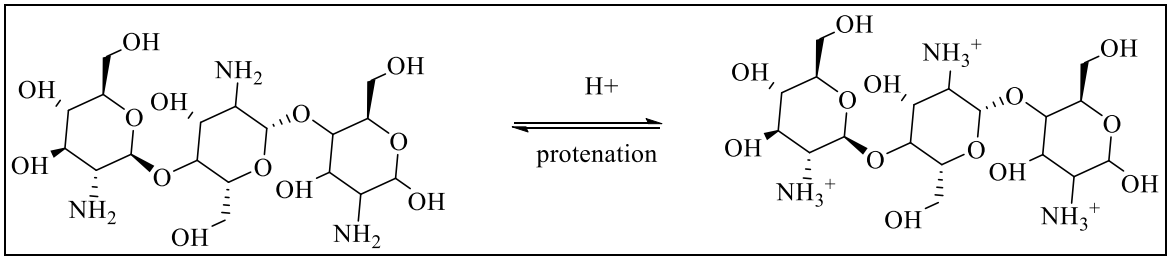

(b)

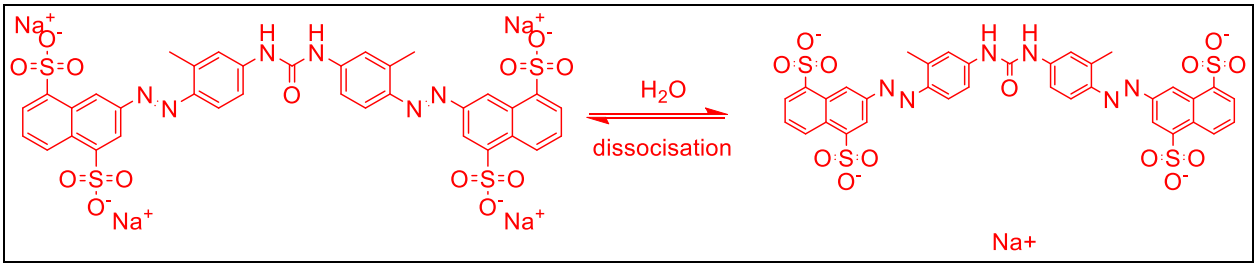

(c)

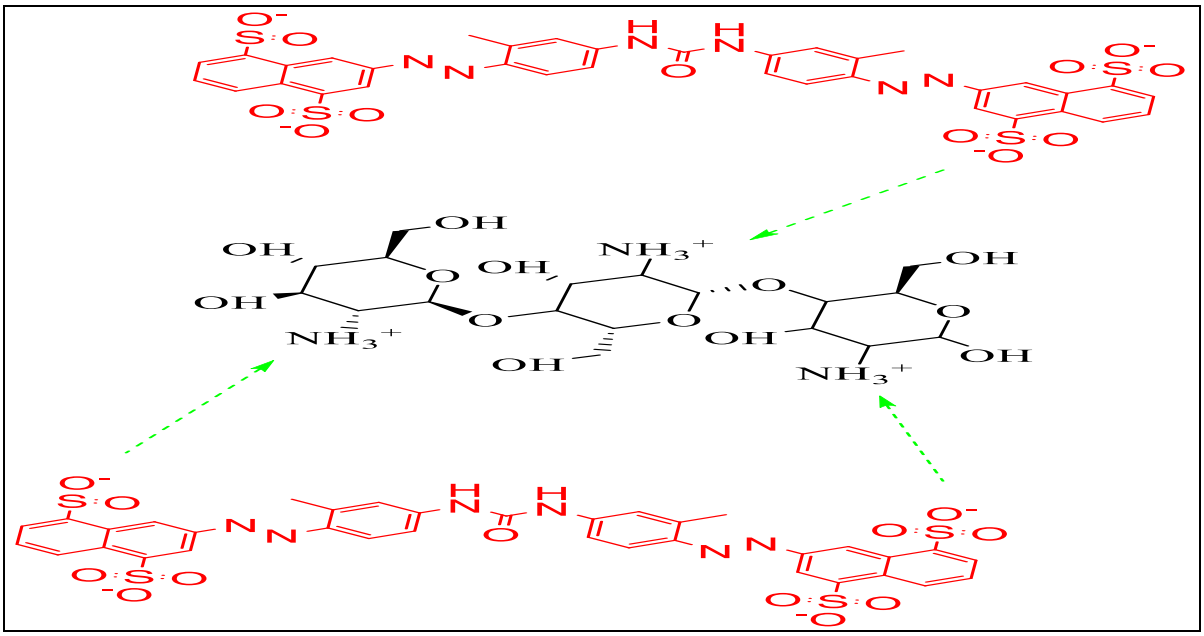

Electrostatic interaction

Figure 3.46 a Chemical structure of CS, b Dissociation of DY50 in aqueous solution and c Adsorption mechanism of anionic DY50 dye on emeraldine salt of CS Nanocomposites

Chapter 4
Conclusions & Recommendation

4.1 Conclusions

The following points can be drawn from the results of this study:

1-The preparation of Polyaniline/Nb_2O_5/MnO_2 and Polyaniline /Nb_2O_5/Cr_2O_3 were successfully prepared by oxidative polymerization.

2-The preparation of Chitosan/Nb_2O_5/MnO_2 and Chitosan/Nb_2O_5/Cr_2O_3 were successfully prepared by oxidative polymerization.

3-Studying the other characterization of the prepared Chitosan/Nb_2O_5/MnO_2 and Chitosan/Nb_2O_5/Cr_2O_3 & Polyaniline/Nb_2O_5/MnO_2 and Polyaniline /Nb_2O_5/Cr_2O_3 nanocomposite such as XRD, SEM, FTIR, technique, and zeta potential.

4- The new method proved to be highly efficient and accurate in removing toxic dyes based on the composite nanoparticles.

5- The optimum conditions for the methyl orange reactions with Polyaniline/Nb_2O_5/MnO_2 where the dose was 100 mg, temperature 298 K, and pH value was 7, while with Polyaniline /Nb_2O_5/Cr_2O_3 Nanocomposites the dose was 50 mg, temperature 298, and pH value was 9.

6- The optimum conditions for the bromocresol green reactions with Chitosan /Nb_2O_5/MnO_2 where the dose was 150 mg, temperature 298 K, and pH value was 7,while with Chitosan /Nb_2O_5/Cr_2O_3 Nanocomposites the dose was 550 mg, temperature 313, and pH value was 10.

7- The optimum conditions for the direct yellow 50 reactions with Chitosan /Nb_2O_5/MnO_2 where the dose was 50 mg, temperature 298 K, and pH value was 3,while with Chitosan /Nb_2O_5/Cr_2O_3 Nanocomposites the dose was 25 mg, temperature298K, and pH value was 4.

4.2 Recommendations and Future Works

The following points can be recommended:

1- Other polymers can be used as adsorbent on the surface of the metal oxide for adsorption dyes.

2- Studying the effective of these nanocomposites in other application such as antibacterial activity.

3- Using different proportions of coating different polymers with the used oxides.

References

1. Rauscher, H., Roebben, G., Mech, A., Gibson, N., Kestens, V., Linsinger, T. P. J. and Sintes, J. R., An overview of concepts and terms used in the European Commission's definition of nanomaterial. Publications Office of the European Union, 2019.
2. Muhammad, S.F., Nanotechnology Particle characteristic, 2021, Salahaddin University-Erbil.
3. Rubel, M.H. and M.K. Hossain, Crystal structures and properties of nanomagnetic materials, in Fundamentals of Low Dimensional Magnets. 2022, CRC Press. p. 183-205.
4. Maria, L., J. Moses, and C. Anandharamakrishnan, Ethical and Regulatory Issues in Applications of Nanotechnology in Food, in *Food Nanotechnology*. 2019, CRC Press. p. 67-92.
5. Khan, I., K. Saeed, and I. Khan, Nanoparticles: Properties, applications and toxicities. Arabian journal of chemistry, 2019. **12**(7): p. 908-931.
6. Singh, K.K., Role of Nanotechnology and Nanomaterials for Water Treatment and Environmental Remediation. International Journal of New Chemistry, 2022. **9**(3): p. 373-398.
7. Bhardwaj, V. and A. Kaushik, Biomedical applications of nanotechnology and nanomaterials, 2017, MDPI. p. 298.
8. Roy, A., Sharma, A., Yadav, S., Jule, L. T., and Krishnaraj, R., Nanomaterials for remediation of environmental pollutants. Bioinorganic Chemistry and Applications, 2021. **2021**.
9. Saleh, T.A., *Nanomaterials:* Classification, properties, and environmental toxicities. Environmental Technology & Innovation, 2020. **20**: p. 101067.
10. Jóźwiak, B., Dzido, G., Zorębski, E., Kolanowska, A., Jędrysiak, R., Dziadosz, J.,and Dzida, M. , Remarkable thermal conductivity enhancement in carbon-based ionanofluids: effect of nanoparticle morphology. ACS applied materials & interfaces, 2020. **12**(34): p. 38113-38123.
11. Rizwan, M., Shoukat, A., Ayub, A., Razzaq, B., and Tahir, M. B. , Types and classification of nanomaterials, in Nanomaterials: Synthesis, Characterization, Hazards and Safety. 2021, Elsevier. p. 31-54.

12. Varghese, R.J., Parani, S., Thomas, S., Oluwafemi, O. S., and Wu, J. , Introduction to nanomaterials: synthesis and applications, in Nanomaterials for solar cell applications. 2019, Elsevier. p. 75-95.
13. Tomar, R.S., A. Jyoti, and S. Kaushik, Nanobiotechnology: Concepts and Applications in Health, Agriculture, and Environment. 2020.
14. Fan, Q., Dehankar, A., Porter, T. K., and Winter, J. O., Effect of Micelle Encapsulation on Toxicity of CdSe/ZnS and Mn-Doped ZnSe Quantum Dots. Coatings, 2021. **11**(8): p. 895.
15. Baig, N., I. Kammakakam, and W. Falath, Nanomaterials: A review of synthesis methods, properties, recent progress, and challenges. Materials Advances, 2021. **2**(6): p. 1821-1871.
16. Hanemann, T. and D.V. Szabó, Polymer-nanoparticle composites: from synthesis to modern applications. Materials, 2010. **3**(6): p. 3468-3517.
17. Balakumar, V., Ramalingam, M., Sekar, K., Chuaicham, C., & Sasaki, K.. Fabrication and characterization of carbon quantum dots decorated hollow porous graphitic carbon nitride through polyaniline for photocatalysis. Chemical Engineering Journal. 2021,426, 131739.
18. Ramalingam, G., Kathirgamanathan, P., Ravi, G., Elangovan, T., Manivannan, N., and Kasinathan, K., Quantum confinement effect of 2D nanomaterials, in Quantum Dots-Fundamental and Applications. 2020, IntechOpen.
19. Divsar, F., Quantum dots: fundamental and applications. 2020: BoD–Books on Demand.
20. Mooss, V., Y. Kesari, and A. Athawale, Conducting polymer and metal-based sensors for the detection of vapours and toxic gases*:* A concise review. Journal of Materials NanoScience, 2022. **9**(1): p. 37-46.
21. Heydari Gharahcheshmeh, M. and K.K. Gleason, Device fabrication based on oxidative chemical vapor deposition (oCVD) synthesis of conducting polymers and related conjugated organic materials. Advanced Materials Interfaces, 2019. **6**(1): p. 1801564.
22. Agobi, A.U., Louis, H., Magu, T. O., and Dass, P. M., A review on conducting polymers-based composites for energy storage application. J. Chem. Rev, 2019. **1**(1): p. 19-34.
23. Kausar, A. and M. Siddiq, Conducting Polymer/Graphene Filler-based Hybrids: Energy and Electronic Applications. Editor: A. Méndez-Vilas & A.

Solano-Martín Polymer Science: Research Advances, Practical Applications and Educational Aspects. Formatex Research Center, 2016: p. 177-87.
24. Tajik, S., Beitollahi, H., Nejad, F. G., Shoaie, I. S., Khalilzadeh, M. A., Asl, M. S.,and Shokouhimehr, M., Recent developments in conducting polymers: Applications for electrochemistry. RSC advances, 2020. **10**(62): p. 37834-37856.
25. Namsheer, K. and C.S. Rout, Conducting polymers: A comprehensive review on recent advances in synthesis, properties and applications. RSC advances, 2021. **11**(10): p. 5659-5697.
26. Cazan, C., A. Enesca, and L. Andronic, Synergic effect of TiO_2 filler on the mechanical properties of polymer nanocomposites. Polymers, 2021. **13**(12): p. 2017.
27. Koo, J.H., Polymer nanocomposites: processing, characterization, and applications. 2019: McGraw-Hill Education.
28. Samadi, A., Xie, M., Li, J., Shon, H., Zheng, C.,and Zhao, S., Polyaniline-based adsorbents for aqueous pollutants removal: A review. Chemical Engineering Journal, 2021. **418**: p. 129425.
29. Genies, E., Boyle, A., Lapkowski, M.,and Tsintavis, C., Polyaniline: A historical survey. Synthetic metals, 1990. **36**(2): p. 139-182.
30. Alesary, H.F., Ismail, H. K., Khudhair, A. F., and Mohammed, M. Q., Effects of dopant ions on the properties of polyaniline conducting polymer. Oriental Journal of Chemistry, 2018. **34**(5): p. 2525.
31. Shakir, I., Shahid, M., Rana, U. A., and Warsi, M. F., In situ hydrogenation of molybdenum oxide nanowires for enhanced supercapacitors. RSC advances, 2014. **4**(17): p. 8741-8745.
32. Baker, C.O., Huang, X., Nelson, W., and Kaner, R. B., Polyaniline nanofibers: broadening applications for conducting polymers. Chemical Society Reviews, 2017. **46**(5): p. 1510-1525.
33. Sun, E., Liao, G., Zhang, Q., Qu, P., Wu, G., Xu, Y.,and Huang, H., Green preparation of straw fiber reinforced hydrolyzed soy protein isolate/urea/formaldehyde composites for biocomposite flower pots application. Materials, 2018. **11**(9): p. 1695.
34. Ajeel, K. and Q. Kareem. Synthesis and characteristics of polyaniline (PANI) filled by graphene (PANI/GR) nano-films. in Journal of Physics: Conference Series. 2019. IOP Publishing.

35. Mudila, H., Prasher, P., Rana, S., Khati, B.,and Zaidi, M. G. H., Electrochemical oxidation-reduction and determination of urea at enzyme free PPY-GO electrode. Carbon letters, 2018. **26**: p. 88-94.
36. Mudila, H., Prasher, P., Kumar, M., Kumar, A., Zaidi, M. G. H., and Kumar, A. , Critical analysis of polyindole and its composites in supercapacitor application. Materials for Renewable and Sustainable Energy, 2019. **8**(2): p. 1-19.
37. Kumar, A., Kumar, V., Sain, P. K., Kumar, M., and Awasthi, K., Synthesis and characterization of polyaniline membranes with–secondary amine additive containing N, N′-dimethyl propylene urea for fuel cell application. International Journal of Hydrogen Energy, 2018. **43**(47): p. 21715-21723.
38. Boeva, Z.A. and V.G. Sergeyev, Polyaniline: Synthesis, properties, and application. Polymer Science Series C, 2014. **56**(1): p. 144-153.
39. Llorens, E., Armelin, E., Pérez-Madrigal, M. D. M., Del Valle, L. J., Alemán,C.,and Puiggalí,J.,Nanomembranes and nanofibers from biodegradable conducting polymers. Polymers, 2013. **5**(3): p. 1115-1157.
40. Gómez, I.J., Vázquez Sulleiro, M., Mantione, D., and Alegret, N., Carbon nanomaterials embedded in conductive polymers: A state of the art. Polymers, 2021. **13**(5): p. 745.
41. Dhand, C., Dwivedi, N., Mishra, S., Solanki, P. R., Mayandi, V., Beuerman, R. W.,and Malhotra, B. D. , Polyaniline-based biosensors. Nanobiosensors in disease diagnosis, 2015. **4**: p. 25.
42. Mazzeu, M.A.C., Faria, L. K., Cardoso, A. D. M., Gama, A. M., Baldan, M. R.,and Gonçalves, E. S, Structural and morphological characteristics of polyaniline synthesized in pilot scale. Journal of Aerospace Technology and Management, 2017. **9**: p. 39-47.
43. Beygisangchin, M., Abdul Rashid, S., Shafie, S., Sadrolhosseini, A. R., and Lim, H. N., Preparations, properties, and applications of polyaniline and polyaniline thin films:A review. Polymers, 2021. **13**(12): p. 2003.
44. Golba, S., M., Miga, S., Jurek-Suliga, J.,and Zubko, M., Electrical Conductivity and Morphology Study of Polyaniline Powder Synthesised with Various Doping Ions. Archives of Metallurgy and Materials, 2019. **64**.
45. Mozafari, M. and N.P.S. Chauhan, Fundamentals and emerging applications of polyaniline. 2019.

46. Heme, H.N., Alif, M. S. N., Rahat, S. S. M.,and Shuchi, S. B., Recent progress in polyaniline composites for high capacity energy storage: A review. Journal of Energy Storage, 2021. **42**: p. 103018.
47. Gao, Y., Wang, X., Zhang, Y., Li, J., Zhang, H., and Li, J., Novel fabrication of bi-metal oxide hybrid nanocomposites for synergetic enhancement of in vivo healing and wound care after caesarean section surgery. International Wound Journal, 2022.
48. Mizwari, Z.M., A.A. Oladipo, and E. Yilmaz, Chitosan/metal oxide nanocomposites: synthesis, characterization, and antibacterial activity. International Journal of Polymeric Materials and Polymeric Biomaterials, 2021. **70**(6): p. 383-391.
49. Christou, C., Philippou, K., Krasia-Christoforou, T., and Pashalidis,, Uranium adsorption by polyvinylpyrrolidone/chitosan blended nanofibers. Carbohydrate polymers, 2019. **219**: p. 298-305.
50. Pavoni, J.M.F., C.L. Luchese, and I.C. Tessaro, Impact of acid type for chitosan dissolution on the characteristics and biodegradability of cornstarch/chitosan based films. International journal of biological macromolecules, 2019. **138**: p. 693-703.
51. Kim, H.-R., J.-W. Jang, and J.-W. Park, Carboxymethyl chitosan-modified magnetic-cored dendrimer as an amphoteric adsorbent. Journal of hazardous materials, 2016. **317**: p. 608-616.
52. Alharby, N.F., R.S. Almutairi, and N.A. Mohamed, Adsorption behavior of methylene blue dye by novel crosslinked O-CM-Chitosan hydrogel in aqueous solution: Kinetics, isotherm and thermodynamics. Polymers, 2021. **13**(21): p. 3659.
53. Grząbka-Zasadzińska, A., A., Ratajczak, I., Król, K., Woźniak, M.,and Borysiak, S., The influence of crystalline structure of cellulose in chitosan-based biocomposites on removal of Ca(II), Mg(II), Fe(III) ion in aqueous solutions. Cellulose, 2021. **28**(9): p. 5745-5759.
54. Ioelovich, M., Crystallinity and hydrophility of chitin and chitosan. J. Chem, 2014. **3**(3): p. 7-14.
55. Huang, P., Xia, D., Kazlauciunas, A., Thornton, P., Lin, L., and Menzel, R., Dye-mediated interactions in chitosan-based polyelectrolyte/organoclay hybrids for enhanced adsorption of industrial dyes. ACS applied materials & interfaces, 2019. **11**(12): p. 11961-11969.

56. Ghorai, S., Sarkar, A., Raoufi, M., Panda, A. B., Schönherr, H.,and Pal, S. , Enhanced removal of methylene blue and methyl violet dyes from aqueous solution using a nanocomposite of hydrolyzed polyacrylamide grafted xanthan gum and incorporated nanosilica. ACS applied materials & interfaces, 2014. **6**(7): p. 4766-4777.
57. Badry, M.D., Wahba, M. A., Khaled, R., Ali, M. M., and Farghali, A. A. , Synthesis, characterization, and in vitro anticancer evaluation of iron oxide/chitosan nanocomposites. Inorganic and Nano-Metal Chemistry, 2017. **47**(3): p. 405-411.
58. Liu, Q., Yang, B., Zhang, L., and Huang, R., Adsorption of an anionic azo dye by cross-linked chitosan/bentonite composite. International journal of biological macromolecules, 2015. **72**: p. 1129-1135.
59. Barbosa, P.F.P., Cumba, L. R., Andrade, R. D. A.,and do Carmo, D. R. , Chemical modifications of cyclodextrin and chitosan for biological and environmental applications: metals and organic pollutants adsorption and removal. Journal of Polymers and the Environment, 2019. **27**(6): p. 1352-1366.
60. Deepika, R., M. Venkateshprabhu, and M. Pandimdevi, Studies on the behaviour of reactive dyes onto the cross-linked chitosan using adsorption isotherms. International Journal of Environmental Sciences, 2013. **4**(3): p. 323.
61. Ladet, S., Francois, S., Claret, J.,and Buffin, M., Method for preparing a chitosan-based porous layer, 2019, Google Patents.
62. Szymańska, E. and K. Winnicka, Stability of chitosan—a challenge for pharmaceutical and biomedical applications. Marine drugs, 2015. **13**(4): p. 1819-1846.
63. Stalder, R., Organic semiconducting molecules and polymers for solution processed organic electronics. 2012: University of Florida.
64. Habiba, U., Afifi, A. M., Salleh, A.,and Ang, B. C., Chitosan/(polyvinyl alcohol)/zeolite electrospun composite nanofibrous membrane for adsorption of Cr^{6+}, Fe^{3+} and Ni^{2+}. Journal of hazardous materials, 2017. **322**: p. 182-194.
65. Wu, S.J., Liou, T. H., Yeh, C. H., Mi, F. L.,and Lin, T. K., Preparation and characterization of porous chitosan–tripolyphosphate beads for copper (II)

ion adsorption. Journal of Applied Polymer Science, 2013. **127**(6): p. 4573-4580.
66. Vincent, C., Barré, Y., Vincent, T., Taulemesse, J. M., Robitzer, M.,and Guibal, E. Chitin-Prussian blue sponges for Cs (I) recovery: From synthesis to application in the treatment of accidental dumping of metal-bearing solutions. Journal of Hazardous Materials, 2015. **287**: p. 171-179.
67. Zhang, H., Dang, Q., Liu, C., Cha, D., Yu, Z., Zhu, W.,and Fan, B., Uptake of Pb (II) and Cd (II) on chitosan microsphere surface successively grafted by methyl acrylate and diethylenetriamine. ACS Applied Materials & Interfaces, 2017. **9**(12): p. 11144-11155.
68. Farrukh, A., Akram, A., Ghaffar, A., Hanif, S., Hamid, A., Duran, H.,and Yameen, B., Design of polymer-brush-grafted magnetic nanoparticles for highly efficient water remediation. ACS applied materials & interfaces, 2013. **5**(9): p. 3784-3793.
69. Ismael, M.N., El Nemr, A., El Ashry, E. S. H.,and Abdel Hamid, H., Removal of hexavalent chromium by cross-linking chitosan and N, N'-methylene bis-acrylamide. Environmental Processes, 2020. **7**(3): p. 911-930.
70. Timur, M. and A. Paşa, Synthesis, characterization, swelling, and metal uptake studies of aryl cross-linked chitosan hydrogels. ACS omega, 2018. **3**(12): p. 17416-17424.
71. Kumar, D., Gihar, S., Shrivash, M. K., Kumar, P.,and Kundu, P. P., A review on the synthesis of graft copolymers of chitosan and their potential applications. International Journal of Biological Macromolecules, 2020. **163**: p. 2097-2112.
72. Abraham, S., Rajamanickam, D., and Srinivasan, B., Research article preparation, characterization and cross-linking of chitosan by microwave assisted synthesis. *Sci. Int*, 2018.*6*, 18-30.
73. Zhao, D., Yu, S., Sun, B., Gao, S., Guo, S.,and Zhao, K. , Biomedical applications of chitosan and its derivative nanoparticles. Polymers, 2018. **10**(4): p. 462.
74. Elwakeel, K., El-Bindary, A. A., Ismail, A.,and Morshidy, A. M., Magnetic chitosan grafted with polymerized thiourea for remazol brilliant blue R recovery*:* Effects of uptake conditions. Journal of Dispersion Science and Technology, 2017. **38**(7): p. 943-952.

75. Mahaninia, M.H. and L.D. Wilson, Modular cross-linked chitosan beads with calcium doping for enhanced adsorptive uptake of organophosphate anions. Industrial & Engineering Chemistry Research, 2016. **55**(45): p. 11706-11715.
76. Mahaninia, M.H. and L.D. Wilson, Phosphate uptake studies of cross-linked chitosan bead materials. Journal of colloid and interface science, 2017. **485**: p. 201-212.
77. Zhang, X., Guo, H., Xiao, N., Ma, X., Liu, C., Zhong, L.,and Xiao, G. , Preparation and properties of epichlorohydrin-cross-linked chitosan/hydroxyethyl cellulose based CuO nanocomposite films. Cellulose, 2022. **29**(8): p. 4413-4426.
78. Elmehbad, N.Y. and N.A. Mohamed, Terephthalohydrazido cross-linked chitosan hydrogels: Synthesis, characterization and applications. International Journal of Polymeric Materials and Polymeric Biomaterials, 2022. **71**(13): p. 969-982.
79. Koh, K.Y., Chen, Z., Zhang, S.,and Chen, J. P. , Cost-effective phosphorus removal from aqueous solution by a chitosan/lanthanum hydrogel bead: material development, characterization of uptake process and investigation of mechanisms. Chemosphere, 2022. **286**: p. 131458.
80. Hamza, M.F., Abdel-Rahman, A. A. H., Negm, A. S., Hamad, D. M., Khalafalla, M. S., Fouda, A.,and Goda, A. E. S., Grafting of Thiazole Derivative on Chitosan Magnetite Nanoparticles for Cadmium Removal—Application for Groundwater Treatment. Polymers, 2022. **14**(6): p. 1240.
81. Sanchez-Salvador, J.L., J. L., Balea, A., Monte, M. C., Negro, C.,and Blanco, A. , Chitosan grafted/cross-linked with biodegradable polymers: A review. International Journal of Biological Macromolecules, 2021. **178**: p. 325-343.
82. Fang, S., Wang, G., Xing, R., Chen, X., Liu, S., Qin, Y.,and Li, P., Synthesis of superabsorbent polymers based on chitosan derivative graft acrylic acid-co-acrylamide and its property testing. International journal of biological macromolecules, 2019. **132**: p. 575-584.
83. Al-Mughrabi, W., A.O. Al-Dossary, and A. Abdel-Naby, Free Radical Copolymerization of Diallylamine and Itaconic Acid for the Synthesis of Chitosan Base Superabsorbent. Polymers, 2022. **14**(9): p. 1707.

84. Chang, K., Handbook of Microwave and Optical Components, Fiber and Electro-Optical Components. Vol. 4. 1991: Wiley-Interscience.
85. Ahmed, L.M., Bulk and Nanocatalysts Applications in Advanced Oxidation Processes, in Oxidoreductase. 2020, IntechOpen.
86. Cheng, Zeng, G., Huang, D., Lai, C., Xu, P., Zhang, C.,and Liu, Y., Hydroxyl radicals based advanced oxidation processes (AOPs) for remediation of soils contaminated with organic compounds: a review. Chemical Engineering Journal, 2016. **284**: p. 582-598.
87. Ahmed, L.M. and F.H. Hussein, Roles of Photocatalytic Reactions of Platinized TiO_2 Nanoparticales. 2014: LAP Lambert Academic Publishing.
88. Qumar, U., Hassan, J. Z., Bhatti, R. A., Raza, A., Nazir, G., Nabgan, W.,and Ikram, M., Photocatalysis vs adsorption by metal oxide nanoparticles. Journal of Materials Science & Technology, 2022.
89. Bard, A.J., Semiconductor particles and arrays for the photoelectrochemical utilization of solar energy. Berichte der Bunsengesellschaft für physikalische Chemie, 1988. **92**(11): p. 1187-1194.
90. Li, Z., Li, H., Wu, Z., Wang, M., Luo, J., Torun, H.,and Fu, Y., Advances in designs and mechanisms of semiconducting metal oxide nanostructures for high-precision gas sensors operated at room temperature. Materials Horizons, 2019. **6**(3): p. 470-506.
91. Portilla, L., Functionalization of Metal Oxide Nanostructures via Self-Assembly. Implications and Applications, Friedrich-Alexander-Universität Erlangen-Nürnberg (FAU),2017.
92. Choi, S.-J., I.-D. Kim, and H.J. Park, 2D layered Mn and Ru oxide nanosheets for real-time breath humidity monitoring. Applied Surface Science, 2022. **573**: p. 151481.
93. Wadullah, H.M., M.T. Mohammed, and T.K. Abdulrazzaq, Structure and characteristics of Nb_2O_5 nanocoating thin film for biomedical applications. Materials Today: Proceedings, 2022.
94. Umpierres, C.S., Prola, L. D., Adebayo, M. A., Lima, E. C., Dos Reis, G. S., Kunzler, D. D.,and Benvenutti, E. V, Mesoporous Nb_2O_5/SiO_2 material obtained by sol–gel method and applied as adsorbent of crystal violet dye. Environmental technology, 2017. **38**(5): p. 566-578.

95. Prado, A., Malafatti, J. O. D., Oliveira, J. A., Ribeiro, C., Joya, M. R., Luz, A. P., and Paris, E. C., Preparation and application of Nb_2O_5 nanofibers in CO_2 photoconversion. Nanomaterials, 2021. **11**(12): p. 3268.
96. Hashemzadeh, F., A. Gaffarinejad, and R. Rahimi, Porous p-NiO/n-Nb_2O_5 nanocomposites prepared by an EISA route with enhanced photocatalytic activity in simultaneous Cr (VI) reduction and methyl orange decolorization under visible light irradiation. Journal of Hazardous Materials, 2015. **286**: p. 64-74.
97. Luisa Marin, M., Hallett-Tapley, G. L., Impellizzeri, S., Fasciani, C., Simoncelli, S., Netto-Ferreira, J. C.,and Scaiano, J. C. , Synthesis, acid properties and catalysis by niobium oxide nanostructured materials. Catalysis Science and Technology, 2014. **4**(9): p. 3044-3052.
98. Hashemzadeh, F., R. Rahimi, and A. Ghaffarinejad, Mesoporous nanostructures of Nb_2O_5 obtained by an EISA route for the treatment of malachite green dye-contaminated aqueous solution under UV and visible light irradiation. Ceramics International, 2014. **40**(7): p. 9817-9829.
99. Gomes, G.H.M. and N.D. Mohallem, Insights into the TT-Nb_2O_5 crystal structure behavior. Materials Letters, 2022. **318**: p. 132136.
100. Aljumaily, G., Carver, G. E., Barton, J. B., Locknar, S. A., Chanda, S. K.,and Johnson, R. L. ,Optical and Physical Properties of Annealed Amorphous Nb_2O_5 Thin Films. in Optical Interference Coatings. 2022. Optica Publishing Group.
101. Zhang, Y.X., Guo, X. L., Huang, M., Hao, X. D., Yuan, Y.,and Hua, C. , Engineering birnessite-type MnO_2 nanosheets on fiberglass for pH-dependent degradation of methylene blue. Journal of Physics and Chemistry of Solids, 2015. **83**: p. 40-46.
102. Ganeshan, S., Ramasundari, P., Elangovan, A., Arivazhagan, G.,and Vijayalakshmi, R., Synthesis and characterization of MnO_2 nanoparticles: study of structural and optical properties. Int J Sci Res Phys Appl Sci, 2017. **5**(6): p. 5-8.
103. Taranu, B.-O., Novaconi, S. D., Ivanovici, M., Gonçalves, J. N.,and Rus, F. S., α-MnO_2 Nanowire Structure Obtained at Low Temperature with Aspects in Environmental Remediation and Sustainable Energy Applications. Applied Sciences, 2022. **12**(13): p. 6821.

104. Zhang, L.-X., Wang, Y. Z., Jiu, H. F., Wang, Y. L., Sun, Y. X.,and Li, Z., Controllable synthesis of Co-doped spinel $LiMn_2O_4$ nanotubes as cathodes for Li-ion batteries. Electronic Materials Letters, 2014. **10**: p. 439-444.
105. Mohammed, M.K., D. Hassan, and A. Hashim, Exploring the optical properties of MnO_2 nanoparticles doped PVP for optoelectronics devices. World Journal of Advanced Research and Reviews, 2023. **17**(1): p. 1178-1185.
106. AbdulKareem, S., M. Suhail, and I. Adehmash, Fabrication of Cr_2O_3: ZnO Nanostructure Thin Film Prepared by PLD Technique as NH_3 Gas Sensor. Iraqi Journal of Science, 2021: p. 2176-2187.
107. Zhang, D., Li, X., Qin, B., Li, X., Guo, X.,and Lai, C., Fabrication of chromium (III) oxide (Cr_2O_3) coating by electrophoretic deposition. Journal of the American Ceramic Society, 2014. **97**(11): p. 3413-3417.
108. Almaev, A.V., Kushnarev, B. O., Chernikov, E. V., Novikov, V. A., Korusenko, P. M.,and Nesov, S. N, Structural, electrical and gas-sensitive properties of Cr_2O_3 thin films. Super lattices and Microstructures, 2021. **151**: p. 106835.
109. Huang, N., Zhai, L., Xu, H.,and Jiang, D. , Stable covalent organic frameworks for exceptional mercury removal from aqueous solutions. Journal of the American Chemical Society, 2017. **139**(6): p. 2428-2434.
110. Wei, W., Lu, R., Xie, H., Zhang, Y., Bai, X., Gu, L.,and Liu, X., Selective adsorption and separation of dyes from an aqueous solution on organic–inorganic hybrid cyclomatrix polyphosphazene submicro-spheres. Journal of Materials Chemistry A, 2015. **3**(8): p. 4314-4322.
111. Yu, J.-G., Yue, B. Y., Wu, X. W., Liu, Q., Jiao, F. P., Jiang, X. Y.,and Chen, X. Q., Removal of mercury by adsorption: a review. Environmental Science and Pollution Research, 2016. **23**: p. 5056-5076.
112. Inyang, M. and E. Dickenson, *T*he potential role of biochar in the removal of organic and microbial contaminants from potable and reuse water: A review. Chemosphere, 2015. **134**: p. 232-240.
113. Zheng, H., Wang, Z., Zhao, J., Herbert, S.,and Xing, B. , Sorption of antibiotic sulfamethoxazole varies with biochars produced at different temperatures. Environmental Pollution, 2013. **181**: p. 60-67.
114. Worch, E., Adsorption technology in water treatment: fundamentals, processes, and modeling. 2021: Walter de Gruyter GmbH & Co KG.

115. Job, G. and R. Rüffler, Physical Chemistry from a Different Angle. Springer International Publishing. doi, 2016. **10**: p. 978-3.
116. Turhan, K. and S. Uzman, Removal of phenol from water using ozone. Desalination, 2008. **229**(1-3): p. 257-263.
117. Iftekhar, S., Ramasamy, D. L., Srivastava, V., Asif, M. B.,and Sillanpää, M., Understanding the factors affecting the adsorption of Lanthanum using different adsorbents*:* a critical review. Chemosphere, 2018. **204**: p. 413-430.
118. Adom, S., Effects of pH on Adsorption of Copper (II) onto Ground Peanut Hulls. 2020: Western Carolina University.
119. Zhang, Y., Zhu, C., Liu, F., Yuan, Y., Wu, H.,and Li, A. , Effects of ionic strength on removal of toxic pollutants from aqueous media with multifarious adsorbents: A review. Science of the Total Environment, 2019. **646**: p. 265-279.
120. Schramke, J.A., J. A., Murphy, S. F., Doucette, W. J.,and Hintze, W. D., Prediction of aqueous diffusion coefficients for organic compounds at 25 C. Chemosphere, 1999. **38**(10): p. 2381-2406.
121. Do, D.D., *A*dsorption analysis: Equilibria and kinetics (with cd containing computer MATLAB programs), World Scientific. 1998,Vol. **2**.
122. Salam, O.E.A., N.A. Reiad, and M.M. ElShafei, A study of the removal characteristics of heavy metals from wastewater by low-cost adsorbents. Journal of Advanced Research, 2011. **2**(4): p. 297-303.
123. Sadeek, S.A., Negm, N. A., Hefni, H. H.,and Wahab, M. M. A., Metal adsorption by agricultural biosorbents: adsorption isotherm, kinetic and biosorbents chemical structures. International journal of biological macromolecules, 2015. **81**: p. 400-409.
124. Ghasemi, M., Javadian, H., Ghasemi, N., Agarwal, S.,and Gupta, V. K. , Microporous nanocrystalline NaA zeolite prepared by microwave assisted hydrothermal method and determination of kinetic, isotherm and thermodynamic parameters of the batch sorption of Ni (II). Journal of Molecular Liquids, 2016. **215**: p. 161-169.
125. Demiral, H. and C. Güngör, Adsorption of copper (II) from aqueous solutions on activated carbon prepared from grape bagasse. Journal of cleaner production, 2016. **124**: p. 103-113.

126. Petronella, F., Truppi, A., Ingrosso, C., Placido, T., Striccoli, M., Curri, M. L.,and Comparelli, R., Nanocomposite materials for photocatalytic degradation of pollutants. Catalysis Today, 2017. **281**: p. 85-100.
127. Kaykhaii, M., M. Sasani, and S. Marghzari, Removal of dyes from the environment by adsorption process. Chem. Mater. Eng, 2018. **6**(2): p. 31-35.
128. Yang, J., Chen, D., Zhu, Y., Zhang, Y.,and Zhu, Y., 3D-3D porous Bi_2WO_6/graphene hydrogel composite with excellent synergistic effect of adsorption-enrichment and photocatalytic degradation. Applied Catalysis B: Environmental, 2017. **205**: p. 228-237.
129. Abbas, A.M., Abdulrazzak, F. H., Sabbar, W. J.,and Faraj, R. A. S., Adsorption of dyes by activated carbon surfaces were prepared from plant residues, A Review. J. Mater. Environ. Sci, 2020. **11**: p. 2007-2015.
130. Macías-García, A., Corzo, M. G., Domínguez, M. A., Franco, M. A.,and Naharro, J. M. , Study of the adsorption and electroadsorption process of Cu (II) ions within thermally and chemically modified activated carbon. Journal of hazardous materials, 2017. **328**: p. 46-55.
131. Natarajan, S., H.C. Bajaj, and R.J. Tayade, Recent advances based on the synergetic effect of adsorption for removal of dyes from waste water using photocatalytic process. Journal of Environmental Sciences, 2018. **65**: p. 201-222.
132. Xiao, Y. and J.M. Hill, Benefit of hydrophilicity for adsorption of methyl orange and electro-Fenton regeneration of activated carbon-polytetrafluoroethylene electrodes. Environmental science and technology, 2018. **52**(20): p. 11760-11768.
133. Sánchez-Sánchez, Á., Suárez-García, F., Martínez-Alonso, A.,and Tascón, J. M. D., Synthesis, characterization and dye removal capacities of N-doped mesoporous carbons. Journal of colloid and interface science, 2015. **450**: p. 91-100.
134. Huang, R., Liu, Q., Huo, J., & Yang, B., Adsorption of methyl orange onto protonated cross-linked chitosan. Arabian Journal of Chemistry, 2017. **10**(1): p. 24-32.
135. Carmen, Z. and S. Daniela, Textile organic dyes-characteristics, polluting effects and separation/elimination procedures from industrial effluents-a critical overview. IntechOpen Rijeka,2012: Vol. **3.**

136. Shankarling, G.S., P.P. Deshmukh, and A.R. Joglekar,Process intensification in azo dyes. Journal of environmental chemical engineering, 2017. **5**(4): p. 3302-3308.
137. Solís, M., Solís, A., Pérez, H. I., Manjarrez, N.,and Flores, M, Microbial decolouration of azo dyes: a review. Process Biochemistry, 2012. **47**(12): p. 1723-1748.
138. Mota, I.G.C., Neves, R. A. M. D., Nascimento, S. S. D. C., Maciel, B. L. L., Morais, A. H. D. A.,and Passos, T. S., Artificial dyes: Health risks and the need for revision of international regulations.Food Reviews International, 2021: p. 1-16.
139. Tanhaei, B., Ayati, A.,Lahtinen, M.,and Sillanpää, M., Preparation and characterization of a novel chitosan/Al_2O_3/magnetite nanoparticles composite adsorbent for kinetic, thermodynamic and isotherm studies of Methyl Orange adsorption.Chemical Engineering Journal, 2015. **259**: p. 1-10.
140. Zhai, L., Bai, Z., Zhu, Y., Wang, B., & Luo, W., Fabrication of chitosan microspheres for efficient adsorption of methyl orange. Chinese Journal of Chemical Engineering, 2018. **26**(3): p. 657-666.
141. Yadav, P. and M. Goutam, Forensic Analysis of Phenolphthalein in Trap Cases-A Critical Review. International Journal of Multidisciplinary Approach & Studies, 2014. **1**(4).
142. Yu, F., Chen, J., Chen, L., Huai, J., Gong, W., Yuan, Z.,and Ma, J., Magnetic carbon nanotubes synthesis by Fenton's reagent method and their potential application for removal of azo dye from aqueous solution. Journal of colloid and interface science, 2012. **378**(1): p. 175-183.
143. Aamir, M., Synthesis of Polyaniline Composites and Their Applications, 2016, Bahauddin Zakariya University, Multan, Pakistan.
144. Shair, A.S., A.S.A. Dena, and I.M. El-Sherbiny, Matrix-dispersed PEI-coated SPIONs for fast and efficient removal of anionic dyes from textile wastewater samples: Applications to triphenylmethanes. Spectrochimica Acta Part A: Molecular and Biomolecular Spectroscopy, 2021. **249**: p. 119301.
145. Dena, A.S.A. and W.M. Hassan, Experimental and quantum mechanical studies on the ion–pair of levocetirizine and bromocresol green in aqueous

solutions.Spectrochimica Acta Part A: Molecular and Biomolecular Spectroscopy, 2016. **163**: p. 108-114.
146. Alabbad, E., Removal of Direct Yellow 50 From Aqueous Solutions Using Chitosan-ISO-Vanillin Derivatives Chelating Polymers. 2020.
147. Ansari, R. and Z. Mosayebzadeh, Application of polyaniline as an efficient and novel adsorbent for azo dyes removal from textile wastewaters. Chemical Papers, 2011. **65**: p. 1-8.
148. Rizzi, V.,Longo,A.,Fini,P., Semeraro, P., Cosma, P., Franco, E.and Ferrándiz, M. , Applicative study (part I): the excellent conditions to remove in batch direct textile dyes (direct red, direct blue and direct yellow) from aqueous solutions by adsorption processes on low-cost chitosan films under different conditions. Advances in Chemical Engineering and Science, 2014. **4**(04): p. 454.
149. Smita, J., J. Dipika, and K. Shraddha, Polyaniline for removal of methyl orange dye from waste water. Int J Sci Eng Manag, 2016: p. 1-6.
150. Tanzifi, M., Hosseini, S. H., Kiadehi, A. D., Olazar, M., Karimipour, K., Rezaiemehr, R.,and Ali, I. , Artificial neural network optimization for methyl orange adsorption onto polyaniline nano-adsorbent: kinetic, isotherm and thermodynamic studies. Journal of Molecular Liquids, 2017. **244**: p. 189-200.
151. Chakraborty, P., A. Kothari, and R. Nagarajan, Highly ordered polyaniline as an efficient dye remover. Adsorption Science & Technology, 2018. **36**(1-2): p. 429-440.
152. Nerkar, N.V., Kondawar, S. B., Brahme, S. K.,and Kim, Y. H., Polyaniline/ZnO nanocomposites for the removal of methyl orange dye from waste water. International Journal of Modern Physics B, 2018. **32**(19): p. 1840085.
153. Haitham, K., S. Razak, and M. Nawi, Kinetics and isotherm studies of methyl orange adsorption by a highly recyclable immobilized polyaniline on a glass plate. Arabian Journal of Chemistry, 2019. **12**(7): p. 1595-1606.
154. Vidya, J., Bosco, A. J., Haribaaskar, K.,and Balamurugan, P., Polyaniline-$BiVO_4$ nanocomposite as an efficient adsorbent for the removal of methyl orange from aqueous solution. Materials Science in Semiconductor Processing, 2019. **103**: p. 104645.

155. Mohammadi, R., B. Massoumi, and F. Galandar, Polyaniline-TiO_2/graphene nanocomposite: an efficient catalyst for the removal of anionic dyes. Desalination and Water Treatment, 2019. **142**: p. 321-330.

156. Salmalian, E., H. Rezaei, and A. Shahbazi, Removal of bromocresol green from aqueous solutions using chitin nanofibers. Environmental Resources Research, 2019. **7**(2): p. 79-86.
157. Liu, D., Yuan, J.,Li, J.,and Zhang, G., Preparation of chitosan poly (methacrylate) composites for adsorption of bromocresol green. ACS omega, 2019. **4**(7): p. 12680-12686.
158. Duhan, M. and R. Kaur, Adsorptive removal of methyl orange with polyaniline nanofibers: an unconventional adsorbent for water treatment. Environmental Technology, 2020. **41**(23): p. 2977-2990.
159. Xing, C., Xia, A., Yu, L., Hao, Y., Dong, L., Zhao, Z.,and Sun, M. Adsorption Behavior Of Polyaniline Micro/Nanostructures For Methyl Orange. Materials & Technologies/Materiali in Tehnologije,2020.54(4).
160. Lv, C., Zhang, J., Li, G., Xi, H., Ge, M.,and Goto, T., Facile fabrication of self-assembled lamellar PANI-GO-Fe_3O_4 hybrid nanocomposites with enhanced adsorption capacities and easy recyclicity towards ionic dyes. Colloids and Surfaces A: Physicochemical and Engineering Aspects, 2020. **585**: p. 124147.
161. Rathore, B.S., Chauhan, N. P. S., Rawal, M. K., Ameta, S. C.,and Ameta, R., Chitosan–polyaniline–copper (II) oxide hybrid composite for the removal of methyl orange dye. Polymer Bulletin, 2020. **77**(9): p. 4833-4850.
162. Pete, S., R.A. Kattil, and L. Thomas, Polyaniline-multiwalled carbon nanotubes (PANI-MWCNTs) composite revisited: An efficient and reusable material for methyl orange dye removal. Diamond and Related Materials, 2021. **117**: p. 108455.
163. Ali, L.A., Ismail, H. K., Alesary, H. F.,and Aboul-Enein, H. Y., A nanocomposite based on polyaniline, nickel and manganese oxides for dye removal from aqueous solutions. International Journal of Environmental Science and Technology, 2021. **18**: p. 2031-2050.
164. Abniki, M. and A. Moghimi, Synthesis of chitosan functionalized magnetic carbon nanotubes for dispersive solid-phase extraction of bromocresol green. Micro & Nano Letters, 2021. **16**(9): p. 455-462.

165. Bekhoukh, A., Moulefera, I., Zeggai, F. Z., Benyoucef, A.,and Bachari, K., Anionic methyl orange removal from aqueous solutions by activated carbon reinforced conducting polyaniline as adsorbent: Synthesis, characterization, adsorption behavior, regeneration and kinetics study. Journal of Polymers and the Environment, 2022. **30**(3): p. 886-895.
166. Alabbad, E.A., S. Bashir, and J.L. Liu, Efficient removal of direct yellow dye using chitosan crosslinked isovanillin derivative biopolymer utilizing triboelectric energy produced from homogeneous catalysis. Catalysis Today, 2022. **400**: p. 132-145.
Rizzi, V.,Longo,A.,Fini,P., Semeraro, P., Cosma, P., Franco, E.and Ferrándiz, M. , Applicative study (part I): the excellent conditions to remove in batch direct textile dyes (direct red, direct blue and direct yellow) from aqueous solutions by adsorption processes on low-cost chitosan films under different conditions. Advances in Chemical Engineering and Science, 2014. **4**(04): p. 454.
167. Al-Odayni, A.-B., F.S. Alsubaie, and W.S. Saeed, Nitrogen-Rich Polyaniline-Based Activated Carbon for Water Treatment: Adsorption Kinetics of Anionic Dye Methyl Orange. Polymers, 2023. **15**(4): p. 806.
168. Palapa, N.R.,Yuliasari, N., Siregar, P. M. S. B. N., Wijaya, A., Amri, A., Ahmad, N.,and Lesbani, A., Selective Adsorption of Direct Group Anionic Dyes on Layered Double Hydroxide-Chitosan Composites. Bulletin of Chemical Reaction Engineering & Catalysis, 2023. **18**(1): p. 37-47.
169. Ismail, H.K., Alesary, H. F., Al-Murshedi, A. Y.,and Kareem, J. H., Ion and solvent transfer of polyaniline films electrodeposited from deep eutectic solvents via EQCM. Journal of Solid State Electrochemistry, 2019. **23**(11): p. 3107-3121.
170. Bian, L.-J., H.-L. He, and X.-X. Liu, Self-doped polyaniline/molybdenum oxide composite nanorods for supercapacitors. RSC advances, 2015. **5**(92): p. 75374-75379.
171. Ikram, M., Chaudhary, K., Shahzadi, A., Haider, A., Shahzadi, I., Ul-Hamid, A. & Butt, A. R., Chitosan/starch-doped MnO_2 nanocomposite served as dye degradation, bacterial activity, and insilico molecular docking study. Materials Today Nano, 2022. **20**: p. 100271.
172. Leoni, M., The Scherrer formula and integral-breadth methods. 2019.

173. Buldu, D.G., Investigation of Sulfurization Temperature Effects on Cu_2 $ZnSnS_4$ Thin Flims Prepared by Magnetron Sputtering Method on Flexible Titanium Foil Substrates for Thin Flim Solar Cells, Izmir Institute of Technology (Turkey). 2017.
174. Khan, S.A., Khan, S. B., Khan, L. U., Farooq, A., Akhtar, K.,and Asiri, A. M. , Fourier transform infrared spectroscopy: fundamentals and application in functional groups and nanomaterials characterization. Handbook of materials characterization, 2018: p. 317-344.
175. Skoog, D.A., F.J. Holler, and S.R. Crouch, Principles of instrumental analysis. 2017: Cengage learning.
176. Das, S., Ng, W. K., Kanaujia, P., Kim, S.,and Tan, R. B., Formulation design, preparation and physicochemical characterizations of solid lipid nanoparticles containing a hydrophobic drug: effects of process variables. Colloids and surfaces b: biointerfaces, 2011. **88**(1): p. 483-489.
177. Zhou, X., Yu, X., Hao, J.,and Liu, H., Comments on the calculation of the standard equilibrium constant using the Langmuir model.Journal of Hazardous Materials. 2022, **429**: p. 128407.
178. Fouad, M., Physical characteristics and Freundlich model of adsorption and desorption isotherm for fipronil in six types of Egyptian soil. Current Chemistry Letters, 2023. **12**(1): p. 207-216.
179. Zhou, X., R. Maimaitiniyazi, and Y. Wang, Some consideration triggered by misquotation of Temkin model and the derivation of its correct form. Arabian Journal of Chemistry, 2022: p. 104267.
180. Bakhtiarian, E., P.J. Foot, and P.C.M. Tate,Conductive poly (epichlorhydrin)–polyaniline dodecylbenzenesulfonate rubber blends prepared in solution. Progress in Rubber Plastics and Recycling Technology, 2016. **32**(4): p. 183-200.
181. Shahabuddin, S., Muhamad Sarih, N., Mohamad, S.,and Joon Ching, J., $SrtiO_3$ nanocube-doped polyaniline nanocomposites with enhanced photocatalytic degradation of methylene blue under visible light. Polymers, 2016. **8**(2): p. 27.
182. Cai, X., Cui, X., Zu, L., Zhang, Y., Gao, X., Lian, H.and Wang, X., Ultra high electrical performance of nano nickel oxide and polyaniline composite materials. Polymers, 2017. **9**(7): p. 288.

183. Abureesh, M.A., Oladipo, A. A., Mizwari, Z. M.,and Berksel, E., Engineered mixed oxide-based polymeric composites for enhanced antimicrobial activity and sustained release of antiretroviral drug. International journal of biological macromolecules, 2018. **116**: p. 417-425.
184. Bahramzadeh, E., E. Yilmaz, and T. Adali, Chitosan-graft-poly (N-hydroxy ethyl acrylamide) copolymers: Synthesis, characterization and preliminary blood compatibility in vitro. International journal of biological macromolecules, 2019. **123**: p. 1257-1266.
185. Alqahtani, F.Y.,Aleanizy, F. S., El Tahir, E., Alquadeib, B. T., Alsarra, I. A., Alanazi, J. S.,and Abdelhady, H. G., Preparation, characterization, and antibacterial activity of diclofenac-loaded chitosan nanoparticles. Saudi pharmaceutical journal, 2019. **27**(1): p. 82-87.
186. Ikram, M., Shujait, S., Haider, A., Ul-Hamid, A., Haider, J., Shahzadi, I.and Butt, A. R., Molybdenum and chitosan-doped MnO_2 nanostructures used as dye degrader and antibacterial agent. Applied Nanoscience, 2022. **12**(12): p. 3909-3924.
187. Inzelt, G., Conducting polymers: a new era in electrochemistry. 2012: Springer Science & Business Media.
188. Wu, T.-M., Y.-W. Lin, and C.-S. Liao, Preparation and characterization of polyaniline/multi-walled carbon nanotube composites. Carbon, 2005. **43**(4): p. 734-740.
189. Mylarappa, M., Chandruvasan, S., Kantharaju, S.,and Rekha, S., Synthesis and Characterization of Rgo Doped Nb_2O_5 Nano Composite for Chemical Sensor Studies. ECS Transactions, 2022. **107**(1): p. 269.
190. Dessie, Y., S. Tadesse, and R. Eswaramoorthy, Surface Roughness and Electrochemical Performance Properties of Biosynthesized α-MnO_2/NiO-Based Polyaniline Ternary Composites as Efficient Catalysts in Microbial Fuel Cells. Journal of Nanomaterials, 2021. **2021**: p. 1-21.
191. Dinh, V.-P., Le, N. C., Tuyen, L. A., Hung, N. Q., Nguyen, V. D.,and Nguyen, N. T., Insight into adsorption mechanism of lead (II) from aqueous solution by chitosan loaded MnO_2 nanoparticles. Materials Chemistry and Physics, 2018. **207**: p. 294-302.
192. Yadav, M., Rhee, K. Y., Park, S. J., and Hui, D. , Mechanical properties of Fe_3O_4/GO/chitosan composites. Composites Part B: Engineering, 2014. **66**: p. 89-96.

193. Saleh, T.A., An overview of nanomaterials for water technology. Advanced Nanomaterials for Water Engineering, Treatment, and Hydraulics, 2017: p. 1-12.
194. Taş, R., M. Can, and S. Sönmezoğlu, Preparation and characterization of polyaniline microrods synthesized by using dodecylbenzene sulfonic acid and periodic acid. Turkish Journal of Chemistry, 2015. **39**(3): p. 589-599.
195. Djara, R., Holade, Y., Merzouki, A., Masquelez, N., Cot, D., Rebiere, B.,and Tingry, S., Insights from the physicochemical and electrochemical screening of the potentiality of the chemically synthesized polyaniline. Journal of the Electrochemical Society, 2020. **167**(6): p. 066503.
196. Hassan, S.E.-D., Fouda, A., Saied, E., Farag, M. M., Eid, A. M., Barghoth, M. G.& Awad, M. F. , Rhizopus Oryzae-mediated green synthesis of magnesium oxide nanoparticles (MgO-NPs): A promising tool for antimicrobial, mosquitocidal action, and tanning effluent treatment. Journal of Fungi, 2021. **7**(5): p. 372.
197. Fuseini, M., A.H. El-Shazly, and M.F. El-Kady. Effects of Doping on Zeta Potential and pH of Polyaniline Colloidal Suspension. in Materials Science Forum. 2020. Trans Tech Publ.
198. Nawrocki, J., The silanol group and its role in liquid chromatography. Journal of Chromatography A, 1997. **779**(1-2): p. 29-71.
199. Roosz, N., Euvrard, M., Lakard, B.,and Viau, L., A straightforward procedure for the synthesis of silica/polyaniline core-shell nanoparticles. Colloids and Surfaces A: Physicochemical and Engineering Aspects, 2019. **573**: p. 237-245.
200. Kim, K.N., H.-R. Jung, and W.-J. Lee, Hollow cobalt ferrite–polyaniline nanofibers as magnetically separable visible-light photocatalyst for photodegradation of methyl orange. Journal of Photochemistry and Photobiology A: Chemistry, 2016. **321**: p. 257-265.
201. Al-Sagheer, F.A., E.I. Ibrahim, and K.D. Khalil, Crystallinity, antimicrobial activity and dyeing properties of chitosan-g-poly (N-acryloyl morpholine) copolymer. European polymer journal, 2014. **58**: p. 164-172.
202. Kalaycıoğlu, Z., Kahya, N., Adımcılar, V., Kaygusuz, H., Torlak, E., Akın-Evingür, G.,anf Erim, F. B.,Antibacterial nano cerium oxide/chitosan/cellulose acetate composite films as potential wound dressing. European Polymer Journal, 2020. **133**: p. 109777.

203. Buşilă, M., Muşat, V., Textor, T.,and Mahltig, B., Synthesis and characterization of antimicrobial textile finishing based on Ag: ZnO nanoparticles/chitosan biocomposites. Rsc Advances, 2015. **5**(28): p. 21562-21571.
204. Shahabuddin, S., Gaur, R., Mukherjee, N., Chandra, P.,and Khanam, R., Conducting polymers-based nanocomposites: Innovative materials for waste water treatment and energy storage. Materials Today: Proceedings, 2022. **62**: p. 6950-6955.
205. Ansari, R. and Z. Mosayebzadeh, Application of polyaniline as an efficient and novel adsorbent for azo dyes removal from textile wastewaters. Chemical Papers, 2011. **65**(1): p. 1-8.
206. Nasar, A. and F. Mashkoor, Application of polyaniline-based adsorbents for dye removal from water and wastewater—a review. Environmental Science and Pollution Research, 2019. **26**(6): p. 5333-5356.
207. Karri, R.R., Tanzifi, M., Yaraki, M. T.,and Sahu, J. N., Optimization and modeling of methyl orange adsorption onto polyaniline nano-adsorbent through response surface methodology and differential evolution embedded neural network. Journal of environmental management, 2018. **223**: p. 517-529.
208. Al-Ghouti, M.A. and D.A. Da'ana, Guidelines for the use and interpretation of adsorption isotherm models: A review. Journal of hazardous materials, 2020. **393**: p. 122383.
209. Ibrahim, R. K., El-Shafie, A., Hin, L. S., Mohd, N. S. B., Aljumaily, M. M., Ibraim, S., and AlSaadi, M. A., A clean approach for functionalized carbon nanotubes by deep eutectic solvents and their performance in the adsorption of methyl orange from aqueous solution. Journal of environmental management, 2019. **235**: p. 521-534.
210. Manzar, M.S., Waheed, A., Qazi, I. W., Blaisi, N. I. and Ullah, N., Synthesis of a novel epibromohydrin modified crosslinked polyamine resin for highly efficient removal of methyl orange and eriochrome black T. Journal of the Taiwan Institute of Chemical Engineers, 2019. **97**: p. 424-432.
211. Elwakeel, K. Z., El-Bindary, A. A., El-Sonbati, A. Z.,and Hawas, A. R., Magnetic alginate beads with high basic dye removal potential and excellent regeneration ability. Canadian Journal of Chemistry, 2017. **95**(8): p. 807-815.

212. Sharifpour, E., Alipanahpour Dil, E., Asfaram, A., Ghaedi, M.,and Goudarzi, A., Optimizing adsorptive removal of malachite green and methyl orange dyes from simulated wastewater by Mn-doped CuO-Nanoparticles loaded on activated carbon using CCD-RSM: Mechanism, regeneration, isotherm, kinetic, and thermodynamic studies. Applied Organometallic Chemistry, 2019. **33**(3): p. e4768.
213. Murmu, B., Behera, S. S., Das, S., Mohapatra, R. K., and Parhi, P., Extensive investigation on the study for the adsorption of Bromocresol Green (BCG) dye using activated Phragmites karka. Indian Journal of Chemical Technology, 2019. **25**(5), 409-420.
214. Zhang, F., Chen, X., Wu, F.,and Ji, Y., High adsorption capability and selectivity of ZnO nanoparticles for dye removal. Colloids and Surfaces A: Physicochemical and Engineering Aspects, 2016. **509**: p. 474-483.
215. Ohale, P., Adsorptive removal of bromocresol green dye using activated corn cob. Journal of engineering and applied sciences, 2022.
216. Elijah, O.C., Nonso Collins, O., Callistus Obumneme, O.,and Jessica, N. B., Application of modified agricultural waste in the adsorption of bromocresol green dye. Asian Journal of Chemical Science, 2020. **7**(1): p. 15-24.
217. Theydan, S.K., Effect of process variables, adsorption kinetics and equilibrium studies of hexavalent chromium removal from aqueous solution by date seeds and its activated carbon by $ZnCl_2$. Iraqi Journal of Chemical and Petroleum Engineering, 2018. **19**(1): p. 1-12.
218. Alqaragully, M.B., Removal of textile dyes (maxilon blue, and methyl orange) by date stones activated carbon. Int J Adv Res Chem Sci, 2014. **1**(1): p. 48-59.
219. Arabkhani, P. and A. Asfaram, Development of a novel three-dimensional magnetic polymer aerogel as an efficient adsorbent for malachite green removal. Journal of Hazardous Materials, 2020. **384**: p. 121394.
220. Asadu, C.O., Anthony, E. C., Elijah, O. C., Ike, I. S., Onoghwarite, O. E.,and Okwudili, U. E., Development of an adsorbent for the remediation of crude oil polluted water using stearic acid grafted coconut husk (Cocos nucifera) composite. Applied Surface Science Advances, 2021. **6**: p. 100179.

221. Onu, C.E., Ekwueme, B. N., Ohale, P. E., Onu, C. P., Asadu, C. O., Obi, C. C.and Onu, O. O., Decolourization of bromocresol green dye solution by acid functionalized rice husk: artificial intelligence modeling, GA optimization, and adsorption studies. Journal of Hazardous Materials Advances, 2022: p. 100224.
222. Alabbad, E.A., Efficient removal of methyl orange from wastewater by polymeric chitosan-iso-vanillin. Open Chemistry Journal, 2020. **7**(1).
223. Salgot, M., Oron, G., Cirelli, G. L., Dalezios, N. R., Díaz, A.,and Angelakis, A. N., Criteria for wastewater treatment and reuse under water scarcity, in Handbook of Drought and Water Scarcity. 2017, CRC Press. p. 263-282.
224. Saeed, T., Naeem, A., Mahmood, T., Khan, A., Ahmad, Z., Hamayun, M.and Khan, N. H., Kinetic and thermodynamic studies of polyvinyl chloride composite of manganese oxide nanosheets for the efficient removal of dye from water. Water Science and Technology, 2021. **84**(4): p. 851-864.
225. Saeed, T., Naeem, A., Din, I. U., Farooq, M., Khan, I. W., Hamayun, M.,and Malik, T, Synthesis of chitosan composite of metal-organic framework for the adsorption of dyes; kinetic and thermodynamic approach. Journal of Hazardous Materials, 2022. **427**: p. 127902.
226. Joshi, S., Garg, V. K., Kataria, N., and Kadirvelu, K., Applications of Fe_3O_4/AC nanoparticles for dye removal from simulated wastewater. Chemosphere, 2019. **236**: p. 124280.
227. Al Hamouz, O.C.S., Synthesis and characterization of a novel series of cross-linked (phenol, formaldehyde, alkyldiamine) terpolymers for the removal of toxic metal ions from wastewater. Arabian Journal for Science and Engineering, 2016. **41**(1): p. 119-133.
228. Laçin, D. and A. Aroguz, Removal of dye pollution by modified halloysite as eco-friendly adsorbent. The International Journal of Materials and Engineering Technology,2020. **3**(1): p. 47-56.
229. Santhosh, C., Daneshvar, E., Kollu, P., Peräniemi, S., Grace, A. N.,and Bhatnagar, A., Magnetic SiO_2/$CoFe_2O_4$ nanoparticles decorated on graphene oxide as efficient adsorbents for the removal of anionic pollutants from water. Chemical Engineering Journal, 2017. **322**: p. 472-487.
230. Mahmoud, A.S., Effect of nano bentonite on direct yellow 50 dye removal; Adsorption isotherm, kinetic analysis, and thermodynamic behavior.

Progress in Reaction Kinetics and Mechanism, 2022. **47**: p. 14686783221090377.

231. Ismail, L F. M., Sallam, H. B., Farha, S. A., Gamal, A. M., and Mahmoud, G. E. A, Adsorption behaviour of direct yellow 50 onto cotton fiber: equilibrium, kinetic and thermodynamic profile. Spectrochimica Acta Part A: Molecular and Biomolecular Spectroscopy, 2014. **131**: p. 657-666.
232. Jabeen, A. and H.N. Bhatti, Adsorptive removal of reactive green 5 (RG-5) and direct yellow 50 (DY-50) from simulated wastewater by Mangifera indica seed shell and its magnetic composite: Batch and Column study. Environmental Technology & Innovation, 2021. **23**: p. 101685.
233. Wang, W., Huang, G., An, C., Xin, X., Zhang, Y.,and Liu, X., Transport behaviors of anionic azo dyes at interface between surfactant-modified flax shives and aqueous solution: Synchrotron infrared and adsorption studies. Applied Surface Science, 2017. **405**: p. 119-128.

الخلاصة

تتكون الدراسة الحالية من جزئيين:

يتناول الجزء الاول من الاطروحة تحضير متراكب نانوي جديد من Polyaniline / Nb_2O_5 / MnO_2 و Polyaniline / Nb_2O_5 / Cr_2O_3 بواسطة البلمرة الكيميائية من بادئ الأنيلين في جود اكاسيد معدنية (Nb_2O_5,Cr_2O_3 MnO_2) واستخدام بيرسلفات الامونيوم(APS) كمادة مؤكسدة في محلول حامض الهيدروكلوريك المخفف لإزالة الاصباغ من الماء .هنا، وجد ان المتراكبين مواد ممتزة جيدة لمعالجة مياه الصرف الصحي بسبب كفاءتها وتكلفتها المنخفضة وسهولة التحضير كما يمكن اعادة استخدامها اكثر من مرة. تم تشخيص المتراكبات بتقنيات مختلفة مثل الاشعة تحت الحمراء(FT-IR) ،إنحراف الاشعة السينية (XRD)، الاشعة فوق البنفسجية والمرئية (UV-VIS) ، تحليل جهد زيتا(ZPA)، المجهر الالكتروني الماسح(FE-SEM) والتحليل الوزني الحراري(TGA). تم فحص طبيعة السطح بواسطة SEM، كما تم التعرف على بنية المركبات Polyaniline/nanomatrial بواسطة XRD والتعرف على المجاميع الوظيفية في البوليمر باستخدام FT-IR.

تم استخدام المتراكبات Polyaniline / Nb_2O_5 / MnO_2 وPolyaniline /Nb_2O_5 / Cr_2O_3 في امتزاز صبغة المثيل البرتقالي، اظهرت النتائج ان كفاءة الامتزاز للمتراكب Polyaniline / Nb_2O_5 / MnO_2 اعلى من المتراكب Polyaniline /Nb_2O_5 / Cr_2O_3 حيث كانت 97.75% و 94.3% على التوالي. كانت سعة الامتزاز للمتراكبين Polyaniline / Nb_2O_5 / MnO_2 وPolyaniline /Nb_2O_5 / Cr_2O_3

(84mg/g، 148) على التوالي.

الظروف المثلى لتفاعل صبغة المثيل البرتقالي مع المتراكب Polyaniline / Nb_2O_5 / MnO_2 (وزن المتراكب =100mg، درجة الحرارة= 298K، تركيز الصبغة= 10 جزء بالمليون وقيمة الدالة الحامضية =7)، بينما كانت الظروف المثلى للمتراكب Polyaniline /Nb_2O_5 / Cr_2O_3 (وزن المتراكب =50mg، درجة الحرارة= 298K، تركيز الصبغة= 25 جزء بالمليون وقيمة الدالة الحامضية =9).

في الجزء الثاني من الاطروحة تم تحضير متراكبات نانوية جديدة Chitosan / Nb_2O_5 / MnO_2و Chitosan / Nb_2O_5 / Cr_2O_3 بطريقة سهلة وبسيطة بوجود حامض الخليك المخفف وكذلك اضافة محلول قاعدي من هيدروكسيد الصوديوم (0.1M). تم تشخيص المتراكبات بتقنيات مختلفة مثل الاشعة تحت

الحمراء(FT-IR) ،إنحراف الاشعة السينية (XRD)، الاشعة فوق البنفسجية والمرئية (UV-VIS) ، جهد زيتا(ZPA)، المجهر الالكتروني الماسح(FE-SEM) والتحليل الوزني الحراري(TGA). استخدمت المتراكبات في ازالة صبغة بروموكريسول الاخضر (BCG) وكذلك صبغة (Direct yellow 50) .

تم الحصول على اقصى فعالية لإزالة اللون لصبغة (BCG) باستخدام المتراكب Chitosan / Nb_2O_5 / MnO_2 حيث كانت نسبة الازالة 90.65% بينما نسبة الازالة للمتراكب Chitosan / Nb_2O_5 / Cr_2O_3 كانت 88.5%. تم تحديد سعة الامتزاز للمتراكبات CS / Nb_2O_5 / MnO_2 و CS /Nb_2O_5 / Cr_2O_3(43,93 mg/g) على التوالي.

تمت دراسة الظروف المثلى للمتراكب $CS/Nb_2O_5/MnO_2$ في امتزاز صبغه بروموكريسول الاخضر

حيث كان(وزن المتراكب =150mg، درجة الحرارة= 298K، تركيز الصبغة= 5 جزء بالمليون وقيمة الدالة الحامضية =7) ، بينما كانت الظروف المثلى للمتراكب CS /Nb_2O_5 / Cr_2O_3 (وزن المتراكب =550mg، درجة الحرارة= 313K، تركيز الصبغة= 5 جزء بالمليون وقيمة الدالة الحامضية =10).

اظهرت النتائج ان اقصى فعالية لإزالة اللون لصبغة (DY50) للمتراكب CS/ Nb_2O_5/MnO_2 اعلى من المتراكب CS/Nb_2O_5/ Cr_2O_3 حيث كانت 98.1% و 95.41% على التوالي.

تمت دراسة الظروف المثلى للمتراكب $CS/Nb_2O_5/MnO_2$ في امتزاز صبغه (DY50) حيث كان(وزن المتراكب =50mg، درجة الحرارة= 298K، تركيز الصبغة= 10 جزء بالمليون وقيمة الدالة الحامضية =3) ، بينما كانت الظروف المثلى للمتراكب CS /Nb_2O_5 / Cr_2O_3 (وزن المتراكب =25mg، درجة الحرارة= 298K، تركيز الصبغة=15 جزء بالمليون وقيمة الدالة الحامضية =4).

جمهورية العراق

وزارة التعليم العالي والبحث العلمي

جامعة بابل/ كلية العلوم

قسم الكيمياء

إزالة بعض الاصباغ باستخدام متراكبات نانوية مشتقة من متعدد الانلين والكيتوسان مع اكاسيد بعض الفلزات كممتزات جديدة

أطروحة مقدمة

إلى مجلس كلية العلوم ـ جامعة بابل كجزء من متطلبات

نيل درجة الدكتوراه فلسفة في علوم الكيمياء

تقدم بها

كرار مجيد عبيد محمد

بأشراف

أ.م. د. أحمد سعدون عباس

أ.م. د. يحيى فاهم عبيد

2023 م

1445 ه